

SEQUENTIAL ON-COLUMN SINGLE MOLECULE MEASUREMENT

By

ROBERT DOUGLAS GUENARD

A DISSERTATION PRESENTED TO THE GRADUATE SCHOOL
OF THE UNIVERSITY OF FLORIDA IN PARTIAL FULFILLMENT
OF THE REQUIREMENTS FOR THE DEGREE OF
DOCTOR OF PHILOSOPHY

UNIVERSITY OF FLORIDA

1996

*This dissertation, and all great successes I achieve in life,
I dedicate to the loving memory of my mother, Shirley*

ACKNOWLEDGMENTS

First and foremost, I would like to express my deepest gratitude to my advisor and mentor Professor James Winefordner. Working with such a large and dynamic group of post doctoral researchers, visiting professors and scientists and, of course, graduate students has been a most valuable experience. The availability of this type of group can all be attributed to Jim's wonderful acumen of spectroscopy and his down-to-earth personality. Jim's philosophies of research and life will be with me always and it is my hope that I will have an impact on my chosen path in life as he has.

My greatest appreciation goes to Dr. Benjamin Smith for compelling me to view his love of science and because of his practical advice and ideas on achieving success in the lab. Ben's confident mild manner with his timely given dose of positive reinforcement can account for a large portion of the successful completion of my research and the personal growth I experienced over my stay. I owe a great deal of thanks to my predecessor Yuan-Hsiang Lee for the great work he did on the project before I took it over and also for the advice and discussions we had since his departure. It is my hope that I continued the research in a manner that he would have found to meet his standards. I would like to thank Dr. Mikhail Bolshov for his contribution to the theoretical studies on the metal vapor filter. Without his help,

these studies would not have been so thorough. Thanks also go to Mr. Chi-Hse Teng and Dr. Mark Yang of the Department of Statistics for their contribution of the statistical models and simulations of the detection of single molecules. I would like to express my gratitude to the members of my Ph.D. committee, Dr. Robert Kennedy, Dr. Anna Brajter-Toth, Dr. John Reynolds and Dr. Joseph Delfino. I would especially like to thank Dr. Kennedy for his helpful discussions and advice.

Heartfelt thanks go to all of the members of the J.D.W. group for all of their help, enthusiasm and friendship. I would specifically like to acknowledge Eugene Wagner, Cindy Baker, Ken Riter, Wendy Clevenger, Anil Raghani, Scott Baker, Bryan Castle, Dave Rusak, Bill Walden, Dave Besteman and Andea Croslyn for their support and friendship. I would like to thank Leslie King for the work she performed on the project in the last year. She deserves special thanks for her patience over my last few months in the lab.

I would like to thank Texaco for the financial support of my third year through the award of a fellowship.

My appreciation goes out to my parents, Richard and Shirley, and to my siblings Richard, Glenn, Laura, Carrie and Charles for their support, confidence and encouragement. Glenn and Charles were invaluable to me and without them I wouldn't have made it through it all. Words cannot describe the impact that my mother Shirley has had on my life before and during my graduate career. Her love and confidence in me have given me the perseverance and passion needed to accomplish things which were never expected from me, like obtaining a Ph.D.

I want to express my deepest thanks to Rebecca Litteral for the love and support she has given me and has enabled me to return. I am looking forward to starting our life together and will be with her always.

TABLE OF CONTENTS

	<u>page</u>
ACKNOWLEDGEMENTS.....	iii
ABSTRACT.....	vii
 CHAPTER ONE	
REVIEW OF SINGLE MOLECULE DETECTION.....	1
Introduction.....	1
Single Molecule Detection Basics.....	2
Overview.....	2
Fluorescence Analysis.....	4
Background Signal Reduction.....	9
Data Reduction.....	12
Figures of Merit.....	19
Techniques of Single Molecule Detection.....	24
Flowing Techniques.....	24
Levitated Microdroplet Technique.....	31
Microscopy Techniques.....	33
Far-Field Microscopy.....	33
Near-Field Microscopy.....	37
Applications.....	38
 CHAPTER TWO	
EXPERIMENTAL.....	40
Introduction.....	40
Description of Apparatus.....	40
General Experimental Apparatus.....	40
Light Source.....	42
Capillary Flow Cell and Sample Introduction.....	47
Detection Scheme.....	52
Metal Vapor Filter.....	53
Photon Detection and Data Acquisition.....	58
Optical Alignment.....	65
Chemical System.....	71

CHAPTER THREE

RUBIDIUM METAL VAPOR FILTER STUDIES.....	76
Introduction.....	76
Experimental.....	80
Results and Discussion.....	84
Simulation.....	98
Conclusions.....	110

CHAPTER FOUR

SEQUENTIAL SINGLE MOLECULE MEASUREMENT.....	113
Overview.....	113
Preliminary Studies.....	113
Background Signal.....	113
Linear Flow Velocity.....	119
Fluorescence Signal Saturation.....	132
Calibration Curve.....	134
Single Molecule Measurement.....	137
Sequential Single Molecule Measurement.....	151

CHAPTER FIVE

CONCLUSIONS AND FUTURE WORK.....	160
Conclusions.....	160
Future Work.....	162

APPENDIX

STATISTICS OF SINGLE MOLECULE DETECTION.....	164
Occupancy of a Single Molecule.....	164
Photon Detection Model.....	165
Simulation of Data.....	167

REFERENCES.....	170
-----------------	-----

BIOGRAPHICAL SKETCH.....	177
--------------------------	-----

Abstract of Dissertation Presented to the Graduate School
of the University of Florida in Partial Fulfillment of the
Requirements for the Degree of Doctor of Philosophy

SEQUENTIAL ON-COLUMN SINGLE MOLECULE MEASUREMENT

By

Robert Douglas Guenard

December 1996

Chairperson: James D. Winefordner
Major Department: Chemistry

The main objective of the work described in this dissertation was to achieve the efficient detection of a single molecule in a flowing stream, on-column, sequentially in two channels. Preliminary work included the theoretical and experimental characterization of a rubidium metal vapor filter (MVF) used to reject scattered laser radiation. These studies included monitoring the transmission of background photons under various conditions with the goal of improving the performance of the MVF. It was found that the metal vapor filter should be operated at a high temperature with a high fill-gas pressure and at a low laser power to achieve the maximum attenuation of laser light.

Other studies prior to the measurement of single IR 140 molecules included characterizations of solution flow, laser saturation of IR 140 fluorescence, IR 140 photobleaching and the construction a calibration curve for each channel. To detect

a single molecule, titanium:sapphire laser was focused onto a quartz capillary with an inside diameter of 9 micrometers. A dilute solution (0.1 pM) of IR 140 molecules dissolved in methanol was flowed through the capillary with pressure. The fluorescence was orthogonally collected using a microscope objective. Significant laser scatter was attenuated using the MVF. Fluorescence was passed through a bandpass filter centered at the fluorescence maxima of IR 140 and detected with a single photon avalanche photodiode. Detection channels were placed at two spots on the column so that single fluorophores were detected sequentially. Channels were characterized individually to investigate their detection efficiencies for single molecule detection. The detection efficiencies were found to be 0.95 and 0.93 for channels one and two, respectively. Using the distance between the channels and the measured average linear velocity, the inter-channel molecular transit time was calculate to be 232 ms. The measured molecular transit value was 225 ± 5 ms which was in good agreement with the calculated value confirming the efficient measurement of single molecules sequentially on-column.

CHAPTER ONE

REVIEW OF SINGLE MOLECULE DETECTION

Introduction

Analytical chemistry involves techniques for the measurement of the type and amount of chemicals in a given system or sample. On a fundamental level of analytical research, this includes improvement to existing techniques, development of new ones and application of both in new and different areas. A definitive goal for the analytical chemist is to quantitate the smallest particle form in the realm of chemistry: the single molecule or the single atom. The motivation for such an achievement, however, is not based solely on a rudimentary goal for the analytical chemist. As the demand becomes greater in terms of quantitation of chemical species in biological and environmental systems, amongst others, the need for highly sensitive and selective methods is of paramount importance. Microchemical analysis is a prime candidate for the use of ultrasensitive detection capabilities. For example, capillary electrophoresis (CE) has become one of the most widely researched microchemical techniques. Because of its high mass sensitivity, small sample sizes (nL injections) combined with the analysis of dilute solutions (nM or less), the sensitivity requirements on the detection are on the order of attomole or less quantities.

In analytical chemistry, the most widely analyzed state of matter is the liquid sample. Therefore, analytical research directed toward the detection of single molecules has been

primarily on liquid analytes. The review presented in this Chapter will entail the observation of individual molecules existing in solution. It is not meant to detract from impressive work done in solids from such groups such as Moerner *et al.*^{1,2}, Orrit *et al.*³ Basche *et al.*^{4,5} Wild *et al.*^{6,7} and several others. In fact, working with low temperature solids, optical detection of nuclear magnetic resonance⁸ and electron paramagnetic resonance⁹ on single molecules has been achieved. Laser induced fluorescence has been the most widely published technique for analytical single molecule detection. It is this method that will be discussed in detail in the following review of single molecule detection as well as the doctoral research reported subsequently. Several other analytical methods have been evaluated for the detection of single molecules (events) in solution have included chemiluminescence¹⁰ and electrochemical methods.¹¹

Single Molecule Detection Basics

Overview

To obtain the sensitivity necessary to observe events from an individual molecule, two major accomplishments must be achieved. The first is that the mechanism by which the signal is obtained must be amplified in some manner so as to differentiate it from random or spurious events. Secondly, the background signal must be decreased to a level whereby the signal from the molecular event be discernable from the events in the background. Upon initial inspection of these two reasons, they may seem virtually indistinguishable. However, within the experimental framework of single molecule detection (SMD), these

difficulties must be approached independently. Methods to amplify an intrinsic signal by spectroscopic techniques include detecting:

1. multiple molecules in the same event,
2. multiple labels on the same molecule,
3. multiple products from the same molecule, and
4. multiple photons from the same molecule

Method 1 entails amplifying the signal in a given event by increasing the number of analyte molecules. Obviously, this method would intrinsically preclude the detection of individual molecules. By placing multiple labels on a given molecule, as in method 2, the signal obtained in its measurement would be amplified by a factor proportional to the number of labels attached to the analyte of interest. It was with this method that the detection of a single molecule was first attempted^{12,13} and first reported.¹⁴ By the standards set in the literature of SMD as of today, this method is not true SMD because multiple fluorophores are used in the measurement. A unique method of amplifying the signal is revealed in method 3. Molecules which act as catalysts or reaction mediators, such as enzymes, can be detected indirectly by monitoring the products from the chemical reaction which the analyte molecule is facilitating. This technique has been used to monitor enzymes¹⁵ and for fluorescence-based enzymatic assays.¹⁶ Method 4 is the basis for the technique of laser-induced fluorescence (LIF) spectroscopy in that, from one molecule many photons may be emitted with repeated excitation. An individual molecule detected in this manner is considered, throughout the literature, to be a true single molecule detection technique. True SMD methods, that is, measurement of individual molecular events, can be evaluated in terms of the ability to

observe events directly without signal processing, real-time measurement, measurement efficiency, etc, which will be discussed in subsequent sections within this chapter.

Fluorescence Analysis

Figure 1-1 illustrates the technique of laser-induced fluorescence as a single molecule passes through a laser beam. While in the laser beam, the fluorescent molecule repeatedly cycles through photon excitation of a ground state to a singlet state (S_1) and photon emission back down to the ground state (S_0). This SMD detection process is called photon-burst detection. The rate at which this process can occur is dependent upon the pumping rate (k_a) to the excited state by the laser and by the rate at which the molecule then radiationally relaxes (k_r) as governed by the characteristic fluorescence lifetime (τ_f) of the molecule. Mathies *et al* reported a mathematical model describing high sensitivity fluorescence and its optimization in the presence of ground-state depletion (optical saturation) and photodestruction (photobleaching).^{17,18} The authors describe in detail the basic fluorescence equations and parameters needed to optimize an ultrasensitive LIF method. Figure 1-2 is a kinetic scheme for the model and should be used as a reference throughout the explanation of the basic equations. In Figure 1-2, S_1' is an optically excited vibronic singlet state, k_a is the radiationless decay rate, k_i is the intersystem crossing rate to the triplet state (T), k_D is the photodestruction rate and k_T is the overall triplet state decay rate. All rates in the model have units of s^{-1} . In the model, it is assumed that the relaxation rate $S_1' \rightarrow S_1$ is fast compared to any of the decay rates.

To obtain the maximum number of photons in a burst, the photoexcitation rate must

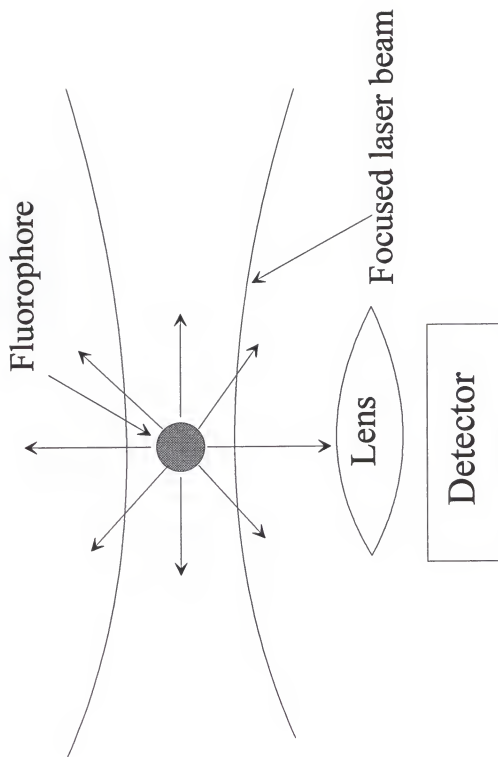


Figure 1-1 Schematic of photon burst detection

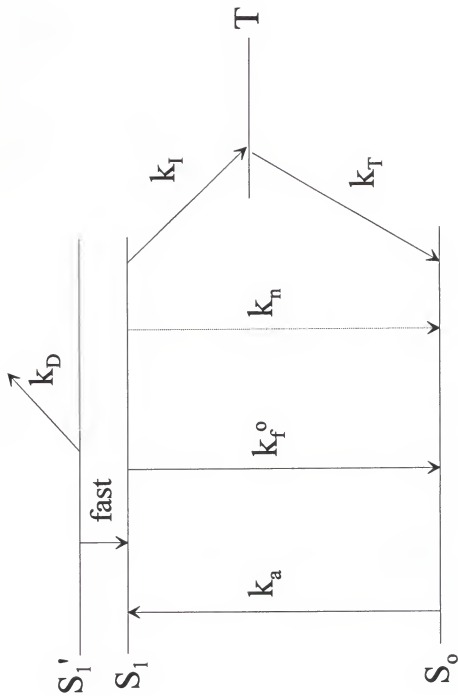


Figure 1-2 Kinetic scheme for fluorescence model

be maximized while simultaneously minimizing the photobleaching rate. The rate of photoexcitation is described by

$$k_s = \sigma_a I = 3.8 \times 10^{-21} \epsilon I \quad (1-1)$$

where σ_a is the absorption crosssection of the molecule (cm^2), I is the laser intensity (photons $\text{cm}^{-2} \text{s}^{-1}$) and ϵ is the decadic molar absorption coefficient ($\text{cm}^{-1} \text{M}^{-1}$). For a laser beam with a Gaussian intensity profile, the mean light intensity is given by

$$I_0 = \frac{P}{\pi \omega^2} \quad (1-2)$$

where P is the laser power (photons/s) and ω is $1/e^2$ intensity radius of the beam. The S_1 state decays with a rate ($k_f (\text{s}^{-1})$) which is the sum of all the decay processes

$$k_f = k_f^0 + k_n + k_t = 1/\tau_f \quad (1-3)$$

where τ_f is the observed fluorescence lifetime. The observed lifetime is usually quoted in the literature rather than the reciprocal of the k_f^0 , the natural radiative lifetime. The fluorescence quantum yield (Q_f) is given by

$$Q_f = k_f^0 / k_f \quad (1-4)$$

Under nonsaturating conditions, the rate of fluorescence (photons/s) from the molecule excited with a Gaussian laser intensity is

$$k_f = \sigma_a Q_f \frac{P}{\pi \omega^2} \quad (1-5)$$

Photodestruction is a process in which the molecule is permanently taken out of the fluorescence manifold; it is caused by a structural change in the molecule itself. It is often assumed that the photodestruction process takes place from the singlet state of the molecule with a first order rate constant (k_d). The quantum efficiency of this process is defined as the ratio of the photodestruction rate constant to the sum of all the singlet state decay processes

$$Q_d = k_d / k_f \quad (1-6)$$

Based on Poissonian statistics and a flowing system, Mathies *et al.* have derived an equation for the number of photons emitted (n_f) from a molecule traversing the laser volume

$$n_f = (Q_f / Q_d) \left[1 - \exp \frac{-k \tau}{k (1 + k_f / k_T + 1)} \right] \quad (1-7)$$

where k_i is the intersystem crossing rate, k_T is the triplet state decay rate, $k = k_d / k_f$, $\tau = \tau_f / \tau_d$, τ_i is the triplet state lifetime and τ_d is photodestruction lifetime. The average number of emitted photons from a given molecule prior to photodestruction is Q_f / Q_d and is usually on the order of a million photons. From equation 1-7, the maximized number of emitted photons

requires a high fluorescence quantum efficiency, a low photodestruction quantum yield and a fast overall excited state decay. In general, the important photophysics for a fluorophore is its molar absorptivity, fluorescence quantum yield and fluorescence lifetime. At the single molecule detection levels the quantum yield of photodestruction becomes important.

Of the molecules which have been detected individually, all of them possess near ideal photophysical properties favorable to fluorescence analysis. The ideal molecule must have a high fluorescence quantum yield (near unity), a large molar extinction coefficient ($> 10^5 \text{ cm}^{-1} \text{ M}^{-1}$), a fast fluorescence lifetime (ns or less) and a low probability of photobleaching. The ideal molecule for applications must have moieties that can be used to tag other molecules and a low molecular weight. Molecules that fit the ideal description for SMD are organic dyes. To the knowledge of the author, direct observation of single molecules in solution has only been achieved on organic dyes with these good photophysics.

Table 1-1 summarizes the photophysical properties of many of the dyes successfully detected on an individual level.

Background Signal Reduction

To observe the fluorescence from individual molecules, the signal from the measurement must be reduced to the shot noise limit. Noise can be generally broken down into extrinsic and intrinsic noise. Extrinsic noise is the excess noise due to nonspecific background even in the absence of the analyte. These include instrumental factors such as scatter and background emission. Intrinsic noise is the ultimate limit of a method in that it is dictated by the nature of discrete matter; for example the random emission of photons.

Sources of background photons in ultrasensitive LIF analysis include background fluorescence from the solvent, optics, contaminants and sample cell; specular scatter from areas of dramatic changes in refractive index, such as air/sample cell and sample cell/solvent interfaces; and Raman and Rayleigh scattering from the solvent and sample cell. Typically in ultrasensitive LIF, the most difficult sources of background photons to minimize are specular scatter from the interfaces and the Raman scatter from the solvent. Background fluorescence can usually be removed by using purified and well chosen solvents as well as utilizing high quality optics.

Table 1-1 Photophysical properties of dyes used in SMD

Dye	MW (g/mol)	ϵ (k cm ⁻¹ M ⁻¹)	λ_e/λ_r	Q_f	τ_f (ns)	ref
rhodamine 6G	479	105	528/550	0.45	3.5	²⁰
β -phycoerythrin	240,000	2,400	546,565/575	0.98		¹⁷
rhodamine 110	366	69	506/532		3.8	¹⁹
IR 132*	954	194	805/847	0.19	0.76	²⁰
IR 140*	779	366		~1	0.8	²¹
fluorescein	332	90	490/514	0.95		²²
sulforhodamine 101	367	87	554/583	0.35		²³
texas red	625	85	589/615			²⁴
tetramethyl rhodamine	515	80	555/580	0.15		²⁵
C-phycoyanin	104,000	700	650/660	0.68		²⁶
TOTO†	1303	115	514/533			²⁷
BODIPY†	484	97	492/515			²²
DiI†	934	148	550/565			²⁸
DiIc†	766	145	550/565			²⁹

* In methanol, † Molecular Probes trademark name

Detecting individual molecules in solution has often been compared to the metaphor of trying to find a needle in a haystack, viz an analyte molecule is engulfed by a sea of solvent molecules. A fundamental solution to such a problem is to decrease the interference of the solvent molecules on the measurement by minimizing the size of the viewing area of the solution. In this manner the haystack would be partitioned into smaller sections to more easily find the needle. Dovichi *et al.* showed, through technology borrowed from flow cytometry, that by decreasing the region probed by the laser, the ratio of fluorescence to Raman scatter increased.³⁰ In that study, feasibility calculations were performed to predict the probability of single molecule detection using LIF in a subpicoliter probe volume. It was this group at Los Alamos that brought direct observation of fluorescence bursts from individual molecules to fruition in 1990 using a 0.44 pL probe volume.³¹ The size of the probe volume has become one of the central issues in decreasing the background in single molecule detection. Probe volumes may be restricted by the size of the sample cell itself or optically by the size of the focus spot of the laser beam or the region that is imaged onto the detector. Depending on the specific technique, these methods have advantages and disadvantages as will be shown in the subsequent section on the techniques of SMD. As a rule of thumb, an upper limit on the size of the probe volume to have fluorescence dominate solvent scattering is 10 pL.³² In an aqueous system having a probe volume of 10 pL, the ratio of solvent molecules to one analyte molecule is 3.3×10^{14} .

The remaining scatter from the small probe volume can be discriminated against through temporal, spatial and spectral filtering. All SMD techniques must use some type of spectral filtering; however, temporal and spatial filtering are not necessarily required.

Spectral filtering is typically done on the detection side of the cell with interference filters with a bandpass function centered around the emission maxima of the fluorophore. These filters are used mainly because they offer high transmittance in the center of the bandpass function (~50%) and fairly large attenuation outside the bandpass (O.D.>3). Spectrometers are typically used in fluorimetry, however their throughput is much too low to be used in ultrasensitive analysis. Other means of spectral filtering includes selective attenuation of specific background photons through the use of high and low pass filters, notch filters and even atomic filters as used in the presented dissertation research. Temporal filtering is based on removing events which occur at different times from the signal. By using a pulsed laser, (with a pulse width < 1 ns) scattering events, such as Raman, Rayleigh and specular scattering which occur on the order of femtoseconds can be separated from fluorescence events which typically have lifetimes on the nanosecond scale. Synchronizing the detection electronics with the laser pulse, the fast events can be temporally separated from the fluorescence events. Finally, spatial filtering can be very useful to attenuate scattered laser radiation from the edges of the probe volume image where there are steep gradients in refractive index. Depending on the type of information desired, spatial filtering could reduce the efficiency of the measurement by limiting the viewed area of the interrogated region. Interesting combinations of filtering have been used in order to achieve SMD and will be describe in the techniques section of this chapter.

Data Reduction

One of the most important aspects of SMD is the treatment of the data. The collected

data must be able to show that molecules are being detected on an individual basis with a high degree of certainty. Prior to performing an experiment in the laboratory, the conditions in which the probability of having a single molecule in the probe region must first be determined. A first approximation of the molecule occupation probability (P_v) in the probe volume is given by ²⁰

$$P_v = C V_p N_A \quad (1-8)$$

where C is the concentration of the analyte in solution (M), V_p is the probe volume (L) and N_A is Avagadros number. This was found to be an inadequate method because the arrival of the molecules in dilute solutions occurs randomly. Equation 1-8 is thus only an average value and not the probability. The probability of n molecules occupying the probe volume must be calculated from a Poisson probability (P_v) as given by ²¹

$$P_v = \frac{(\bar{N})^n e^{-\bar{N}}}{n!} \quad (1-9)$$

where N is the average number of molecules in the probe region (P_v in eqn. 1-8). For a probe region of 1 pL and a 0.1 pM concentration, the probabilities of 0, 1, 2, and 3 molecules occupying the probe volume are 0.887, 0.106, 0.006 and ~0.000 respectively. Once the probability of double occupation in the probe volume has been minimized, signals measured above the background can be considered to be from single molecules.

Several different criteria can be used to indicate the detection of a single molecule

as it passes through a laser beam.³³

1) higher signal counts per integration time for the analyte than the blank in the histograms of the data.

2) Autocorrelation analysis of the data stream yielding a nonrandom correlation peak with a width corresponding to the molecular transit time through the laser beam.

3) Observation of bursts of photons resulting from the cycling of the molecule from the ground state to the first excited singlet state fluorescent emission upon decay.

The first two criteria are indirect methods which are useful in terms of confirming the detection of singular events and other corollary information. Observation of photon bursts in the data stream is considered to be direct observation of single molecule events.

Autocorrelation analysis is a useful tool in evaluating correlated single molecule events resulting from the molecule passing through a focussed laser beam.³⁴ Photon counting detection is used exclusively in SMD, therefore the data obtained is inherently digital. For discretely sampled data, the autocorrelation function ($G(\tau)$) can be given by

$$G(\tau) = \frac{1}{N} \sum_{t=0}^{N-1} h(t) h(t + \tau) \quad (1-10)$$

N is the number of data points in the calculation and is used to normalize the function, $h(t)$ is a data point at time (t), and $h(t + \tau)$ is a data point at a delay time (τ). The autocorrelation function is made up of a random (g_r) and nonrandom (g_m) correlations ($G(t) = g_r + g_m$). Nonrandom correlations corresponding to photon bursts from individual molecules are critical to SMD. The duration of the nonrandom correlation are indicative of the molecular

transit time across the focused laser beam. Rewriting the autocorrelation function, under the assumption of a "flat top" response of the photon burst amplitude (S) and the background counts over the integration time of the (b) at $\tau = 0$, the following relationship is obtained

$$G(t) = \frac{1}{N} \sum_{i=0}^{N-1} (S_i + b_i)^2 \quad (1-11)$$

Three different cases can be explored with regard to equation 1-11 and are shown in figure 1-3. The first case considered is when $S \ll b$ so that the signal is buried within the background and the random contribution dominates ($G(t) = g_r = (1/N)(\sum b_i^2)$). As shown in figure 1-3A, no nonrandom correlation is observed because the amplitude of the photon burst is too low compared to the background count rate. The second case is when $S \leq b$; the signal is slightly less than or equal to the background count rate (Figure 1-3b). In this case, neither random or nonrandom contribution dominates so that $G(t) = g_r + g_{nr}$ (equation 1-11). The point a on Figure 1-3B is the extrapolated point at which $G(\tau = 0) = g_r + g_{nr}$; point b is the extrapolated point $G(\tau = 0) = g_r$ and T is the molecular transit time. In the last case $S \gg b$ with the nonrandom contribution dominating and $G(t) = g_{nr} = 1/N \sum S_i^2$ (see Figure 1-3c). In this case the autocorrelation function is directly related to the square of the amplitude of the photon burst. If $S \leq b$, the number of photoelectrons detected per molecule per transit time can be obtained from the value of the autocorrelation function when it is extrapolated to $\tau = 0$. The autocorrelation function is a powerful tool in evaluating SMD data as it yields information about the transit time of the molecule, the signal-to-noise ratio (SNR) and the number of

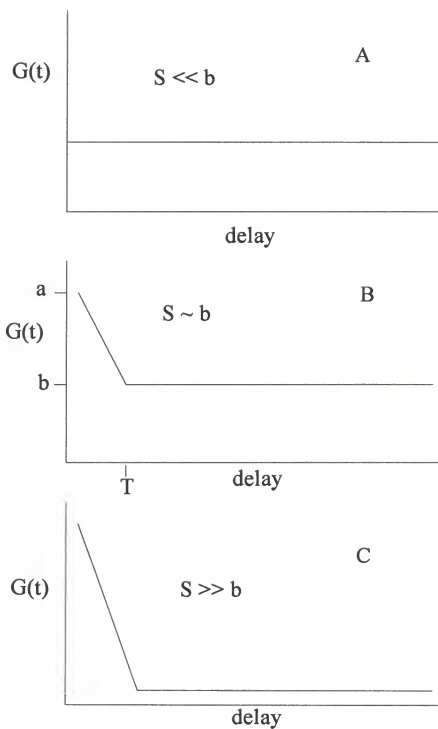


Figure 1-3 Autocorrelation function: 3 basic cases

All of the advantages of autocorrelation analysis notwithstanding, data reduction by this method is still indirect in terms of the observation of single molecules. As mentioned in the foregoing, explicit observation of photon bursts from individual molecular events is the only direct method. In many SMD techniques, the SNR is moderate at best so that visual observation of bursts is not clear. To enhance the visibility of the photon bursts, the data stream may be run through a sliding summing filter. By summing consecutive integration bins together, the nonrandom photon bursts are selectively enhanced over the random background. Many researchers have used a weighted quadratic summing (WQS) filter to enhance photon bursts.^{21,23-25} This filter is given by

$$S(t) = \sum_{\tau=0}^{k-1} w(\tau) d(t + \tau)^2 \quad (1-12)$$

where k is the number of time intervals for the transit time of the molecule, $w(t)$ is a weighting factor and $d(t + \tau)$ is the raw data point at a time $t + \tau$ (τ is a delay time usually set to the transit time of the molecule). The weighting factor ($w(t)$) describes the shape of the photon burst as the molecule traverses the beam. Gaussian, triangular, square and ramp functions have been used for this factor. Figure 1-4 shows the enhancement obtained on SMD data using the WQS filter with an asymmetric ramp weighting function ($w(t) = (\tau + 1)/k$).²¹ For such a weighting function, it has been assumed that as the molecule enters the laser beam, the signal increases slowly with an abrupt cessation due to the photodecomposition of the molecule. Statistical studies were done to evaluate various types detected photons per molecular burst.

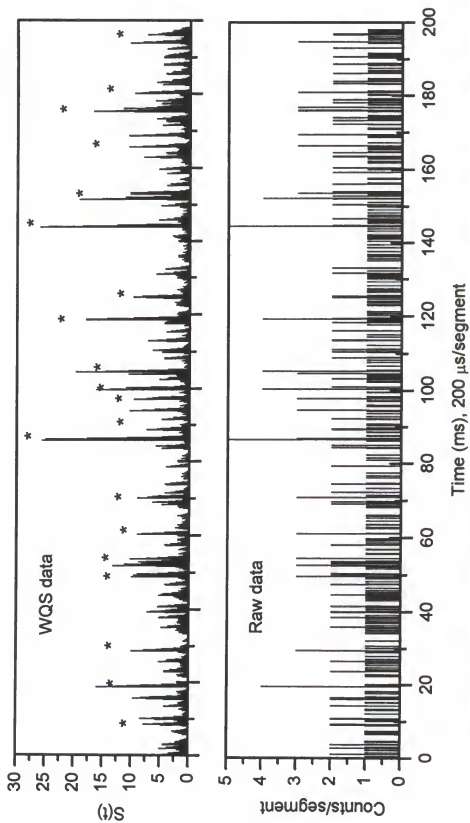


Figure 1-4 Comparison of WQS and raw data for IR140 (* represent bursts from single molecules).

of summing filters in order to reveal the type which gave the best results in terms of accuracy in identifying molecules based on their photon burst. The filter which gave the best results is a simple linear summing filter given by

$$S(t) = \sum_{\tau=0}^{k-1} d(t + \tau) \quad (1-13)$$

As can be seen in equation 1-13, the weighting factor is equal to one and the data is not squared before it is summed. Simulated data was run through different summing filters and weighting factors at fixed error rates to study how sensitivity of the measurement was enhanced. Results and discussion of this and other statistical studies of various SMD concepts will be explained in the appendix of this dissertation.

Figures of Merit

One of the most important analytical figures of merit for the detection of individual molecules by LIF is the signal-to-noise ratio (SNR). As discussed above, measurements made on single molecules are at the shot noise limiting case. Thus, the SNR is simply

$$SNR = \frac{n_f}{n_b^{1/2}} \quad (1-14)$$

where n_f is the number of fluorescent photons and n_b is the number of background photons. A simple method of increasing the SNR would be to collect more light overall because the SNR is inversely proportional to the square root of the background. A statistical approach

for the detection limit has been given by Kaiser which gives a value of k to the SNR.³⁵ Under his approach, the limit of detection (LOD) has a $k = 3$ (SNR = 3) and for the limit of guarantee of purity (LOG) $k = 6$ (SNR = 6). Figure 1-5 shows Gaussian probability distribution functions for the signal from the blank (X_b) and from the analyte (X_d) with mean values of μ_b and μ_d respectively. The value of X_d at the LOD is $3\sigma_b + X_b$ and for the LOG $X_d = 6\sigma_b + X_b$. Near the detection limit, it is assumed that the noise on the blank and the analyte is the same.^{36,37}

Both concepts of detection limit are associated with a false positive error (α) and a false negative error (β). A false negative would result if a signal was mistaken for the blank and a false positive would count a signal as an analyte when none are present. As can be seen in figure 1-5, these errors can be described as the overlap between the blank signal distribution and the analyte signal distribution. The LOD carries a low chance of false positive error ($\alpha = 0.14\%$), but has a high chance of false negatives ($\beta = 50\%$). The LOG detection limit is more conservative by definition with an $\alpha < 0.14\%$ and a $\beta = 0.14\%$. Therefore, at the LOD 50% of the analyte present will go undetected, whereas the LOG, the analyte will be detected with a 99.86% confidence level. A major goal of an SMD measurement would be to reach the LOG detection limit.

The detection efficiency has been described by Alkemade as the probability that a given species appearing in the probe volume produces an event during the transit time.^{38,39}

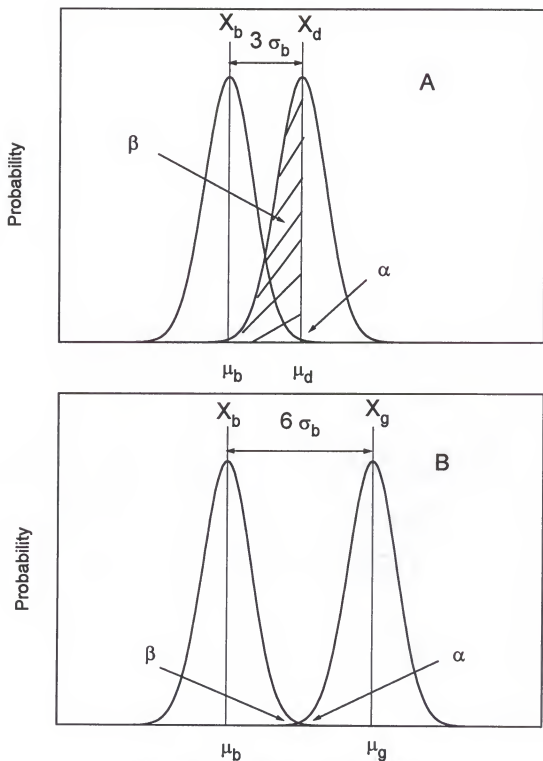


Figure 1-5 Concept of LOD (A) and LOG (B).

X_b is the background distribution, X_d is the analyte distribution at the LOD, X_g is the analyte distribution at the LOG and μ are the respective means.

Alkemade^{38,39} dealt only with cases without extrinsic noise and for cases where the transit time was determined by the pulse width of the laser or the width of the time gate. A more general approach was taken by Winefordner and Stevenson^{40,41,42} to take into account the transit time of a molecule and extrinsic noise. In their approach the detection efficiency is defined with respect to the transit time of the molecule and the need to detect the analyte over extrinsic noise. The detection efficiency (ϵ_d) is determined by the interaction of individual molecules with the laser over the measurement time (T_m) by

$$\epsilon_d = P(X_t \geq X_d) \quad (1-15)$$

where X_t is the number of counts produced by the molecule in T_m and X_d is the signal counts at the detection limit. Thus, as defined in equation 1-15, the detection efficiency is the probability that the number of counts from the analyte are greater than the number at the detection limit. With a Poissonian detection process as in SMD, the detection efficiency can be written as

$$P(X_t \geq X_d) = 1 - e^{-\phi_s \Delta t_i} \quad (1-16)$$

where ϕ_s is the mean signal flux from a molecule (cts/s) and Δt_i is the interaction time (transit time) of the molecule in the laser beam. A general definition of SMD is that the method detects all molecules interacting with the laser. Hence:

$$\epsilon_d \geq 1 - \beta \quad (1-17)$$

where, again, β is the probability of false negatives. The minimum requirement to obtain SMD by LIF with is therefore given by

$$X_t \geq X_d - X_b \quad (1-18)$$

where X_t is the required sensitivity of the measurement to detect individual molecules and X_b is the mean background flux. Table 1-2 gives the sensitivity needed to detect single molecules by LIF at different mean blank levels for both the LOD and LOG.

The overall measurement efficiency of a method is defined as the probability that a given analyte in the sample is detected above the background noise in the probe region. The relationship between the measurement efficiency, ϵ_m and the detection efficiency, ϵ_d , is given by

$$\epsilon_m = \epsilon_T \epsilon_p \epsilon_d \quad (1-19)$$

Table 1-2 Detection Limit for a single molecule detection experiment

Mean Blank, X_b (counts)	Mean Sensitivity, X_p (counts)	
	LOD = 1 molecule	LOG = 1 molecule
0.00	1	6.6
0.05	2	8.9
0.25	4	12.4
1.00	5	15
5.00	9	23
10.00	12	29
100.00	32	69

where ϵ_T is the efficiency of transporting the sample from the point of introduction and the probe region, ϵ_p is the laser probing efficiency which is the product of the spatial probing

efficiency (ϵ_d) and the temporal probing efficiency (ϵ_t). For a continuous-wave (CW) or a high repetition rate laser (where the analyte is interrogated at least once while in the probe region), the temporal probing efficiency is unity. Because ϵ_m accounts for sample loss during introduction and inefficiencies in laser probing, it may have a value less than unity even if $\epsilon_d = 100\%$. It is this point that is frequently neglected when describing how efficient an SMD technique is and when comparing different methods. Often in SMD, the spatial probing efficiency is dramatically compromised to avoid such difficulties as laser specular scatter. As will be shown, the technique presented in this dissertation is capable of achieving SMD with a *measurement* efficiency near unity.

Techniques of Single Molecule Detection

It is the intent of this section to briefly describe each of the techniques with which single molecule detection has been previously achieved. The experimental design, unique characteristics and figures of merit of each method will be discussed. Depending upon the application for SMD, each technique may have advantages over others in terms of throughput, SNR, measurement efficiency, experimental complexity, physical information and the type of sample.

Flowing Techniques

Techniques which involve flowing the analyte solution through the probe volume are unique and powerful methods. These methods are capable of detecting individual molecules

with very high throughput. A flowing technique made the seminal direct observation of photon bursts from single molecules in solution.³¹ Only a few groups have achieved SMD in a flowing stream including Mathies *et al.*,^{17,18,43} Lee *et al.*,²¹ Keller *et al.*,^{31,44,45,46,47,48,49,50} Soper *et al.*,^{24,51,52} and Davis and Li.^{53,54} The techniques used by Soper and Davis are very similar to Keller's, so there are only three basic techniques which have performed SMD in flowing streams. Mathies' approach uses epifluorescence collection, the technique by Keller's group uses a pulsed laser/time gating and hydrodynamic flow approach and our method, developed by Lee *et al.* uses CW excitation and a unique method of laser scatter rejection.

Figure 1-6 shows the experimental apparatus developed by the Los Alamos group (Keller). A good review of their work has been recently published.⁵⁵ With only minor permutations, this set up has been used for many years in most of their published literature. A pulsed laser is used as an excitation source and is focused onto the flow cell (beam waist diameter ~10-15 μm). The flow cell in most studies was a sheath flow cuvette as used in flow cytometry and in others a square capillary (250 μm on a side). In the cuvette, the sheath buffer flows at a higher rate than the analyte solution. Upon exiting the sample tube, the analyte solution is hydrodynamically focused down to a stream diameter of ~40 μm ; this helps reduce the Rayleigh scatter from the solvent. Light is collected orthogonally with a microscope objective and is spatially filtered with a pair of vertical slits, parallel to the flow axis, to attenuate laser scatter from the cell and the edges of the sheath flow. Linear flow velocities are in the range 1-10 mm/s yielding transit times on the order of a few

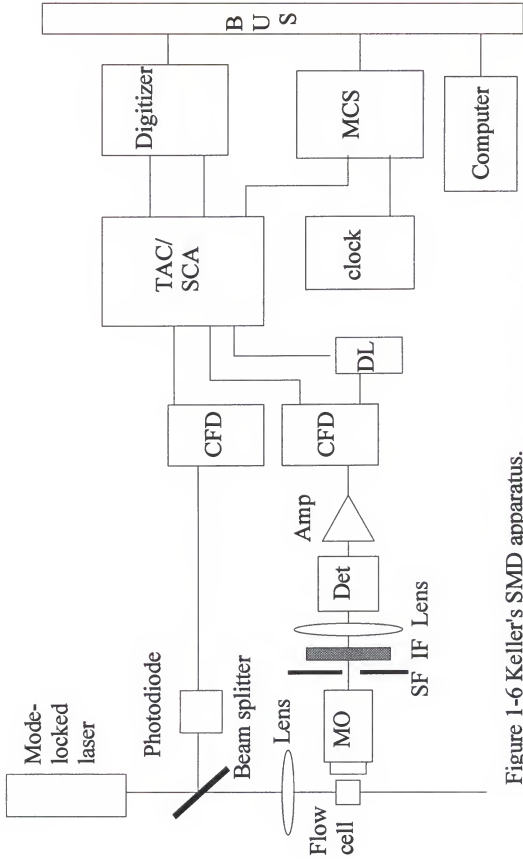


Figure 1-6 Keller's SMD apparatus.

MO = microscope objective, SF = spatial filter IF = interference filter, CFD = constant fraction discriminator, DL = delay line, TAC=time to amplitude converter, SCA = single channel analyzer, MCS = multichannel scaler

milliseconds. The probe volume is defined by the slits (optically) to be 0.3- 2 pL. Spectral filtering is done with an interference filter centered at the emission maxima of the analyte. In early studies, detectors were multichannel plates, but later to photomultipliers and finally single photon avalanche photodiodes (SPAPD) were used. With pulsed excitation and time-gated detection, much of the optically unfiltered scatter was removed electronically. Both Raman and Rayleigh scattering occurs within femtosecond of the laser pulse, while fluorescence occurs on the order of nanoseconds. Through complex electronic techniques, collection of the analyte signal from the detector was gated to discriminate against the fast scattering phenomena. Photon detection efficiencies (detected photons/emitted photons) for this method was $\sim 1\%$ which is a good value. It has been shown that the collection efficiency could be doubled by collecting light with two microscope objectives placed on each side of the flow cell.⁴⁶

One of the major disadvantages of Keller's method was that the measurement efficiency was severely compromised because of its low spatial probing efficiency (0.01-10%). Low spatial probing efficiency is caused by having a laser spot size much smaller than the stream diameter and by optically restricting the probe volume. Increased SNRs are gained by reducing the probe volume in this manner, however these come at the expense of the overall measurement efficiency. Li and Davis have addressed this problem by using an elliptical laser focus spot and small capillary (sub micron) as the exit port for the analyte solution. The elliptical laser spot allowed efficient interrogation of the sample stream. An overall measurement efficiency of $\sim 80\%$ was achieved with these modifications. Again, the optically defined probe volume precluded 100 % measurement efficiency.

Soper et al, have used the time-gated method to distinguish efficiently between two different fluorophores based on differences in their emission spectra.²⁴ They used essentially the same apparatus as shown in Figure 1-6 but they placed a dichroic mirror in the path of the collected photons with a detector at 90 and 180° to the mirror. Flowing 0.1 fM solution of the dye mixture, they were able to detect emission from rhodamine 6G (@ 550 nm) in one detector and from Texas red in the other (@ 605 nm). This was significant because it allowed the detection and identification of different individual molecules in the same solution.

Soper's group realized the advantages of working in the near-IR (NIR) and successfully detected fluorophores which excited and fluoresced at wavelengths greater than 690 nm.⁵¹ By working in the NIR, several advantages are gained 1) absorption of solvent and optical materials in the NIR was small or negligible, 2) because few compounds fluoresce in that region so that background fluorescence is very low, 3) many NIR dyes have very good photophysical properties with high molar absorptivities, large fluorescence quantum yields and are generally less susceptible to photobleaching as compared visible dyes and 4) significant reduction in Raman because the cross-sections of Raman scatter are inversely proportional to the fourth power of wavelength, so at longer wavelengths the Raman scatter is significantly reduced. Despite detecting fewer photoelectrons per molecule compared to rhodamine 6G (18 vs 39), Soper *et al* obtained a detection efficiency of 97 % for the dye IR 132 with lower error rates and a faster transit time. The improvement was attributed to being able to set a lower discriminator level with the lowered background in the NIR. Soper has also performed detailed studies on the photophysical properties of NIR

fluorophores.⁵⁷

Patonay's group have been the leaders in the development and synthesis of NIR fluorophores.^{58, 59, 60, 61} Because NIR dyes are typically larger and are fairly hydrophobic, they have not been widely applied in analytical chemistry. They have been used in applications such as detection of amino acids in CE,⁶² semiconductor laser detector for LC,⁶³ for immunoassay,⁶⁴ and in DNA sequencing.^{65, 66} As better NIR dyes are developed, the number of feasible applications will grow.

The other major technique for detecting single molecules in a flowing stream was developed in our laboratory. This method utilized an ultramicrocapillary (diameters 9-11 μm) as the sample cell and was performed in the NIR. The uniqueness of the method was that detection was performed *on-column* with 100 % laser probing efficiency. Background in this case was dominated by specular scatter from the index gradients at the capillary interfaces. Under the conditions of other techniques this scatter is overwhelming and would preclude SMD. However, Lee, et al,^{21, 67} applied a metal vapor vapor filter to attenuate scattered laser radiation reaching the detector. Figure 1-7 shows the experimental apparatus used in this work. A argon-ion laser pumped, CW, tunable Ti:sapphire laser is used as the light source. The beam from this laser was focused onto the capillary (11 μm i.d.), overfilling it with laser light, yielding a 1 pL probe volume. Mechanically defined by the inner walls of the capillary and optically by the width of the laser beam, the probe region was completely imaged using a microscope objective. Because of the optical characteristics and CW excitation, a laser probing efficiency of unity was obtained. Tuning the laser to an absorption maxima of the metal in the MVF (rubidium) at 780 nm, the scattered radiation

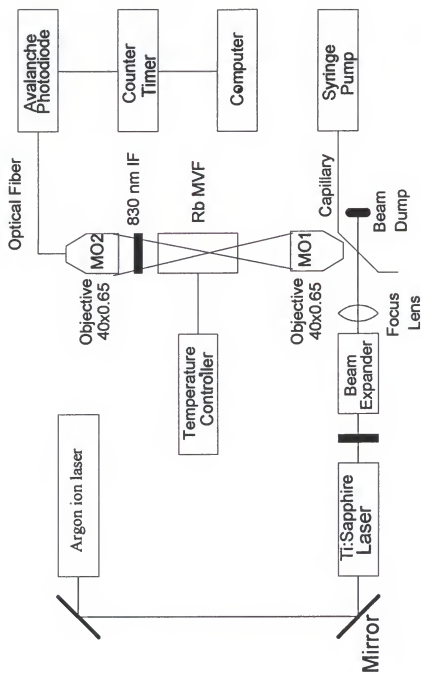


Figure 1-7 Lee's near-IR single molecule detection apparatus.

was attenuated by over 8 decades while efficiently passing the fluorescent photons from the analyte. Such a high absorption was possible because the linewidth of the laser was narrower than the absorption linewidth of the rubidium atoms. Emission was detected using SPAPD optimized for the emission wavelength. A measurement efficiency of near unity was obtained detecting the fluorophore IR 140; no other workers have achieved a measurement efficiency of unity. Transit times through the probe volume were on the order of 1 ms at a flow velocity of 1 cm/s. The number of detected electrons was lower than what Soper achieved (10 photo electrons/molecule) as a trade off for the increased measurement efficiency. However, as can be seen in comparing Figures 1-6 and 1-7, Lee's method was electronically much simpler. Furthermore, the Lee technique was amenable to separations techniques offering high efficiency for single molecule counting experiments. A more detailed description of the experimental apparatus will be given in Chapter 2 of this dissertation.

Levitated Microdroplet Technique

A completely unique method of SMD was developed by Ramsey *et al* at Oak Ridge National Lab.^{68, 69, 70, 71} This technique involved trapping and suspending a small droplet of solution in an electrodynamic trap. In this manner, a molecule contained within the droplet could be interrogated until either the molecule degraded or the droplet evaporated yielding a maximized number of emitted photons. In this case, the probe volume is defined by the size of the microdroplet. A droplet with a diameter of 12 μm has a volume of approximately 1 pL thus making SMD possible. The electrodynamic trap was very similar to the three-

electrode configured ion trap, with two end-cap electrodes above and below a horizontal ring electrode all with geometries optimized to suspend microdroplets. Windows were placed in the ring electrode for the laser, the detection optic and a window to view the droplet for centering and measurement of its diameter. An ac potential at 60 Hz was applied to the ring electrode to confine the particle, while a dc potential is applied to the end-caps to balance the force of gravity. An opening on the top end-cap electrode allowed the introduction of the drop by a piezoelectric pipet. The size of the droplet was controlled by adjusting the voltage pulse amplitude applied to the piezoelectric crystals. The droplet was charged at the exit tip of the pipet with a copper electrode held at a dc potential. To minimize evaporation, glycerol was added to the aqueous solutions of rhodamine 6G.

Molecules were excited using a CW argon ion laser focused to a spot size of 15 μm . Fluorescence was collected orthogonally to the laser and was filtered spatially with slits and spectrally with a bandpass filter. With PMT detection, a SNR up to 40 was achieved for rhodamine 6G levitated in microdroplets. Advantages of the technique were the time independency so that the maximum number of photons were obtained and the lack of diffusive losses of analyte. In later work, it was discovered that the spontaneous emission rates from molecules in the excited state could be enhanced by coupling to the resonance of the droplet: this was called cavity quantum electrodynamic (QED) enhancement.^{72, 73} In other words, when the light being emitted from the molecule has a wavelength comparable to that of its optical cavity, the decay rate may be significantly modified. As the size of the droplet was decreased down to 4 μm , the spontaneous emission rate was enhanced by a factor of 10. Despite the advantages the microdroplet technique, it suffered from slow

analysis time and low throughput. It takes 10-15 minutes for to levitate and align the droplet. A free-falling droplet method was evaluated, but its success has been very limited. Because the droplets fall at such a fast rate (1m/s), saturation of the optical transition would take a laser power of ~20 kW (beam diameter ~1.5 mm).³²

Microscopy Techniques

The fastest growing methods in the field of single molecule detection are the ones performed by different types of specialized microscopy. Proliferation of confocal microscopy techniques in the biological sciences has stimulated interest into the realm of analytical chemistry and hence SMD. Moreover, the advent of subwavelength sized light sources has manifested a natural progression of near-field optical microscopy to SMD. It is, thus, ironic that early attempts on the observation of individual molecules were made using optical microscopy.^{12, 13} The next section will cover true SMD by both far-field and near-field optical microscopy. Excluded from this review will be techniques which measure multiply labelled single molecules. These techniques include the visualization of stained individual DNA molecules,⁷⁴ individual DNA undergoing electrophoresis,^{75, 76} as well as some interesting direct observations as to the motion of DNA in solution^{77, 78} and optical mapping of genes.⁷⁹ Kabata et al have imaged single RNA polymerase molecules sliding over a DNA molecule by optical microscopy.⁸⁰

Far-Field Microscopy

Microscopy is one of the oldest and most widely used methods in the scientific community. It should come as no surprise that it has found use in the realm of detecting

individual molecules. The three general configurations of the microscope for fluorescence analysis include confocal, epi- and total internal reflectance (TIR) illumination of the sample. Hirshfield's seminal attempts at single molecule detection utilized evanescent waves generated through TIR illumination.¹² In epi-illumination, a dichroic mirror is used to reflect the laser orthogonally down into the optical axis of the microscope while passing the fluorescence up through mirror to the detector mounted on the top of the scope. The confocal arrangement involves the focusing the collected light and placing a pinhole in the image plane to reject efficiently out-of-focus signals.

Rigler and co-workers first reported the use of a confocal microscope coupled with fluorescence correlation spectroscopy to detect and study translational diffusion of individual rhodamine 6G molecules in water.^{81, 82} The basic experimental configuration for these studies is shown in Figure 1-8. A high numerical aperture (NA = 1.3) water emersion microscope objective was used to focus the laser beam to its diffraction limit with a diameter of 0.4 μm and a confocally defined image depth of 2 μm giving a probe volume of 0.2 fL. This probe volume was 1000 times smaller than any SMD technique mentioned thus far. The sample is in the form of a droplet hanging from the bottom of the objective. Collected light was filtered with an interference filter and detected with an SPAPD. With this method, detection of single rhodamine 6G molecules as they diffused in and out of the probe volume were measured in observation times of 100 μs with signal-to-noise ratios of 1000:1.⁸³ According to Rigler, autocorrelation analysis performed on the data revealed information as to the diffusion coefficient of the molecule and thus information about the behavior and dynamics of the analyte. With this method, studies involved submillisecond detection⁸⁴ and

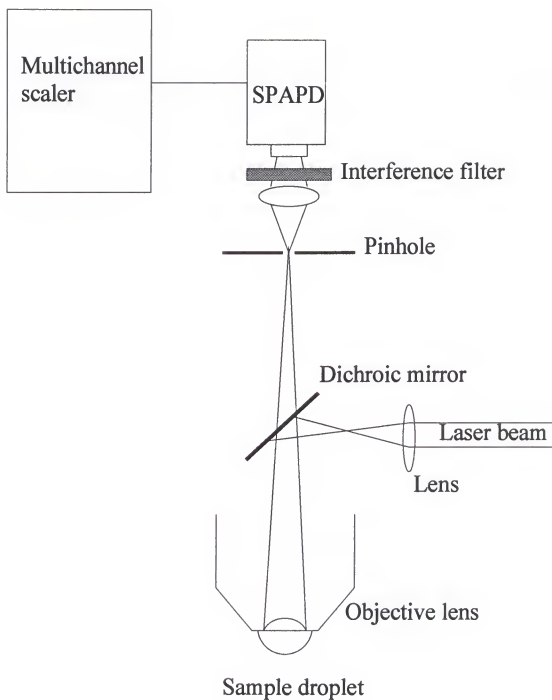


Figure 1-8 Confocal microscope for SMD

triplet state studies of rhodamine 6G.⁸⁵ Rigler *et al*, have performed hybridization analysis on 18mer deoxyribonucleotides⁸⁶ and large number screening using fluorescence correlation spectroscopy.⁸⁷

Nie and coworkers have also probed single molecules in solution using confocal fluorescence microscopy.^{88, 89} The experimental apparatus was very similar to the one used by Rigler as shown in figure 1-8, with some minor changes. Instead of a hanging droplet, samples were present as films of solution placed between a microscope slide and a cover slip to prevent sample evaporation. Furthermore, Nie used an oil emersion objective (NA = 1.3) to focus the laser onto the sample and collect the emitted photons. An improved version of the SPAPD was also used. The probe volume was determined by the diffraction limited focus of the laser was 0.5 fL. In this configuration, ~20 % of the emitted fluorescent photons were collected. Accounting for all instrumental efficiencies, the overall detection efficiency for the system was ~ 1 %. Observation of a single molecule was achieved in real time without the aid of any statistical or correlation analysis. A strong statement made by Nie suggested that Rigler's correlation studies could not make measurements on molecular dynamics and behavior because autocorrelation analysis was statistical by nature.⁸⁹ Dark segments in the data correlated well with the triplet state lifetimes of the analyzed dyes and was confirmed through computer simulations. This work was the first direct observation of diffusing molecules within the probe volume with measurements made on the triplet state.⁸⁹ The versatility of the technique was shown as SMD was achieved with many probes including fluorescein, tetramethyl rhodamine, carbocyanines, boradipyrromethane dyes as well as labeled proteins, nucleotides and DNA primers.⁸⁸

Recently, time-resolved imaging was achieved on single lipid molecules as they diffused through phospholipid membranes.⁹⁰ To do this, epifluorescence microscopy, laser excitation and a cooled charge-coupled device with millisecond time resolution were used. Diffraction limited spatial resolution of the measurements was determined by the width of the peaks of single molecule fluorescence at $0.14 \mu\text{m}^2$. Liquid bilayers were deposited onto a glass substrate using Langmuir-Blodgett techniques. Doped into the lipid bilayers were fluorescently labeled lipids (TRITC-DHPE, Molecular Probes) at concentrations from 0.01 to 1000 dye molecules per μm^2 . In this study, they were able to image the random diffusion of the tagged lipids in two dimensions with a SNR of 20. Small diffusional steps of the lipids in the membrane could be resolved with 30 nm precision. This research could have a major impact on the studies of processes occurring in membranes, specifically the surfaces of living cells.⁹⁰

Near-field microscopy

In near-field optical microscopy (NFOM), sub-wavelength apertures are used to break the diffraction limit of light to provide a nanometer sized light source. These optical probes are very useful in terms of imaging surfaces because they can obtain shear-force and fluorescence information simultaneously.⁹¹ Single molecule detection has been achieved by several researchers with NFOM.^{92, 93, 94} However, thus far the technique has only been used for detecting single molecules which are adsorbed onto surfaces and not in solution. For this reason, discussion of SMD by NFOM is beyond the scope of this review. Some interesting studies on detecting individual molecules using NFOM include imaging single proteins,²⁶ measuring fluorescence lifetimes,⁹⁵ and even on how to construct a NFOM apparatus.⁹⁶

Kopellman and Tan have suggested the use of NFOM to detect single molecules in vivo but this has to yet to come to fruition.⁹¹

Applications

Probably the most well known application of single molecule detection is the proposed method of DNA sequencing put forth by Keller's group at Los Alamos National Laboratory. This has been the central theme and the driving force from which their SMD technique developed. Since they first indirectly detected fluorescence from single molecules in 1987, much of their research has been on sequencing DNA bases on an individual basis. Their proposed technique involved attaching a single strand of DNA to a latex bead, placing the strand in a flowing stream while holding the bead, sequentially cleaving individual bases through the action of an exonuclease and then detecting the fluorescence of the bases individually as they pass through a focussed laser beam.⁹⁷ Achievement of attaching the bead to the strand and placing it in the flowing stream came early.⁹⁸ Suitable exonucleases were able to achieve significant cleavage rates with tagged nucleotides.⁹⁹ Progress on detection of single molecules developed as mentioned previously.^{24, 31-33} Because of difficulties in obtaining fast, robust exonucleases and problems with spatial probing efficiency, among others, their goal has yet to be realized. They have successfully applied their technology to detect and size multiply tagged single strands of DNA.¹⁰⁰ By placing a second detector downstream from the first they were able to detect single molecules, undergoing electroosmotic flow, sequentially in two channels.^{100, 101} In this manner, the electroosmotic velocity can be measured for individual molecules.

One of the more interesting applications of SMD is the imaging the turnover of ATP molecules by single myosin molecules in aqueous solution.¹⁰² Funatsu and coworkers used both epifluorescence and total internal reflectance fluorescence microscopies to observe individual ATP reactions in free solution. Detection was done with a CCD camera collecting data at a video rate of 1/30 s. Single-headed myosin subfragments were tagged with Cy5 and fixed onto a quartz slide. The ATP turnover events were detected by directly observing association-(hydrolysis) dissociation of the fluorescent ATP analogue labeled with Cy3. This research could have significant impact on the fundamental problem of how mechanical reaction in muscle tissue is coupled to ATPase reaction. There have not been many applications of single molecule detection to date because the field is still young and most techniques have been instrumentally intensive. It has been said that because equipment is inexpensive and readily available, that far-field microscopy techniques will bring routine SMD analysis to many laboratories.⁸⁷

CHAPTER TWO EXPERIMENTAL

Introduction

The apparatus and procedures for detecting single molecules sequentially in two probe regions by laser-induced fluorescence (LIF) are described in detail. As mentioned in the foregoing chapter, this method of direct detection of photon bursts from single molecules in solution utilizes a unique filter to reject specular laser scatter. Selective spectral attenuation of resonant laser radiation allows *on-column* analysis of single molecules in real time with high efficiency. This chapter gives descriptions and considerations of individual components of the experimental system, the chosen fluorophore and solvent system, as well as experimental procedures.

Description of Apparatus

General Experimental Apparatus

Figure 2-1 is a graphical representation of the single molecule detection (SMD) apparatus used in this research and should be referred to throughout the course of this chapter. The system is made up of three main parts: 1. the light source, 2. the sample cell, and 3. the detection scheme. The light source is a solid-state titanium:sapphire laser pumped using an argon ion laser. Broadband radiation is attenuated from the Ti:sapphire

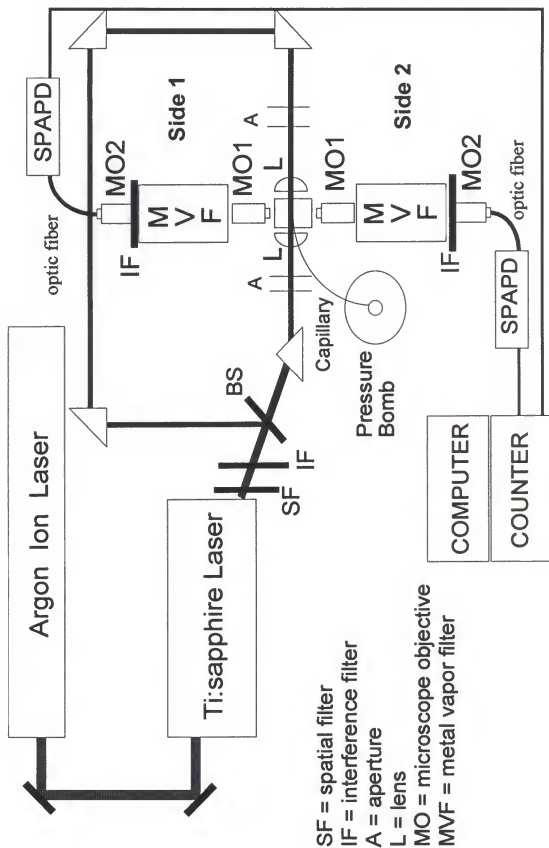


Figure 2-1 Experimental SMD Apparatus

laser beam using a narrow pass interference filter. The beam is then split using a 50/50 beam splitter and guided to the capillary with orthogonal prisms. High quality singlet lenses focus the laser light onto the fused-silica microcapillary. Sample introduction is achieved by pumping the solution through a capillary flow cell by gas pressure from a pressure bomb. Scatter and fluorescence is collected orthogonally to the capillary with a microscope objective and photons passed through a metal vapor filter to attenuate selectively the laser-resonant scattered photons while transmitting all others. These photons are then passed through an interference filter centered around the emission maximum of the fluorophore. This light is coupled to a fiber optic using a microscope objective. The fiber optic is connected to a sensitive avalanche photo diode where the photons are detected. Photons are converted to digital electrical pulses which are counted using a computer. Under optimized conditions of sample concentration, optical alignment, solution flow rate and photon counting rate; fluorescent bursts from single molecules can be observed. The following discussion will elucidate the type and function of individual components of the apparatus and how they work in unison to detect single molecules.

Light source

The approach utilized in this research calls for very strict requirements on the laser light source in terms of its spectral bandwidth, irradiance, spatial intensity, tunability and range of frequencies. As mentioned previously the source is a Ti:sapphire laser (Schwartz Electro-Optics, Orlando, FL) pumped with the all-lines output from an argon ion laser (model 2060, Spectra Physics, Mountain View, CA). The Ti:sapphire laser operates as a

continuous-wave source, in TEM₀₀ and can operate in a standing wave or ring configuration. The diameter of the exit beam was measured by translating a razor blade across the beam using a microtranslational stage and monitoring the power of the beam with a photodiode (Figure 2-2). A first derivative of this curve yields the size and shape of the laser beam (Figure 2-3). With this method the $1/e^2$ diameter of the laser beam was determined to be 1 mm. It is important to have an accurate measurement of the beam diameter to estimate the probe volume in the capillary which is in part due to the spot size achieved by the lens focusing onto the capillary. By operating in the ring configuration (see figure 2-4), the intracavity lasing is unidirectional and a very narrow spectral bandwidth is achieved (< 40 MHz, FWHM) which, as will be shown, is very important to the method of single molecule detection reported here. This configuration sacrifices some laser power as compared to the standing-wave configuration. With 3 sets of mirrors, the tunability of the laser spans from the red at 700 nm to the near-infrared (NIR) at 1020 nm. Course tuning of the wavelength is achieved by adjusting the angle of the intracavity birefringent filter while fine tuning is done by manipulating the tilt on the intracavity Fabry-Perot etalon. The laser has a conversion efficiency of approximately 10%, so at an argon ion laser power of 7.5 W, the Ti:sapphire laser output is approximately 750 mW.

Immediately after the Ti:sapphire beam exits the laser, it passes through a spatial filter (an adjustable iris) and a narrow band interference filter ($\Delta\lambda = 0.18$ nm FWHM, Corion, Holliston, MA). Broadband emission exits the laser coaxial to the beam. Stimulated emission from the Ti:sapphire crystal as well as leakage of argon ion lines contribute to the broadband emission. Spatial filtering aids in the attenuation of the unwanted emission by

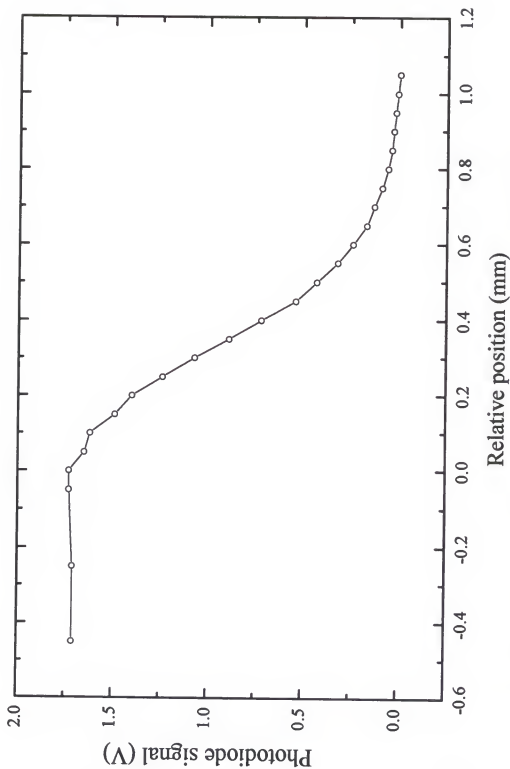


Figure 2-2 Measurement of laser beam by razor blade method

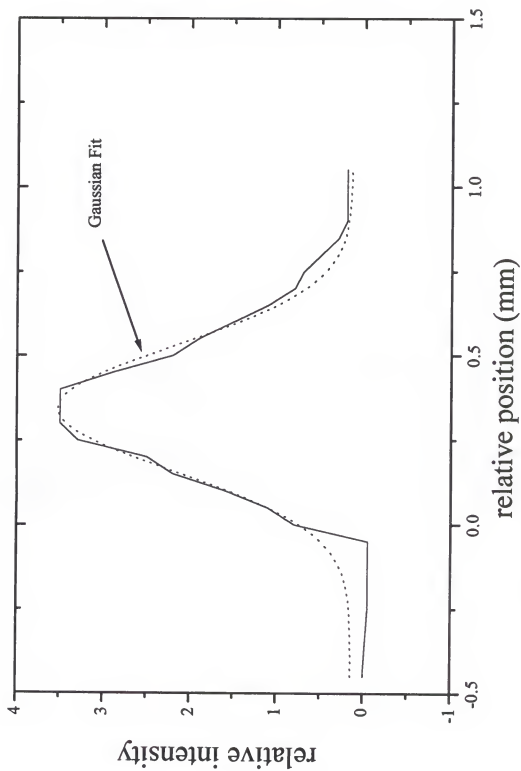


Figure 2-3 Width and shape of Ti:sapphire laserbeam

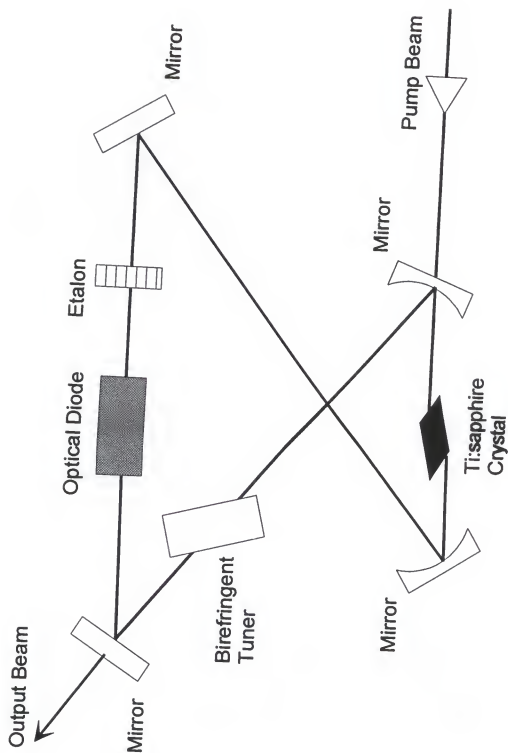


Figure 2-4 Ti:sapphire cavity in ring configuration

physically blocking the broadband photons on the outer portion of the beam. Attenuation of the broadband emission within the cross-section of the laser beam is accomplished with the narrow band interference filter. Upon exiting the interference filter, the beam is split using a 50/50 beam splitter optimized for near-infrared use (Melles Griot, Irvine, CA). The beam is then guided to the capillary using standard orthogonal prisms. The beam which passes through the beam splitter is beam 1 and propagates on the same plane (height) as the beam which exits the laser. Beam 2, the beam which is orthogonally reflected by the splitter, is raised in height by the three turning prisms. In this manner, the beams will be at different heights when they arrive at the capillary. Antireflective plano-convex singlet lenses (CVI Laser Optics, Orlando, FL) were used to focus the laser beams onto the capillary. At the excitation wavelength of 780 nm and a nominal beam diameter of 1 mm, these lenses are capable of focusing the beam down to a waist size of 6 μm . The high spatial coherence typical of CW lasers as used here allows the production of a beam-center irradiance in a tight focus permitting optical saturation of the fluorescence transition of the analyte. Each lens holder is mounted on a high precision x-y microtranslation stage (461-XY-M, Newport, Irvine, CA). With these stages, the lens focus and translation across the capillary can be manipulated with a precision of <0.0001 mm. This stage allows very accurate manipulation of the laser focus on the capillary as well as stable low vibration mounting of the lens.

Capillary Flow Cell and Sample Introduction

A principle facet of this SMD technique is to analyze liquid samples in a flowing stream. This is a main goal because a flowing technique would be amenable to methods

such as flow injection and separations which are high throughput by nature. A fused silica micro capillary (i.d. 9 μm , o.d. 150 μm , nominal, Polymicro Inc. Phoenix, AZ) was used in this work. A capillary was chosen for several reasons: 1. it is an experimentally simple method (especially compared to methods such as the sheath flow cuvette), 2. the efficiency of transporting the sample to the interrogation region is very high ($\epsilon_T = 1$), 3. the small inner diameter of the capillary limits the analyte to a small volume allowing high spatial probing efficiency ($\epsilon_s = 1$) and small probe volumes, 4. solutions could be flowed through the capillary by either pressure-induced or electroosmotic flow and 5. would make the system amenable to separations techniques such as capillary electrophoresis (CE) and microcolumn liquid chromatography (LC).

Fused-silica capillaries are typically coated with a polyimide layer to increase the flexibility of the capillary while decreasing the amount of breakage. To allow *on-column* optical detection, an optical window on the capillary must be made by removing a segment of the polyimide coating. This can be accomplished in several ways: 1. mechanically scraping the coating off, 2. burning the coating off with a flame or 3. chemically removing the coating with a strong acid. The first method is one not widely used because of its difficulty and incomplete removal of the coating. The other two methods are used more widely. In this research, the window was prepared by chemically removing the coating by placing the desired window portion of the capillary into a bath of hot sulfuric acid. This dissolved the polyimide coating yielding an optically clear, smooth silica surface with a much lowered chance of thermal distortion of the capillary compared to the flame method. Maintaining the geometrical integrity of the capillary is important in defining the probe

volume and ensuring a good optical image for the collection of fluorescence photons.

To minimize the noise in the signal, the capillary must be held rigidly to limit the amount of vibration it experiences. Vibration in the capillary caused spatial changes in intensity of laser light within the capillary inner diameter causing fluctuations in the observed signal. Thus, to prevent undesirable vibration, the capillary was held taut within an in-house constructed capillary holder (see Figure 2-5). The holder must be able to hold the capillary tight vertically while allowing all of the excitation and collection optics to be positioned in spatial proximity to the capillary. The construction shown in Figure 2-5 was successful in achieving this goal. This capillary holder assembly was shown to hold the capillary very rigidly allowing quiescent fluorescence measurements to be made.

In contrast to previous work on this project,^{21,67} analyte solutions were forced through the capillary by the means of a pressure pump and not by a syringe pump. In this work, it was found that the flow rate induced by the syringe pump was frequently lower than the calibrated value and when the flow was at the calibrated amount it took a long time (> 1 hour) to obtain the desired rate and obtain stable flow. This was attributed to the high back pressure experienced while flowing solutions through such a small capillary. These difficulties were overcome by using a pressure pump. The pressure pump (also known as a bomb) is a stainless steel vessel with a pressurized bore in which a solution vial can be placed. The capillary is placed into the bomb through the cap and immersed into the solution. Advantages of a pressure pump over syringe type are that the flow generated is free from pulses and mechanical noise and much larger reservoir volumes (> 1000 fold for the syringes used previously) can be used resulting in less frequent replenishment of the analyte solution.

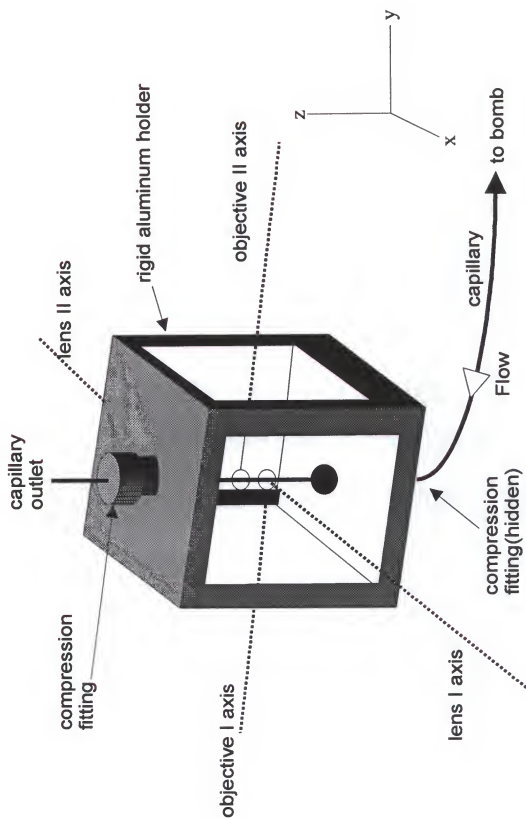


Figure 2-5 Capillary holder and optical configuration

The pressure-induced average linear flow velocity ($\langle v \rangle$) of a solution in a capillary is described by

$$\langle v \rangle = \frac{\Delta p r_c^2}{8 L \eta} \quad (2-1)$$

where Δp is the pressure drop across the capillary ($p_{in} - p_{out}$), r_c is the radius of the inside of the capillary, L is the length of the capillary and η is the viscosity of the solution [Giddings]. Given the specifications of the capillary ($r_c = 5 \mu\text{m}$ and $L = 25 \text{ cm}$) and the viscosity of the solution (methanol $\eta_{25} = 0.55 \text{ cp}$)¹⁰³ the average linear velocity of the solution at various pressures can be calculated (see table 2-1). This value is only an average because the flow profile in the capillary is parabolic; which will become important in the discussion of the single molecule data. Deviations from the calculated velocity observed experimentally may be attributed to error in the diameter of the capillary ($\pm 1 \mu\text{m}$ for a $9 \mu\text{m}$ capillary) and to temperature fluctuations effecting the viscosity of the solution. A unique method of measuring the linear velocity of the solution was devised and will be discussed in chapter 5. In future studies, the solution will flow through the capillary by means of an electric field inducing electroosmotic flow (EOF). EOF has a plug shaped profile which will provide a more uniform linear flow velocity of the molecules. To make use of EOF, buffer systems will have to be designed and optimized to meet the needs of the SMD experiment.

Table 2-1 Calculated linear flow rates

Pressure (psi)	Calculated linear velocity (cm/s)*
50	0.0048
100	1.18
200	2.55
400	5.32
600	8.08
800	10.8
1000	13.6

* For a 9 μm capillary and a dilute methanolic solution at 25 $^{\circ}\text{C}$

Detection Scheme

In order to obtain the maximum number of fluorescent signal, all light was orthogonally collected from the capillary using an achromat microscope objective (40X, 0.65 NA, Melles Griot, Irvine, CA). Collected light was collimated by the objective and passed through the rest of the detection apparatus. The light collected consisted of analyte fluorescence photons, specular scatter from the air-capillary and capillary-solution interfaces, Raman scatter from the capillary fused-silica and the solvent, as well as background fluorescence from impurities in the solvent. In order to observe fluorescence bursts from single molecules, radiation from the other sources must be efficiently filtered out. The major contributor to the background in the measurement is, by far, the specular scatter from the capillary interfaces. It is this limitation that usually precludes spatially

efficient, *on-column*, ultrasensitive LIF detection. In work done by Lee *et al.*,²¹ a unique metal vapor filter was devised to attenuate selectively the laser-resonant photons while allowing efficient transmission of fluorescent photons from a single fluorophore.

Metal Vapor Filter

As can be seen in Figure 2-1, a metal vapor filter (MVF) is placed between the capillary and the detector. In principle, the metal vapor filter acts as a notch-filter to attenuate selectively the scattered laser radiation while efficiently transmitting all other photons. As in many laser-based analytical techniques, such as Raman and LIF spectroscopies, the main contributor to the background signal is scattered laser radiation. By placing a saturated atomic vapor between the sample and the detector and tuning the laser to a strong electronic transition of the vapor, the laser scatter reaching the detector will be significantly attenuated. This technique is based on atomic absorption where the fraction of light absorbed by the filter is dependent upon, among other parameters, the number density of the gaseous metal atoms as well as the path length of the light. In terms of using such a system as a spectral filter, a high number density of atoms and a long path length would be desired to absorb the laser photons. Ideally, for most efficient absorption, the spectral bandwidth of the laser ($\Delta \nu_l$) should be less than the width of the atomic transition ($\Delta \nu_a$). Because atomic transitions are spectrally narrow ($\sim \text{pm}$) the laser must be spectrally more narrow in order to obtain strong absorption by the atomic vapor. To minimize resonance fluorescence of the excited atoms and broaden the atomic transition, a quenching buffer gas is used for the atmosphere for the metal vapor. Collisions with the buffer gas, typically

molecular nitrogen, cause non-radiational deexcitation of the excited metal atoms minimizing the atomic fluorescence of the same wavelength. Detailed theoretical and empirical studies performed to investigate the behavior of the metal vapor filter are presented in chapter 3.

The configuration of the rubidium metal vapor filter assembly used in this work is shown in figure 2-6. The metal vapor filter consisted of cylindrical quartz cell and a heating chamber in which the cell is placed. Commercial rubidium metal vapor cells (Ophos, Rockville, MD) were used in this research. These cells are simply quartz cylindrical cells (2.5 cm diameter, 10 cm length) with parallel quartz windows bonded onto the ends. Construction of the cells includes distilling an excess of rubidium metal (500 mg) into the evacuated cylinder such that sufficient metal would be present to give a saturated vapor at the temperatures used in this work (110-150 °C). Nitrogen fill gas at pressures of 100, 200 and 500 Torr, were used as the buffer gas to quench the resonance fluorescence and broaden the absorption line of the rubidium atoms. The rubidium cell was placed into a specially configured differential heater. The heater was a cylindrical aluminum body which was internally threaded so the cell could be suspended with collars within the body. The cell was heated by hot flowing nitrogen which was warmed using a furnace (Lindberg, Watertown, WI) before entering into the MVF assembly. Heating tape was wrapped around the outside of the MVF device body to allow fairly high temperatures (>140 °C) to be achieved and maintained. As can be seen in figure 2-6, the cell is heated differentially by flowing the hot nitrogen across the ends of the cell first and then recirculated past the cell center. By heating in this manner, the windows on the cell are kept at a higher temperature than the center. This

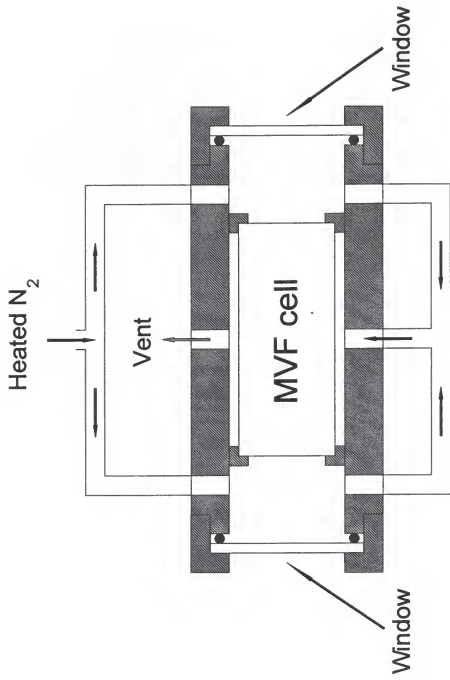


Figure 2-6 Metal vapor filter assembly

prevented the rubidium vapor from condensing onto the windows which reduced the signal throughput and the transmittance of the MVF. If the cell was heated in a spatially equal manner, the rubidium metal would condense on the windows, significantly decreasing the throughput of the filter.

Rubidium was chosen as the absorbing element in the MVF because it is volatile and has strong ground state electronic transitions in the near-IR. To obtain optically thick conditions for the MVF a saturated vapor of the rubidium must be produced. Vapor pressures of rubidium have been measured experimentally¹⁰⁴ and can be described by

$$\log (p) = -\frac{A}{T} - B \log (T) + C + D T \quad (2-2)$$

where p is the vapor pressure of rubidium, T is the absolute temperature and A , B , C and D are empirical values of 4529.6, 2.911, 15.8825 and 0.0059 respectively. The number density (cm^{-3}) of rubidium can be estimated by

$$\log (n) = -\frac{A}{T} - (B + 1) \log (T) + C + D T + 18.985 \quad (2-3)$$

where n is the number density of rubidium at the given absolute temperature T . The empirical constants A , B , C , and D are the same as given previously. A plot of the number density of rubidium atoms as a function of temperature is given in Figure 2-7. As can be seen in Figure 2-7, a large number density of rubidium atoms can be obtained using the temperature range used in this work. Rubidium has ground state transitions which can be

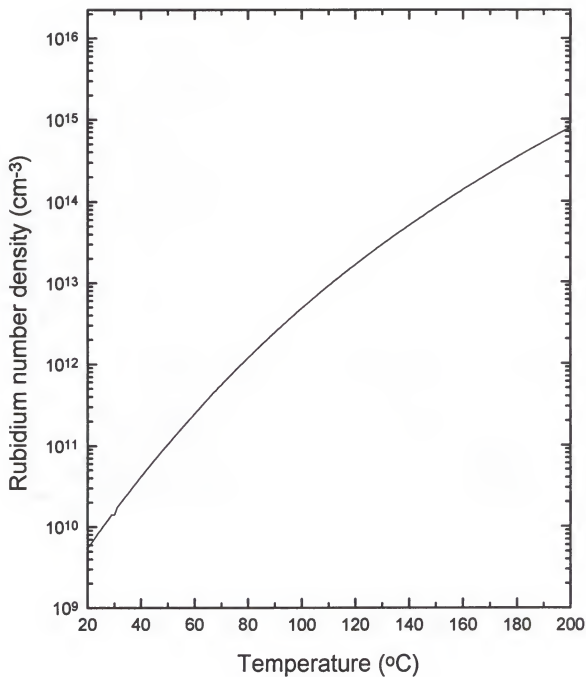


Figure 2-7 Theoretical rubidium number density

excited by the Ti:sapphire laser at 780.02 ($5^2P_{3/2}$) and 794.76 nm ($5^2P_{1/2}$). While both transitions are strong, the 780.02 transition was chosen as the absorption transition because it would give a larger Stoke's shift from the emission maxima from the IR 140 fluorophore. Using the specifications of this laser and MVF with a nitrogen buffer gas pressure of 200 Torr, the absorption of the laser by the filter has been theoretically calculated to be > 1000 . However, in practice, this high absorption is not obtained and will be discussed in the third Chapter.

Photon Detection and Data Acquisition

Before the photons exiting the metal vapor filter were sent to the detector they were passed through an interference filter ($\lambda_{center}=830\pm10$ nm, Melles Griot, Irvine, CA) with the transmission centered at the fluorescence maxima of the fluorophore. At 830 nm, the measured transmission of the filters was $\sim 25\%$ for detector 1 and $\sim 45\%$ for detector 2. This filter attenuated photons which were not blocked by the Rb-MVF and not in the interference filter bandpass. Such photons are unabsorbed laser light, Raman scatter from the fused silica capillary (464 cm^{-1}) or the methanol solvent (1055 cm^{-1} , among others) and fluorescence from solvent impurities. Although all unwanted photons cannot be eliminated with this interference filter, this filter was efficient enough to allow SMD.

A detector utilized in ultrasensitive LIF analysis must have a high quantum efficiency at the wavelength of interest, a low dark count rate, single photon detection sensitivity and a fast response time. The photodetector utilized in the present research was an extremely sensitive single photon avalanche photodiode (SPAPD). SPAPD's are solid

state photon detectors which have become very popular in detecting low levels of light because of their excellent detection characteristics as mentioned in the foregoing, but also due to their ease of use. The specifications of the detectors used in this research (SPCM-200-PQ, EG&G, Canada) are presented in Table 2-2. SPAPD's are essentially self-contained modules which can detect photons having any wavelength between 400 - 1060 nm with sensitivity better than or equal to that of a photomultiplier tube (PMT) and with linearity over 6 orders of magnitude. The detector module houses a square silicone avalanche photodiode which is 200 μm in diameter with the inner 150 μm being the most sensitive. Therefore, the fluorescence radiation must be focused onto the surface to be accurately detected. The small active area aids in the reduction of dark counts and helps to minimize background due to stray light.

A circuit internal to the SPAPD translates the electrons, cascaded by the avalanche photodiode, to digital TTL pulses. These pulses have an amplitude of ~ 2 V and a duration of ~ 180 ns. The dead time of the detector listed in table 2-2 is the amount of time that the detector needs to reset its circuit in order to count another photon. This dead time limits the detection rate at to the low MHz range as indicated by the output saturation of the detector. Because low light levels were detected and the fluorescence measurements were shot noise limited, detection was performed in the photon counting mode. By collecting data in this mode, a SNR advantage can be gained. In addition, the photon counting mode is less susceptible to $1/f$ noise and slow drifts in the dc offset levels and gains made in the SPAPD. Moreover, by photon counting, bursts from individual molecules can be observed directly and in real time.

Table 2-2 Specifications of the SPCM-200-PQ avalanche photodiode

Electrical Characteristics	Minimum	Typical	Maximum
Supply Voltage Required: +12 @0.08A max +5 @1.3 A max -5 @ 0.02 A max	11.9 V 4.9 V -4.9 V	12.0 V 5.0 V -5.0 V	12.1 V 5.1 V -5.0 V
Supply Voltage Ripple	-	-	50 mV
Case Operating Temperature	5 °C	-	40 °C
Photon Detection Efficiency $\lambda = 1060$ nm $\lambda = 830$ nm $\lambda = 633$ nm $\lambda = 400$ nm	- 25 % 40 % -	1.3 % 32 % 46 % 15%	- - - -
Dark Count (counts/s)	1-3	≤ 25	100
Dead Time	-	200 ns	-
Output Count Before Saturation (counts/s)	1.3×10^6	1.8×10^6	-
Threshold For Digital Output Pulse	0.5 V	1.0 V	1.5 V

To perform photon counting, the TTL pulses were counted and binned using a counter/timer module (CTM05, Keithly Metrabyte, Taunton, MA). The counter/timer was in the configuration of a computer interface board and was housed in a 486-66 MHz PC. It has an on-board 1 MHz crystal oscillator which is used as the time base. Software to control the data collection from the board was written in-house in the language of Quick Basic® (Microsoft). The program was written to work in unison with the interrupts of the computer so that there was no dead time between counting bins ensuring that all TTL pulses were counted over the course of the chosen integration time.

The counter board was calibrated to ensure that the number of pulses counted by the

computer program were accurate and to test that both channels were counting synchronously. Digital TTL output pulses from the detector were simulated using a pulse generator (HP3325A, Hewlett Packard), shaped with a pulse generator (PG501, Techtronix, Beaverton, OR) and monitored with a digital storage oscilloscope (TDS 620A, Techtronix, Beaverton, OR). The generated pulse signal was split and sent to the channel one and channel two inputs. The output of the computer program was studied as a function of the interrupt rate, the number of bins and the TTL pulse rate. The interrupt rate is the inverse of the bin integration time. Theoretical counts per bin were calculated by multiplying the bin width (s) by the TTL pulse rate (Hz); e.g. $200 \mu\text{s bin} \times 1 \text{ MHz pulse rate} = 200 \text{ counts/bin}$.

The results of the counter board calibration as a function of interrupt rate (bin width) for channel one are shown in figure 2-8. At a TTL pulse rate of 3 Mhz, 1000 bins were collected and repeated two times to obtain each on Figure 2-8. The precision for each data point and between detectors was less than 1 % for this and all calibration measurements. Because the bin to bin precision of measurement between channels 1 and 2 was less than 1 %, it was concluded that the channels were being counted synchronously. Ideally, the ratio of the measured count to theoretical counts should be unity in each instance. From Figure 2-8 the ratio value, for each interrupt rate had an error of less than 5 %. It is postulated that the deviation from unity for certain interrupt values is caused by an inherent error of the counter board. The interrupt rate is obtained from dividing whole numbers into the 1 MHz base frequency of the on-board oscillator. Thus, the interrupt rates which are not integer fractions of this base rate are in error by a small percent. Upon inspection of Figure 2-8, it

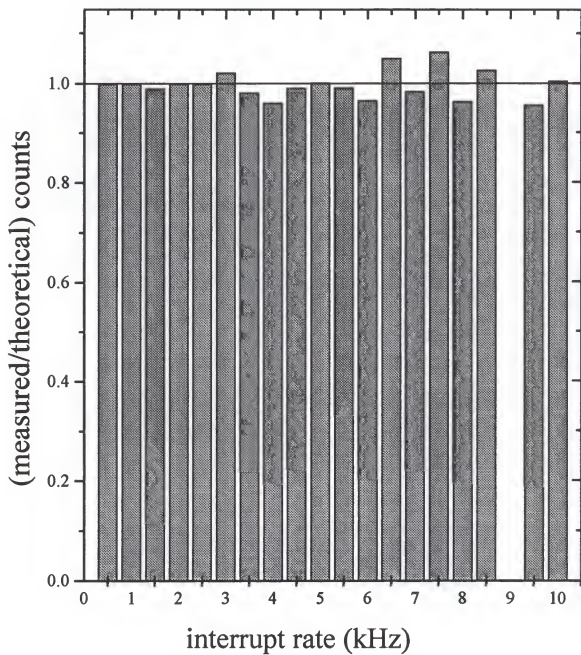


Figure 2-8 Interrupt calibration of counter board

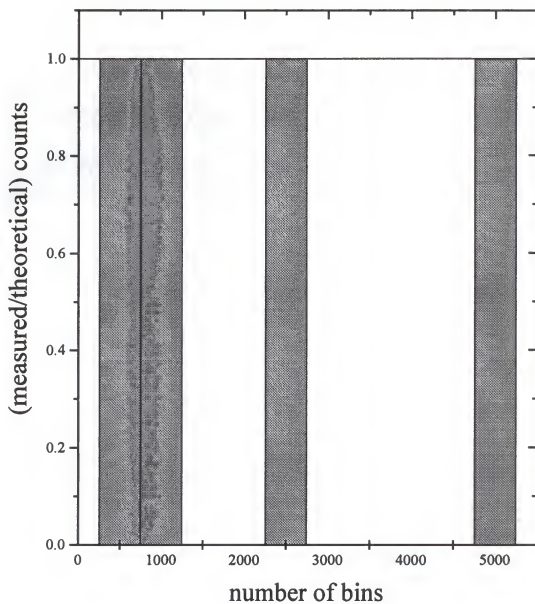


Figure 2-9 Bin number calibration of counter board

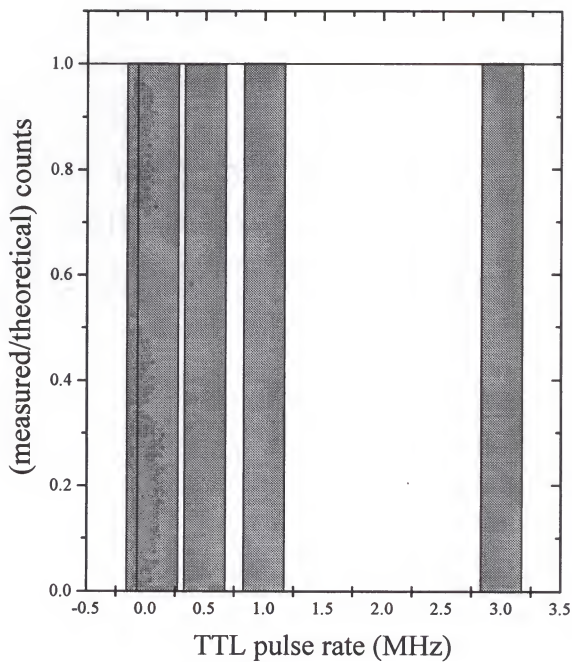


Figure 2-10 Pulse rate calibration of counter board

can be seen that interrupt rates which were not an integer division of 1 Mhz. This confirmed that the error in count accuracy was an inherent property of the counter board. Figures 2-9 and 2-10 are calibration plots as a function of the number of bins counted and TTL pulse rate respectively. A TTL pulse rate of 1 MHz and an interrupt rate of 5 kHz was used for Figure 2-9. An interrupt rate of 5 kHz and 1000 bins were collected for the results in Figure 2-10. From these and previous calibration results it was surmised that an interrupt rate of 5 kHz would be optimal value to work with in SMD experiments.

Optical Alignment

Good optical alignment of the described single molecule detection apparatus was an extremely important in achieving the sensitivity needed to observe fluorescent events from individual fluorophores. Furthermore, alignment procedures for this research are presented because they differ significantly from the previous project.^{21,67} Changes in the focusing optics as well as the added complexity of a second detection channel have warranted new alignment procedures. In this section, a detailed description is given of the optical alignment protocol which was followed to obtain well defined probe regions within the capillary to achieve SMD sensitivity.

Careful optical alignment was performed daily to ensure optimal conditions and good day-to-day precision of fluorescent measurements. Figure 2-1 will serve as a reference for the following general protocol while more detailed figures will be presented to clarify visual images used in the alignment. Throughout the alignment, the laser power was ~300 mW and methanol was flowing through the capillary to prevent thermal damage caused by the laser.

The initial step in the procedure was to adjust the turning prisms so that the laser beam runs parallel to the optical table and centered on the apertures on both sides of the capillary holder. The apertures are on a linear plane normal to the optical table but differ in height by a value $\Delta z = 5$ (refer back to Figure 2-5). Laser alignment was important because it served as a reference for the rest of the alignment. The capillary was then centered in the path of the beams by translating back and forth across the beam path while monitoring the diffraction pattern formed when the capillary was in the path. The capillary was considered to be aligned with the laser when a symmetric interference pattern was observed. A symmetric interference pattern on both sides of the capillary indicated that both beams were centered and propagating parallel with respect to one another. Lenses were then installed and adjusted to yield the best focal image onto the capillary.

Obtaining the most uniform and well aligned spectral irradiance of the laser within the capillary was paramount to achieving single molecule sensitivity. Moreover, without an accurate alignment between the laser beam and the capillary, the high spatial probing efficiency of this method would be compromised. Lens 1 was placed into its holder and adjusted so that the beam was centered in the lens and that the lens was orthogonal with respect to the detection axis. By translating the lens towards the capillary on the beam axis, the beam was focussed onto the capillary while monitoring the diffraction pattern on the other side of the capillary. As before, the symmetry of the pattern indicates whether the beam is centered on its own axis. However, the shape of the pattern yields information as to the alignment of the focus in the axis of the detector. Figure 2-11 shows a drawing of a typical interference pattern of the laser while in the optimized focus position with respect to



Figure 2-11 Diffraction pattern of laser in focus on capillary

both the laser and detector axis. The bright circle in the center indicated that the laser was centered within the capillary in the axis of the detector while the symmetrical interference maxima and minima revealed alignment in the axis of the beam.

The image of the focused beam within the capillary was then obtained with the collection microscope objective (MO1). This objective was mounted onto a precision x-y stage and a precision z-translator (0.001mm precision, Newport, Irvine, CA). By making adjustments in all three dimensions, an image of the capillary was obtained at the exit of the MVF assembly. Like the diffraction pattern of the laser from the capillary, the image of the capillary from MO1 shows the quality of the focus. Figure 2-12 is a pictorial representation of the image of the capillary as obtained from MO1. This image was viewed on a card placed at the exit window of the MVF using an IR viewer. While viewing this image the focus spot was manipulated to give the best focal position and hence the optimal image of the capillary through MO1. To obtain a laser spot size which slightly overfilled the capillary, the image was monitored while the focus lens was adjusted in the axis of the laser. Moving the lens toward and away from the capillary changed the height (h) of the viewed image of the capillary i.d.. The height was adjusted so that h was just slightly larger than the i.d. (d) of the capillary. This ensured that the capillary was slightly overfilled. Overfilling the capillary resulted in a high spatial probing efficiency and reduced background fluctuation caused by capillary vibration. The focus lens was then carefully translated laterally across the capillary to center the focal spot on the detection axis. As the lens was translated in this manner, the brightness of the capillary i.d. walls in the image would change in intensity. At the aligned position both lines would be in equal intensity

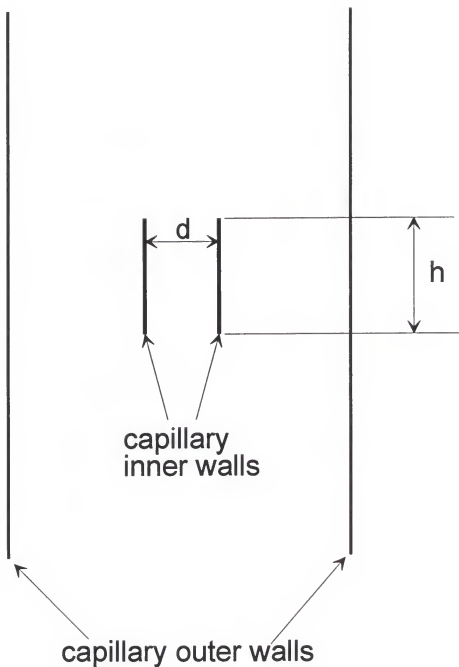


Figure 2-12. Image of capillary as viewed through MO1.
 d is the inner diameter of the capillary and h
is the height of the laser focus spot.

At that stage, MVF number one was heated up to operating temperature ($> 140\text{ }^{\circ}\text{C}$) so that the laser could be spectrally tuned to the MVF.

To tune the laser to the atomic transition of rubidium within the heated MVF, the assembly containing MO2 and the fiber optic mount was placed onto the exit port of the MVF. Light scattered off of the capillary was detected by the SPAPD. The signal from the SPAPD was counted with a photon counter (SR 400, Stanford Research Systems, Sunnyvale, CA) and viewed on a chart recorder. A neutral density filter (4.0) was placed in the path of the laser beam so that the unattenuated light passing through the MVF did not damage the SPAPD during the tuning procedure. By slowly turning the birefringent filter (BRF) of the Ti:sapphire laser the laser was tuned to the electronic transition of the rubidium at 780.0 nm. A sharp characteristic drop in detected scattered radiation was monitored as the BRF was adjusted. Once the signal was minimized (highest absorption), the laser was finely tuned by adjusting the tilt on the intracavity etalon. Upon completion of the tuning, the narrow band interference filter was placed in the path of the laser beam at the immediate exit of the beam from the laser (refer back to Fig 2-1). The tilt on the interference filter was adjusted to yield maximum transmission of laser power ($\sim 250\text{ mW}$). Tilting the interference filter moved the beam slightly in space which complicated the alignment procedure.

The spatial deviation of the beam caused by the tilt of the interference filter does not effect laser beam one significantly, however it does effect laser beam two. Because beam two propagates over a fairly large distance ($\sim 2\text{ m}$) and is reflected by four steering optics, the fairly small spatial deviation in the beam is magnified. For that reason, side 2 had be

aligned with the narrow band interference filter installed and the laser tuned. Thus, it was necessary that the alignment on this side had to be carried out with MVF₂ cold so that the capillary image can be seen at the exit port. Otherwise, the alignment of side two was similar to that of side one with the exception that the laser was already tuned so that the MVF only had to be heated. Once both sides were aligned, the detection bandpass filters were installed and the alignment was optimized giving the maximum fluorescence signal.

Utilizing a fairly dilute concentration of analyte (1 nM IR 140 in methanol), the optics were adjusted to maximize the fluorescence signal. The signal for this optimization was counted using the SR 400 and viewed on a chart recorder. Typically, the most significant adjustments had to be made in the fiber optic (MO2) and collection objective (MO1) alignments. Because the laser focus was so carefully aligned visually, only minor adjustments on it were necessary. With a dwell time of 1 ms on the photon counter, a signal of 120,000 cts/s was obtained at each detector when the alignment was optimized. Upon optimization, all precision mounts were locked down using their adjustment set screws to minimize vibration as well as misalignment during actual analysis.

Chemical System

The analyte/ solvent combination chosen for this research was identical to the system used previously for this project.⁶⁷ Specifically, the analyte molecule was a NIR dye, IR 140, [chemical name, 5,5'-dichloro-11-(diphenylamino)-3-3'-10,12-ethylenethiatricarbocyanine perchlorate, fw = 779, Exciton Chemical Co., Dayton, OH] and the solvent is methanol (Optima grade, Fisher Scientific, Orlando, FL). In previous research^{21,67} it was shown that

this analyte/solvent gave the best signal-to-noise ratio of the dyes which were available at that time. The structure of IR 140 is shown in Figure 2-13. As can be seen in that figure, the molecule has several aromatic moieties and is highly conjugated. This structure gives the molecule excellent photophysical properties for its use as a model compound in ultrasensitive NIR-LIF (see Table 2-3). This molecule has a high molar extinction coefficient at the excitation wavelength ($> 10^5 \text{ L mol}^{-1}\text{cm}^{-1}$), a high fluorescent quantum yield (near unity), a fairly low photodestruction quantum efficiency (2.5×10^{-6})⁶⁷ and a fast fluorescence lifetime (791 ps).¹⁰⁵ The molar extinction coefficient was determined experimentally at the laser wavelength used in the analysis (780.023 nm). A 10 μM IR 140 solution was placed into a 1 cm cuvette which was in the path of the laser beam. The power of the transmitted laser was detected with a photodiode. The IR 140 solution was replaced with pure methanol and the transmitted laser power was measured. The ratio of the blank signal to the IR 140 signal along with the given path length and concentration yielded the measured molar extinction coefficient of $3.66 \times 10^5 \text{ L mol}^{-1} \text{ cm}^{-1}$. The absorption spectrum of IR 140 was obtained and is shown in Figure 2-14.

All glassware, including flasks and pipets, went through a rigorous cleaning procedure. They were first cleaned with a soap solution and then rinsed with distilled water several times. Next, they are soaked for at least 15 minutes in a concentrated sulfuric acid/NOCHROMIX® solution. This highly oxidizing cleaning solution ensures the removal of most residual organics. Finally, the glassware was rinsed five times with ultrapure distilled and deionized water and five times with fresh Optima grade methanol. Dilute solutions ($< \text{nM}$) were made on a daily basis from a 10 μM stock solution which was stored

in the dark. Serial dilutions were carefully done using glass and digital pipets. For low concentrations ($< \mu\text{M}$) and the blanks, the methanol was irradiated with a continuum tungsten lamp for several hours. The goal of this irradiation was to decrease the fluorescent background in the solutions, i.e., to purify the blank.

Table 2-3 Photophysical properties of IR 140 in methanol.

Property	Value
absorption maximum (λ_{ex})	826 nm
emission maximum (λ_{em})	882 nm
fluorescence quantum efficiency (Q_f)	~ 1.0
photodestruction quantum efficiency (Q_d)	2.5×10^{-6}
molar absorptivity (ϵ)	$3.66 \times 10^5 \text{ l mol}^{-1} \text{ cm}^{-1}$
fluorescence lifetime (τ_f)	791 ps

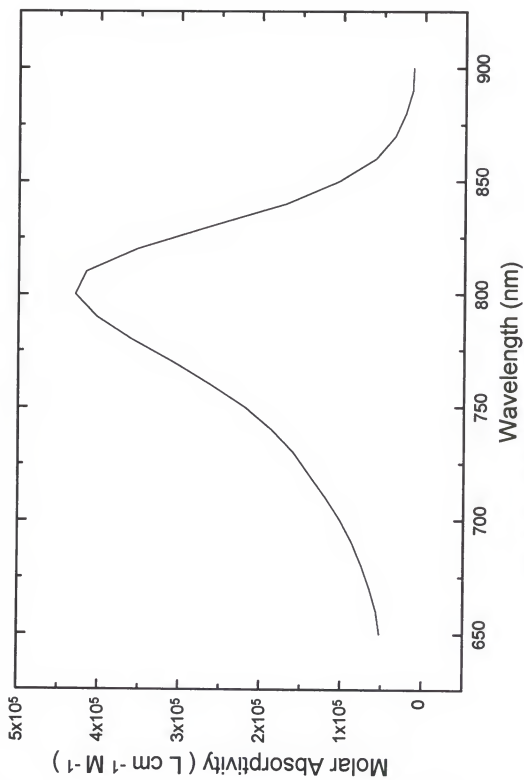


Figure 4-14 Absorption spectrum of IR 140 in methanol.

CHAPTER THREE RUBIDIUM METAL VAPOR FILTER STUDIES

Introduction

Rejection of laser scatter is often the most important consideration in applications of laser-based ultratrace analysis. An ideal optical filter for laser scatter rejection would have to exhibit very high attenuation at the input laser wavelength while remaining transparent at the wavelength of interest. Indralingam et al. have reviewed the use of various optical filters for laser scatter rejection for Raman spectroscopy applications.¹⁰⁶ Each type of optical filter has some disadvantage in terms of light rejection power, signal throughput or ease of use. A grating monochromator has light rejection capability, typically on the order of 10^5 .¹⁰⁷ Unfortunately, the spectral bandpass and the signal throughput are also greatly reduced which lowers the signal as well as the laser scatter.¹⁰⁸ A spectral filter is a common approach in reducing laser scatter for laser-induced fluorescence (LIF) experiments.¹⁷ The light rejection capability of band-pass, short-pass, or long-pass spectral filters is approximately 10^3 , which is poorer than most monochromators. However, spectral filters generally have a much greater optical throughput for the fluorescence signal. Usually, two or more spectral filters are used together or in conjunction with a monochromator. Polarized filtering is another means of reducing laser scatter due to different polarizations of the luminescence signal and laser scatter. Ideally, a polarized filter is rejection capability of 10^9 light polarized 90° to the

transmitted light.⁶⁷ In practice, polarized light filtering does not work as well as expected due to incomplete polarization in the laser scatter and imperfections in the polarizers. The concept of spatial filtering has been successfully applied to ultratrace analysis for signal-to-noise ratio (S/N) improvement.^{20,30,31,68,83} With careful positioning and focusing, a slit or a pinhole can pass a large portion of the fluorescence signal while blocking much of the laser scatter arising from the edge of the sample confinement region. The problem with a spatial filter is that it may limit the observed region of the measurement by collecting luminescence emission from only a portion of the probe volume. Although the S/N can be improved, the overall measurement efficiency may be impaired. Holographic notch filters represent the next generation of optical filters which provide the unique combination of high laser attenuation, narrow spectral bandwidth, and sharper edges without the unwanted secondary reflection bands normally associated with dielectric filters. For dispersive Raman applications, benefits include better system throughput when used with a single monochromator. With Fourier transform Raman applications, the holographic notch filter is more easily installed and aligned when compared to an equivalent dielectric system.¹⁰⁹ Unfortunately, even high-quality holographic notch filters require at least 50 to 100 wavenumbers to pass from high transmission to high rejection (optical densities > 4).

The metal vapor filter (MVF) is a promising optical filter for rejecting narrow-band laser specular scatter based on the resonance absorption of an atomic vapor. The MVF is simply a heated quartz cell with parallel windows containing an inert gas and a volatile metal with a resonance atomic absorption line at the laser wavelength. This MVF,

depending on the volatility of the metal, is heated to an appropriate temperature in order to produce a sufficient number density of metal atoms to absorb efficiently laser specular scatter. Therefore, the metal atoms in the MVF provide a nearly perfect optical filter for laser specular scatter rejection as long as the laser can be tuned to the metal vapor absorption peak and the laser linewidth is narrower than the absorption bandwidth of the atomic vapor. Compared with conventional laser line rejection filters, such as a monochromator, a spectral filter or a notch filter, metal vapor filters offer advantages of very high absorbance, a hemispherical field-of-view, a very narrow rejection linewidth, and high signal throughput. Alkali metal vapors are of particular interest because of the strong discrete optical transitions spanning the regions from the UV to the near-IR. Recently, there has been a reemergence of the use of atomic vapor filters first used for Raman spectroscopy by Rasetti.² Because of the convenience of the Ti:sapphire laser as a tunable excitation source, several MVFs have been demonstrated to be effective in eliminating laser specular scattering for Raman spectroscopy^{106,111,112,113} and single molecule detection.²¹ Most recently, Sabbaghzadeh and Fink have used a laser diode in conjunction with a rubidium MVF to measure pure rotational Raman spectra of CO₂ and N₂.¹¹⁴ A MVF has also been used to confirm the spectral purity of a novel laser source.¹¹⁸

By using a single-stage monochromator and a metal vapor cell, Indralingam et al.¹⁰⁶ demonstrated the use of rubidium (Rb) and mercury (Hg) metal vapor filters as effective in eliminating laser scatter for Raman spectrometry. Pelletier described a simple, inexpensive, mercury metal vapor filter for UV continuum sources¹¹¹ and a near-IR laser line rejection filter¹¹² both for Raman applications. In the latter paper, Stokes and

antistokes Raman spectra, including the laser wavelength, were collected with the use of potassium metal vapor filter. While the Raman bands were not affected by the metal vapor filter, the laser line was attenuated by more than 10 orders of magnitude. Horoyksi and Thewalt presented Raman and Brillouin scattering measurements obtained with a Fourier transform interferometer, in which the laser light rejection was provided by an alkali-metal vapor cell.¹¹³ The narrow absorption band of the vapor cell allowed for the detection of energy shifts as low as 0.85 cm^{-1} (26 GHz) while efficiently blocking scattered light at the laser frequency.

To achieve single molecule detection, the signal throughput of the optical arrangement must be sufficiently high to obtain a discrete signal from a single molecule.¹⁸ Any dispersive optical system, such as a Raman spectrometer using a monochromator as the laser line rejection filter, is not adequate due to its very narrow spectral bandpass which is required for high resolution measurement. For example, the typical detection efficiency of a Raman spectrometer (slit area / (cell area scattering Raman \times fractional solid angle of Raman collection \times spectrograph transmittance \times transmittance of all external optics \times detector quantum efficiency)) is only 10^{-6} - 10^{-7} which precludes the observation of a photon burst from a single molecule. By increasing the spectral bandwidth and by optimizing the optical arrangement, it should be feasible to increase the detection efficiency. The challenge then will be to achieve sufficient rejection of laser scatter to enable a burst of photons from a single molecule to be detected. By tuning a Ti:sapphire laser to the rubidium atomic transition line at 780.023 nm and using a rubidium metal vapor to absorb the intense laser scatter from a capillary,

Lee et al. were able to reliably detect photon bursts from individual single molecules flowing through a 1.05 pL probe volume.²¹ In this scheme, a detector observed the molecular fluorescence as well as the laser scatter from the capillary without any dispersive optics in order to increase the spectral bandpass. The measured apparent absorbance of 8 when the rubidium metal vapor filter was heated to 170 °C was believed to be limited by either the Rb vapor fluorescence or transmission of the laser wings. These factors can complicate the use of the vapor cell for laser scatter rejection. Through a theoretical simulation of the MVF throughput in this chapter, these factors were investigated.

The goal of this work is to describe the performance of the Rb MVF at 780.023 nm used in single molecule detection experiments and characterize the spectral composition of the transmitted light. The laser is sent through the Rb MVF and a monochromator directly before being observed by the detector. Transmission characteristics of the MVF were observed over the entire region between the laser excitation line through the fluorescence Stokes shift of the dye molecules used in our SMD studies. Evaluations of spectral profiles were made at different temperatures and pressures, as well as various laser powers. A theoretical simulation of the experiments was also done to aid in these evaluations. By identifying the spectral composition of the MVF transmission, the practical limitations and possible improvements in the operation of the MVF for single molecule detection may be elucidated.

Experimental

The experiments performed in this part of the research were significantly different than the SMD experiments. Thus, the experiment apparatus and procedures for the MVF studies are explained in detail here. The experimental arrangement for these studies is shown in Figure 3-1. The all-line output from an argon ion laser (model 2060, Spectra Physics, Mountain View, CA) is used to pump a single-mode, tunable, continuous-wave Ti:sapphire laser (Schwartz Electro-Optics, Orlando, FL) in the ring configuration. The laser spectral line width (FWHM) is less than 40 MHz over one second interval based on information from the manufacturer. A narrow band pass interference filter ($\Delta\lambda = 0.18$ nm FWHM at 780.1 nm, Corion, Holliston, MA) attenuated a weak, broad-band Ti:sapphire luminescence, a part of which is within the divergence of the output laser beam. In experiments to investigate peaks in transmission spectrum of the MVF, the laser beam was directed through the metal vapor filter either by a mirror or scattered by a surface such as a quartz capillary or a Teflon block. The commercially available metal vapor cell (OPHTOS, Rockville, MD) consisted of a quartz cylinder (length 10 cm, diameter 2.5 cm) with parallel quartz windows on both ends. This cell is made by distilling an excess of rubidium metal (500 mg) into the evacuated quartz cylinder such that sufficient metal would be present to give a saturated metal vapor at all temperatures used in this work. Nitrogen gas is used as a fill gas in order to quench the atomic resonance fluorescence and broaden the absorption bandwidth of the Rb atomic vapor. Cells filled with 50, 200 and 500 Torr of N_2 were used in this study; these cells resulted in rubidium 780.023 nm lines having calculated Voigt spectral bandwidths (FWHM) of 1.25, 1.52 and 2.19 pm, respectively. The cell was differentially heated to avoid window

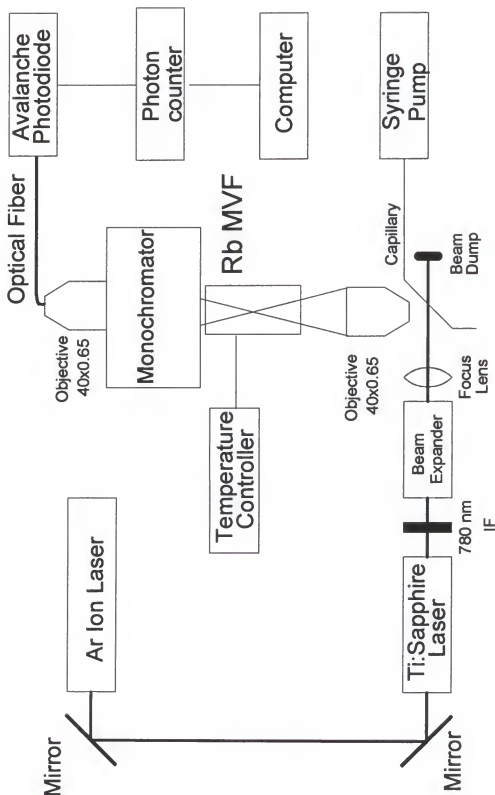


Figure 3-1 Experimental apparatus for MVF studies

discoloring due to the attack of the quartz by the hot Rb metal vapor. The Rb MVF is held inside a cylindrical windows and recycles back to the body of the MVF. In this way, the flat window faces of the MVF are kept warmer than the center of the MVF, preventing metal vapor from condensing onto the windows, which would reduce the signal throughput and the transmittance of the MVF. The Rb MVF used in this work has functioned flawlessly for nearly 2 years.

The spectrometer utilized was a 0.22 m double monochromator (model 1620, Spex Industries, Edison, NJ) equipped with a single photon avalanche photodiode (SPAPD) (model SPCM-200, EG&G Optoelectronics Canada, Vaudreuil, Canada) as the detector. Unless otherwise stated, the width of entrance and exit slits were set to $50\text{ }\mu\text{m}$ ($\Delta\lambda_m = 0.09\text{ nm}$). The output from the monochromator was focused by a microscope objective (0.65 NA, Melles Griot, Irvine, CA) onto an optic fiber pigtail which was prealigned to the SPAPD. The SPAPD is a single-photon counting module with high quantum efficiency (25% at 830 nm) and low dark count rate ($<50\text{ c/s}$, nominal). The digital output pulses from the SPAPD were interfaced to a gated photon counter (SR400, Stanford Research Systems, Sunnyvale, CA) and collected on a 386PC running Stanford's software (SR265 version 3.1x).

The Ti:sapphire laser was tuned to the maximum absorbance of the Rb MVF by slowly adjusting the intracavity birefringent filter. Fine tuning is done by tilting the intracavity Fabry Perot etalon to further maximize absorbance. The maximum absorbance is more like a plateau than a peak because the Fabry Perot etalon can be adjusted significantly before the laser is tuned off-wavelength and the absorbance

decreased sharply. The laser linewidth (FWHM) at 780.023 nm is less than 0.081 pm when the Ti:sapphire laser is operated in the ring configuration with a 40 MHz spectral linewidth.

The calculations for the simulation were performed using the software Mathcad 4.0 (MathSoft Inc. Cambridge, MA) installed onto a pentium-90 MHZ PC (Zeos International LTD. Minneapolis, MN). With the software optimized for these calculations, it took the computer about 8 hours to perform the full simulation.

Results and Discussion

In ultratrace analysis using laser-induced fluorescence, it is imperative that the scattered photons from the laser are efficiently rejected while the fluorescence from the analyte is allowed to pass to the detector. By tuning the laser to the absorption maxima of an atomic vapor in a MVF, essentially all of the resonant laser photons are absorbed by the vapor, while photons outside the absorption profile are passed. When single molecules are counted on our system, all photons which pass through the MVF and a bandpass filter centered at the peak of the molecular fluorescence of the probe molecule are collected.²¹ To investigate the spectral composition of the background photons seen at the detector performing SMD, the fluorescence bandpass filter normally used was removed and a monochromator was placed between the MVF and the avalanche photodiode. Methanol was pumped through a fused silica capillary (10 μm i.d., 150 μm o.d.) and the monochromator was scanned over the range of 770 - 870 nm ($\Delta\lambda_m = 3.6$ nm). This range included the laser line at 780 nm and the 830 nm fluorescence maxima

of the probe molecule (IR 140) used in the SMD experiments. In this manner, the spectral composition of light transmitted through the MVF, within the Stokes shift of our probe molecule, may be obtained. Significant peaks at the laser line and at 795 nm were seen, as well as a small feature at about 850 nm (see Figure 3-2). The transmitted photons at 780 nm can be attributed to either unabsorbed laser light or resonance fluorescence of the Rb vapor or possibly a combination of the two. Because the detector observed the transmitted light colinearly with the incident laser, the distinction between the two processes could not easily be made. It was concluded that the line at 795 nm was due to the non-resonance fluorescence from the rubidium $5^2P_{1/2}$ level (794.76 nm emission) which were probably collisionally populated from the laser resonant $5^2P_{3/2}$ level. The scale of figure 3-2 was decreased to investigate the small feature at 850 nm and a small peak was revealed (Figure 3-3). This peak was identified as a methanol Raman shift at 1055 cm^{-1} . To confirm this, ethanol was flowed through the capillary. As shown in Figure 3-4, a characteristic Raman spectrum of ethanol was obtained with shifts observed at 915, 1080 and 1326 cm^{-1} , while the 1055 cm^{-1} peak disappeared. An interference filter centered at 830 nm ($\Delta\lambda = 10\text{ nm}$) was placed after the MVF to attenuate any photons outside of the fluorescence maxima during SMD. There was some concern as to the presence of the Raman shift at 1055 cm^{-1} in that these photons would be detected during single molecule events due to an overlap of the methanol Raman and the interference filter bandpass function. This potential problem may be solved by optimizing for the best peak transmission and bandpass width of the interference filter. The ability to observe Raman spectra of the methanol from such a small sample volume

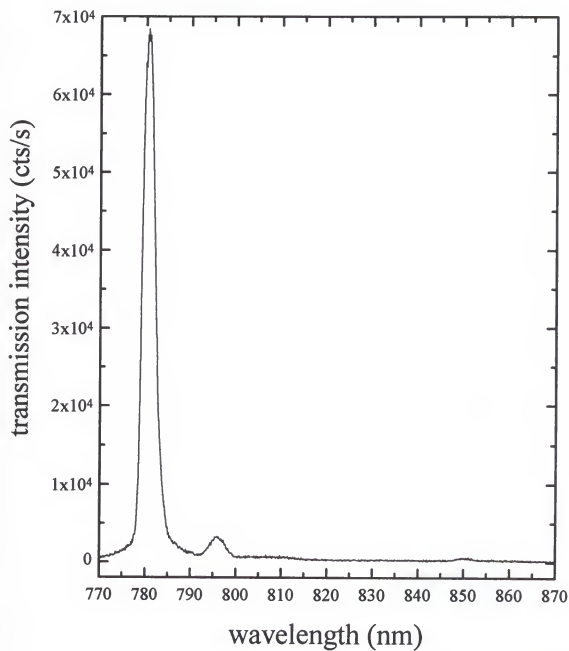


Figure 3-2 Transmission spectrum of background photons

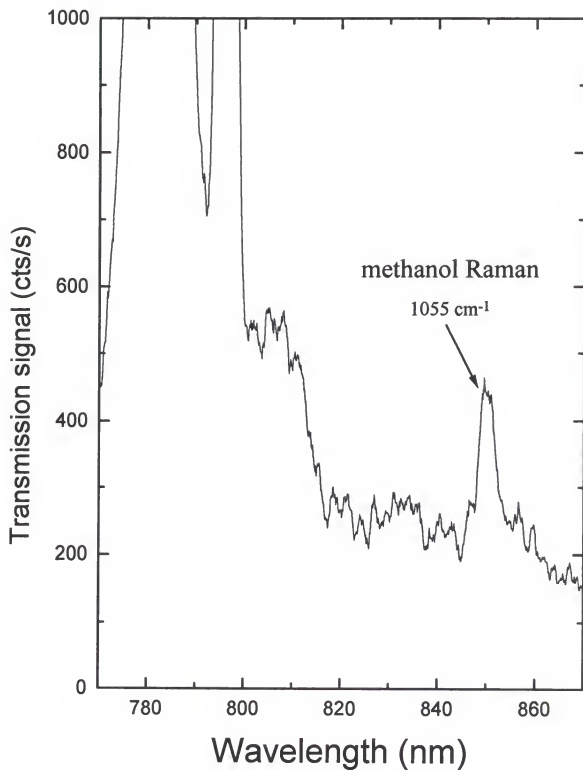


Figure 3-3 Exploded view of transmission spectrum

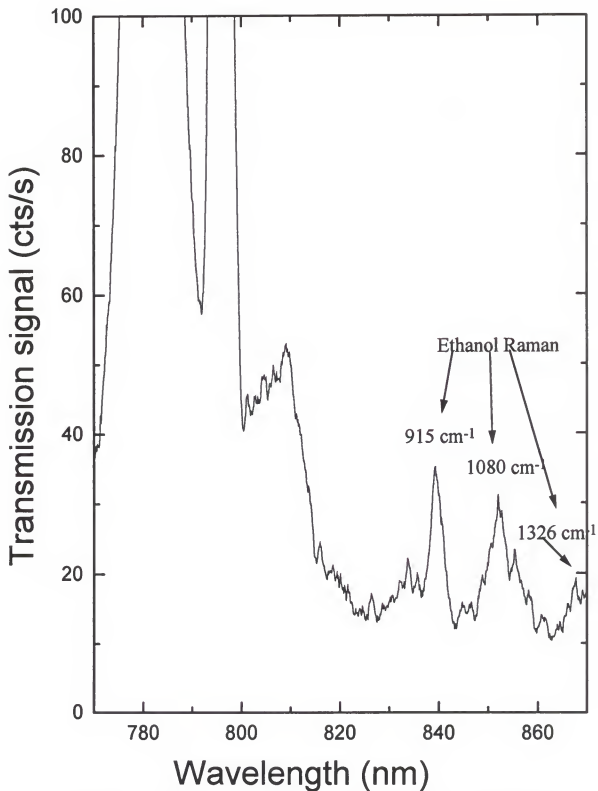


Figure 3-4 Ethanol Raman in transmission spectrum

(1.05 pL) illustrated the high sensitivity of detection using the MVF and SPAPD combination. To confirm that none of the peaks shown in figure 3-2 were due to Raman scattering from the capillary material, the laser was scattered from a block of teflon and into the MVF. Signals at 780 and 794.7 nm were obtained, confirming that these lines were due to the interaction of the laser with the rubidium vapor and the other peak at 850 nm not present and was therefore due to a methanol Raman scatter.

Having elucidated the presence of the two transmission peaks at 780 and 795 nm due to processes of the Rb in the MVF, these peaks were more closely investigated under varying conditions with the goal of improving the filter's performance. During these experiments, the unfocussed laser beam was allowed to pass directly through the MVF by replacing the capillary with a mirror. Given a particular cell size, the extent of the absorption of photons resonant with the vapor is dependent only upon the number density of Rb atoms within the MVF cell and their collisional behavior with the buffer gas. The number density of atoms within the cell, and consequently the optical thickness, can be controlled by the temperature of the cell. Lee, et al, measured the overall apparent absorbance of the Rb-MVF at 200 Torr as a function of temperature by using calibrated neutral density filters.²¹ They found that the absorbance increased from 0 to 8 as the temperature was increased from 23 to 165 °C. The measured absorbance did not account for the transmission of the unabsorbed broadband stimulated emission from the Ti:sapphire crystal and fluorescence by the Rb vapor.

Figures 3-5 and 3-6 show the effect of the MVF temperature upon its absorption character at both the laser and nonresonant fluorescence lines. Transmission of the MVF

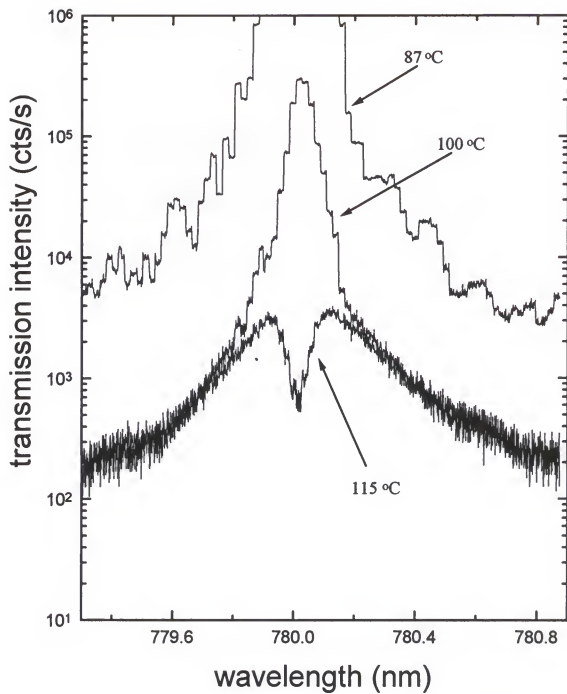


Figure 3-5 Measured transmission profile of laser line at various temperatures.
Monochromator resolution is 0.09 nm.

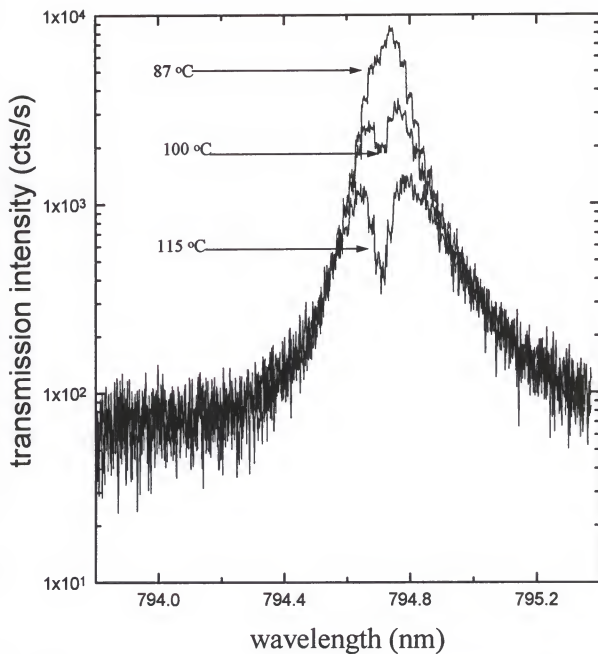


Figure 3-6 Transmission profile of collisionally populated line at various temperatures. Monochromator resolution = 0.09 nm

photons decreases significantly over the rubidium absorption line profile at the laser line with only a modest increase in temperature. Profiles obtained for temperatures under 87 °C were not obtained because of detector saturation occurring at 10^6 counts/s. The 115°C profile in Figure 3-5 is the observed transmission of the Rb-MVF which is a convolution of very strong absorption of the laser line, transmission of the Ti:sapphire crystal emission, resonance fluorescence of the Rb vapor and the spectral response function of the monochromator. As the temperature of the cell increases, the convoluted profile becomes dominated by the crystal emission. The dip in the profile is due to strong absorption of the laser center frequency under optically thick conditions and becomes more pronounced as the number density of Rb increases. This profile is mirrored by the collisionally populated fluorescence line as can be seen in Figure 3-6. It makes sense that the collisionally populated fluorescence state ($^2S_{1/2}$) would have a similar profile shape as the radiationally populated resonance level ($^2S_{3/2}$), since the resonance line is the source for the non-resonance level.

The other major contributor to the behavior of the MVF is the type and pressure of the quenching partner. Nitrogen is used because of its chemical inertness and significant collisional cross-section ($2.49 \times 10^{-19} \text{ m}^2$).¹¹⁶ Figures 3-7 and 3-8 show the dependence of buffer gas pressure on the shape and intensity of the laser transmission and non-resonance fluorescence, respectively. As expected, as the pressure increases, the FWHM of the transmission peak increases and the amount of total transmitted light decreases. This trend is seen in both the 780 and 795 nm profiles. As shown in previous studies using MVF's for Raman applications,^{106, 111-113} it is important to have narrow transmitted

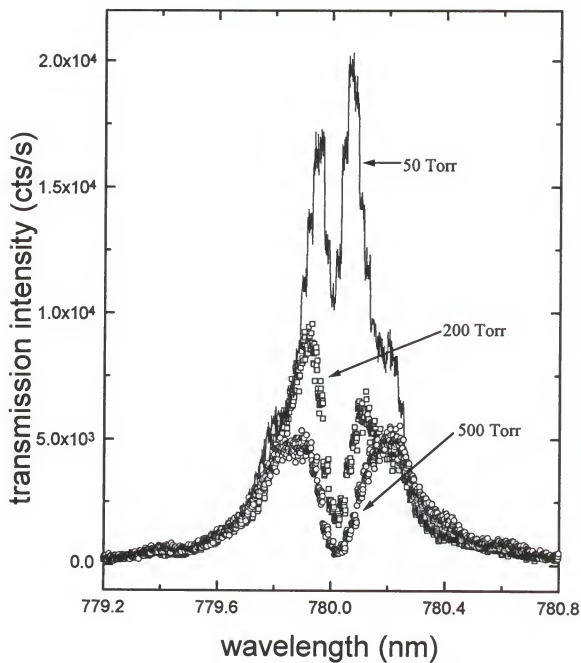


Figure 3-7 Transmission profile of laser line at various buffer gas pressures

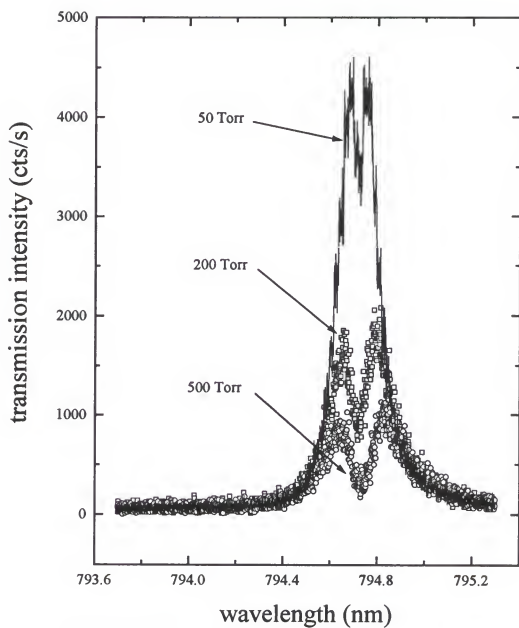


Figure 3-8 Transmission profile of collisionally populated fluorescence line as a function of pressure

laser lines so that resolution of small Raman shifts can be measured without being buried under the laser peak. In using this filter for SMD purposes, however, the total amount of transmitted light is a more important factor rather than the width of the detected laser line. Recall that in our SMD experiments, no dispersive wavelength selective optics were used for the detected photons, only an interference filter. Hence, to reject laser scatter more efficiently in our SMD experiments, the 500 Torr filter will be used because of its greater integrated attenuation. The fact that the width of the dip in these profiles increases with pressure, in both Figures 3-7 and 3-8, indirectly shows the collisional broadening of the Rb absorption line. The ratio of the laser transmission peak intensity to the non-resonance fluorescence peak intensity (I_L/I_F) was obtained at different N_2 pressures, and it was found that this ratio increased at higher pressures. Upon inspection of the population rate equations, it was postulated that at very high quenching rates, stimulated emission became a bigger factor in the transmission of more light at the laser line as compared to the non-resonance fluorescence. Under those conditions, the I_L/I_F ratio would indeed increase.

To further clarify the contribution of the laser crystal to the transmission profile, scans were made at different laser powers (see Figures 3-9 & 3-10). As can be seen, the apexes of the features as well as the dips remained aligned on a vertical axis, while the overall width and intensity of the profiles increased with laser power. This is because the conditions within the MVF are constant and the amount of the transmitted laser wings is in direct proportion to the laser power. The magnitude of the dip in the profile does not change greatly relative to the peak height because of the extremely high absorbance in

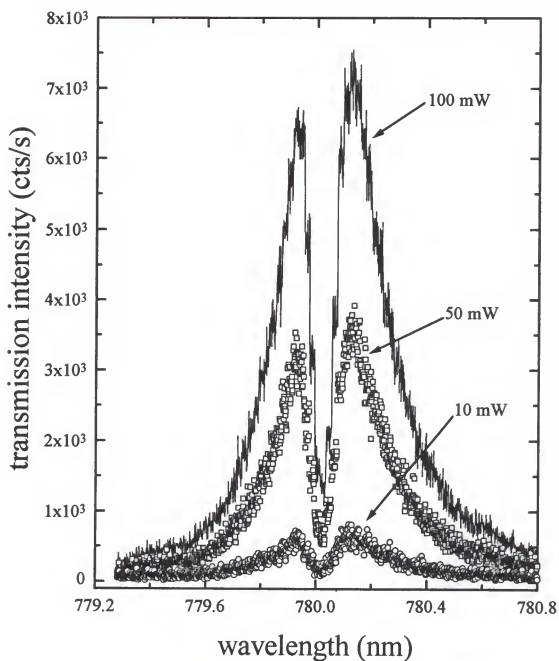


Figure 3-9 Laser Line transmission as a function of laser power
MVF T = 110 °C

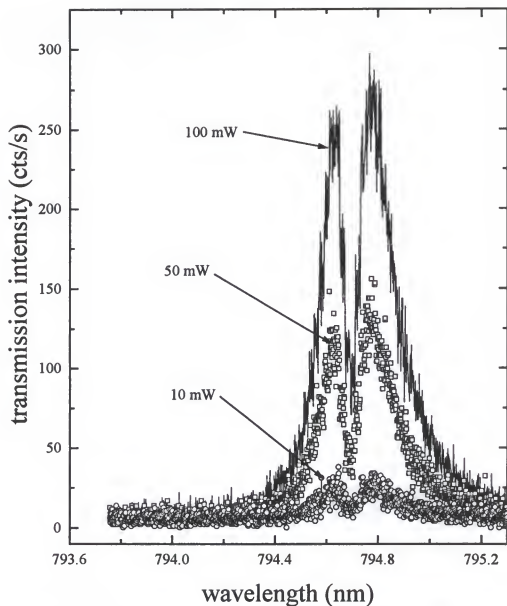


Figure 3-10 Fluorescence line transmission at various laser powers
MVF T = 110 °C

the center of the Rb absorption profile. This shows the significant contribution of the laser crystal emission to the profile due to the the lower absorption in the wings of the Rb absorption profile.

Simulation

To evaluate theoretically the profile of the transmission of the laser line through the Rb-MVF, a computer simulation was performed. The model involved calculating the absorption profile of rubidium, estimating the spectral line shape of the laser, combining the two together, accounting for fluorescence and convoluting the transmission profile with the spectral function of the monochromator. The goal of the simulation was not only to correlate the experimentally obtained transmission profiles with theory, but also to establish a working model so that experimental parameters could be easily changed in the computer simulation and the outcome predicted. In this manner, parameters for the optimal performance of the MVF could be established before performing an experiment. This may allow improvements in the performance of the Rb- MVF for single molecule detection as well as other experiments.

The absorption profile of rubidium was calculated using Puerta and Martins four-pole approximation of the Voigt profile.^{117,118} This function can be approximated by the equation:

$$J(p, d) \approx \sum_{j=1}^4 \frac{\gamma_j(p - \alpha_j) + \delta_j(d - \beta_j)}{(p - \alpha_j)^2 + (d - \beta_j)^2} \quad (3-1)$$

where p is the collisional line width, d is the normalized line separation and $\gamma_j, \alpha_j, \delta_j$

and β_j are the j th-pole expansion parameters. The values for these parameters were given paper by Puerta and Martin.^{117,118} Profiles of each isotope (^{87}Rb and ^{85}Rb) were calculated using the frequency and intensity of each of the 12 hyperfine structure transitions. The individual transitions of each isotope are then added together using:

$$S(v_i) = \sum_i 2 \frac{\sqrt{\ln 2}}{\Delta v_i} \frac{f_i}{f_{\text{tot}}} J(p, d) \quad (3-2)$$

where Δv_i is the Doppler width of the i th fine structure line and f_i and f_{tot} are the i th and total oscillator strengths, respectively. Absorption coefficient profiles for each isotope were obtained using:

$$k(v_i) = \frac{e^2 f_{\text{tot}} S(v_i) n}{4 \epsilon_0 m_e c} \quad (3-3)$$

where e is the fundamental charge, f_{tot} is the total oscillator strength for each isotope (summed over all hyperfine components), $S(v_i)$ is the area-normalized absorption profile, n is the atomic number density, ϵ_0 is the permittivity of free space, m_e is the mass of an electron and c is the speed of light. This "linear form" of the absorption coefficient can be used because it was estimated that the laser intensity is below the saturation intensity¹¹⁸ and radiation trapping was assumed negligible because of the relatively high pressure of the quenching gas, N_2 . The atomic number density (n) was calculated using the method of Gallager and Lewis as described in chapter 2.¹⁰⁴ The absorption profiles for each isotope were weighted according to their natural abundance¹²⁰ ($^{85}\text{Rb} = 0.727$ and

$^{87}\text{Rb} = 0.273$) and added together. The combined absorption profile of both isotopes is plotted in Figures 3-11A and 3-11B. Figure 3-11A shows the detail of the hyperfine transitions of Rb on the absorption profile over a small frequency range. The extent to which the absorption wings of the profile span across the full range of the simulated scan can be seen in Figure 3-11B. Absorption in the wings of the absorption profile will play a significant role in the performance of a MVF.

Simulating the line shape of the laser is an important facet of this model because of its significant contribution to the transmission of light through the MVF. In most situations, it is appropriate to use a Gaussian spectral line shape for the laser. However, in the modeling of our particular case, a Gaussian alone was not a suitable choice because it would not accurately emulate the experimentally observed weak broadband stimulated emission from the Ti:sapphire crystal. Even though this broadband background was very weak compared to the intensity of the laser, it played a significant role in the performance of the MVF. It was attenuated by placing a narrow-band interference filter ($\Delta\lambda = 0.18$ nm, centered at 780.1 nm) in the path of the beam. Attenuation of the Ti:sapphire broadband emission can be seen in the comparison in Figure 3-12. Transmission of the laser through the MVF is much greater without the narrowband filter. The spectrum without the filter exhibits the performance of the MVF very well, in that, small details within only a few wavenumbers of the very intense laser (< 8 decades larger) can be observed. A combination of a Gaussian (lasing) and Lorentzian (interference filter transmission) was used to simulate accurately the spectral profile of light scattered off the capillary, incident to the MVF. These two contributions to the profile were added in a

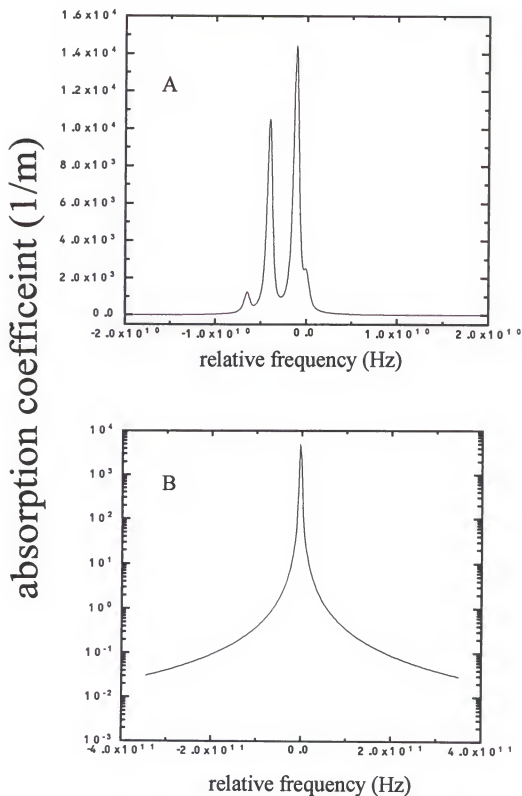


Figure 3-11 Simulated absorption profile of rubidium at $T = 100$ C and 200 Torr.

A) Coefficient shown in a small frequency range to show fine structure

B) Absorption coefficient showing wings of absorption

linear fashion given by:

$$S_L(v) = G(v) + W L(v) \quad (3-4)$$

where $S_L(v)$ is the simulated laser profile, W is a weighting factor and $G(v)$ and $L(v)$ are the Gaussian and Lorentzian profiles, respectively. The weighting factor (W) is an empirical parameter to account for the much lower intensity of the broadband emission in comparison to the peak laser intensity. Values of W were estimated by comparing the simulated MVF spectral transmission profiles with those obtained experimentally. A W value of 10^{-8} was chosen as an initial value because the apparent absorbance obtained by Lee, et al was 8. A simulated laser profile of this combined laser shape is shown in Figure 3-13. As can be seen in Figure 3-13, a very narrow and intense center line is standing on top of a broad and weak pedestal. The experimentally obtained profiles correlate very well with this line shape as will be seen below. The next step in the simulation was to model the transmission of the total laser profile through the MVF and to account for the rubidium fluorescence. The transmitted light intensity can be and is given by the following:

$$I_T(v) = I_0 S_L(v) e^{(-k(v) l)} \quad (3-5)$$

where $I_T(v)$ is the transmission intensity, I_0 is the total integrated laser intensity ($\approx 10^{18}$ photons/s @ 100 mW) and l is the length of the MVF cell. The resulting

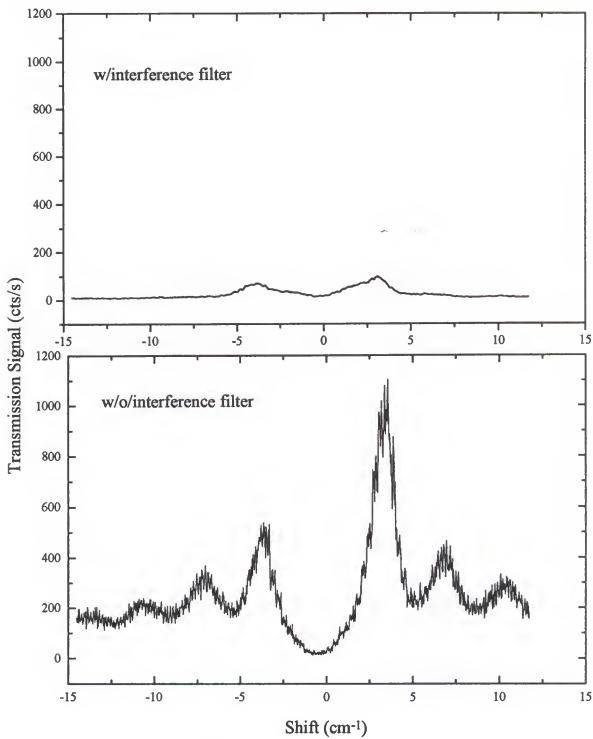


Figure 3-12 Comparison of laser transmission through MVF with and without laser filter

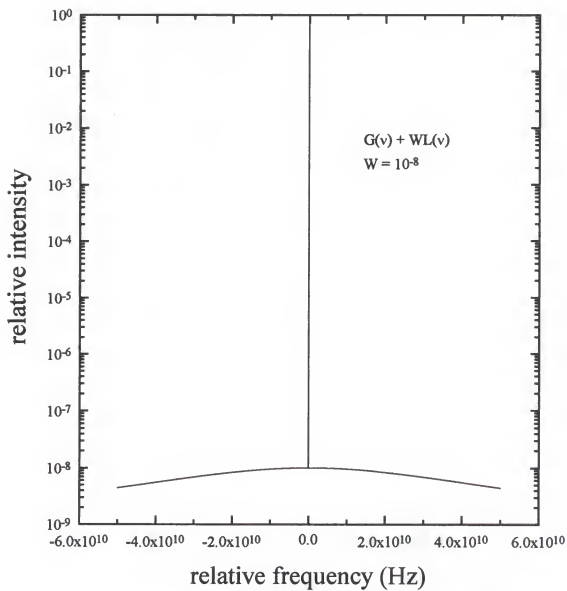


Figure 3-13 Simulated combined spectral profile of laser

profile is shown in Figure 3-14. The most noticeable feature of the profile was the very large dip in the center. This can be attributed to the very strong absorption of the Gaussian component of the laser beam by the pressure broadened rubidium absorption line. The rest of the profile is mostly due to the unabsorbed broadband emission from the Ti:sapphire crystal of the laser.

The following section is a derivation of the integral used to simulate the resonance fluorescence for the model. It was estimated that the laser intensity incident on the MVF is below the saturation intensity of the rubidium atoms. It can then be assumed that the absorption coefficient is in its linear form (see equation 3-3) and that the fluorescence quantum yield is constant as a function of the distance coordinate x (cm) within the MVF. These assumptions greatly simplify the model and its numerical calculation. The laser intensity at a given point x from the front face of the MVF is given by:

$$I(x, \nu) = I_0 S_L(\nu) \exp[-k(\nu)x] \quad (3-6)$$

where I_0 is the total integrated laser intensity, $S_L(\nu)$ is the laser profile function given by equation 3-4, $k(\nu)$ is the absorption coefficient (cm^{-1})(eqn. 3-3) and x is a given distance from the front face of the MVF. The spectral component of the laser absorbed within a thin layer from x to $(x + dx)$ can be written:

$$dI(x) = I(x, \nu) (1 - \exp[-k(\nu) dx]) \approx I(x, \nu) k(\nu) dx \quad (3-7)$$

where the approximation $[1 - \exp(-\alpha)] \approx \alpha$ for $\alpha \rightarrow 0$ was used. The total energy of laser light absorbed within the layer dx will be:

$$dE(x) = I_0 S dx \int_0^{\infty} S_L(v) k(v) \exp[-k(v)] dv \quad (3-8)$$

where S is the cross sectional area of the laser beam (cm^2). Fluorescence radiation emitted by the layer dx within the solid angle (steradians) of the collimating microscope objective ($d\Omega$) will then be:

$$dI_F(v) = dE Y e_v \frac{d\Omega}{4\pi} \quad (3-9)$$

where Y is the fluorescence quantum yield and e_v is the emission profile of the rubidium. The intensity of light at the output plane of length (L , cm) of the MVF will be:

$$dI_F(v) = dI_F(x) \exp[-k(v)(L-x)] \quad (3-10)$$

The spectral distribution of resonance fluorescence behind the MVF can then be expressed as: :

$$I_F(v, L) - I_0 Y \frac{d\Omega}{4\pi} \int_0^L \exp[-k(v)(L-x)] dx \int_0^{\infty} e_v k(v) S_L(v) \exp[-k(v)x] dv \quad (3-11)$$

where Y is the fluorescence quantum efficiency of the rubidium, $d\Omega$ is the solid angle

collected by the microscope objective, dx is a crosssectional thin slice of the MVF and e_v is the spectral emission profile of rubidium fluorescence as given by Hooymayers.¹²³

Figure 3-15 shows the profile of the fluorescence calculated using equation 3-11. Even though 200 Torr of N_2 is present in the MVF cell to quench fluorescence of the rubidium, as can be seen, there is a contribution of fluorescence to the composition of light transmitted through the MVF. The fluorescence is 3 orders of magnitude less intense than the transmitted laser light. In other words, if we were to show a plot of the combination of the transmitted and fluorescence light profiles the fluorescence would be hidden beneath the transmission. This makes the rest of the simulation much less cumbersome because the fluorescence can be neglected.

The convolution integral of the transmitted light convolved with the monochromator function is given by:

$$I_{\text{exp}}(\nu) = \epsilon_s \epsilon_q \int_{-3\Delta\nu_m}^{3\Delta\nu_m} I_T(\nu - \nu') A(\nu') d\nu' \quad (3-12)$$

where $\Delta\nu_m$ is the spectral bandwidth of the monochromator (4.0×10^{10} Hz), ϵ_s is the efficiency of the spectrometric system (0.0038), ϵ_q is the quantum efficiency of the detector (0.25), $I_T(\nu - \nu')$ is the total transmitted intensity through the MVF and $A(\nu')$ is the spectral function of the monochromator. $A(\nu')$ is usually described by a triangle function. However, in our case, to ease the format of the calculation for the computer, a Gaussian function was used, given by:

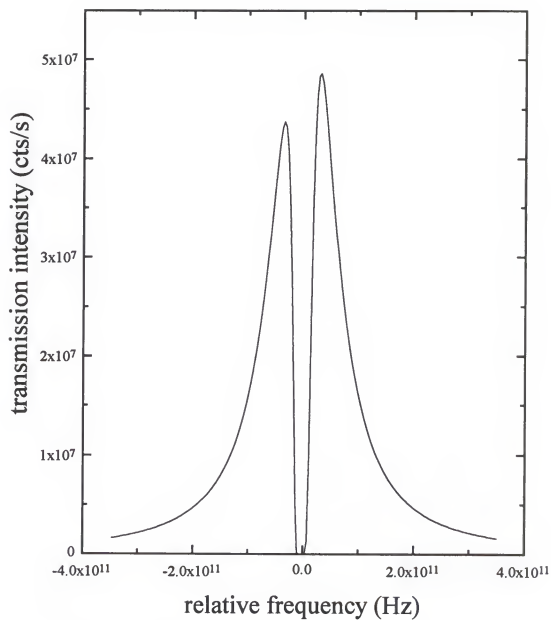


Figure 3-14 Simulated transmission profile of laser through MVF

$$A(v') = \frac{1}{\sqrt{2\pi} \Delta v_m} \exp \frac{-4 \ln 2 (v')^2}{\Delta v_m^2} \quad (3-13)$$

where v' is the domain of the monochromator function (from $-3\Delta v_m$ to $3\Delta v_m$). Figure 3-16 shows the simulated transmission profile convoluted with the monochromator function at a resolution of 0.09 nm ($\Delta v_m = 4 \times 10^{10}$ Hz). The simulated profile shown in Figure 3-16 was calculated under the same conditions as the 100 mW profile shown in Figure 3-9. When Figures 3-9 and 3-16 are compared, it can be seen that the shape and relative magnitudes of intensity match up very well. Such a good match of the model with the experiment indicates that the model and the assumptions made are fairly accurate. Further optimization of the simulation parameters, such as the W-factor in the laser shape and the efficiencies of light collection and throughput of the monochromator, will allow a more closely matched fit of the simulated with the experimental profiles.

Conclusions

It has been previously shown that metal vapor filters can sufficiently attenuate scattered laser light to permit highly resolved Raman spectra and the fluorescence from single molecules to be detected. MVF's are an attractive option to attenuate laser scatter because they are efficient, relatively inexpensive and easy to use. Their drawbacks include the need for a tunable laser source and the restriction of using atomic lines. In this chapter, it has been shown that the transmission profile across the Stokes shift of the

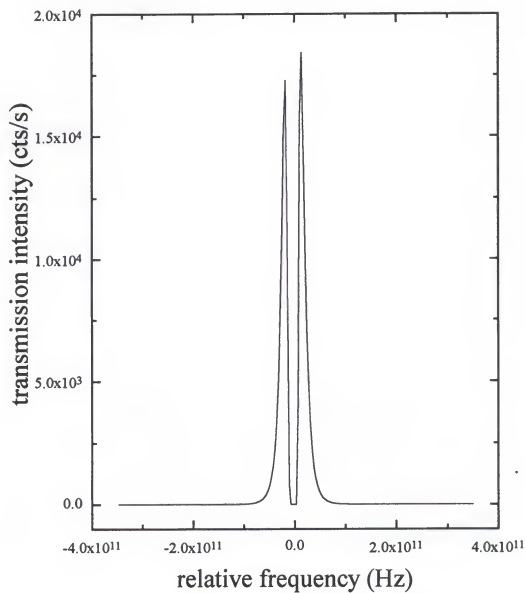


Figure 3-15 Simulated rubidium resonance fluorescence

fluorophore used in SMD is dominated by processes of the laser interacting with the Rb-MVF and not by fluorescence or Raman scattering of the capillary or the solvent. It was also shown that the narrowband interference filter used to attenuate broadband emission from the Ti:sapphire laser plays a important role in the use of the Rb MVF in single molecule detection. Resonance and non-resonance fluorescence as well as unabsorbed source light significantly contribute to the laser stimulated Rb-MVF transmission profiles. The relative contributions of these factors was determined using a theoretical simulation. It was found that the most significant contribution of photons transmitted through the MVF was due to the broadband background emission from the Ti:sapphire crystal. According to the calculation, this transmission was 3 orders of magnitude larger than the contribution of resonance fluorescence. To increase the accuracy of the calculation, non-resonance fluorescence should be added into the model. This would make the simulation more difficult to perform, but it would make the model more complete. Because it was found that background photons were dominated by the transmission of broadband stimulated emission from the Ti:sapphire crystal, it was concluded that the background can be reduced by using a higher pressure of nitrogen buffer gas. Because of the large Stokes shift (30 - 50 nm) of the near-IR fluorophore used (e.g., IR 140), collisional-broadening of the Rb line will not attenuate fluorescence appreciably. Other ways of reducing the transmission of the crystal emission would be to improve the laser itself or to utilize a narrower bandpass interference filter. However, neither of these options are by any means trivial.

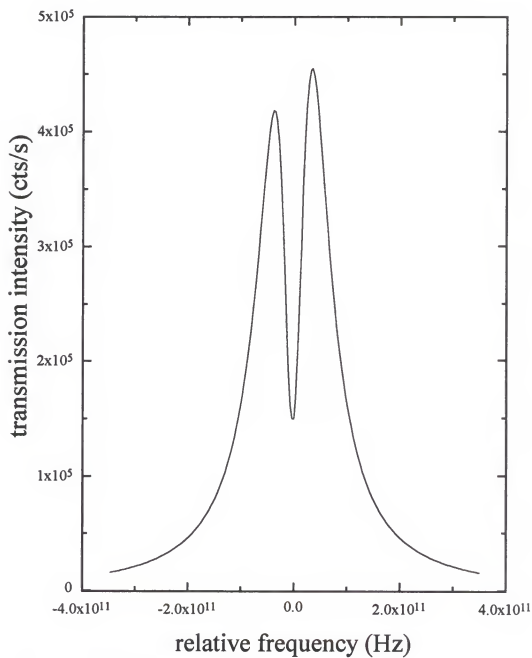


Figure 3-16 Simulated transmission spectrum convoluted with monochromator

CHAPTER FOUR

SEQUENTIAL SINGLE MOLECULE MEASUREMENT

Overview

This chapter will describe in detail the results of research performed to successfully achieve the sequential measurement of an individual fluorophore in solution in a flowing stream. Important aspects of the research include the detection of single molecules on-column with a laser probing efficiency of unity and confirmation of the measurement by sequential detection in two separate channels. Preliminary studies involved ensuring a low background, measurement of the solution flow within the capillary by a novel means, laser saturation of IR 140 fluorescence, IR 140 photobleaching and calibration of both channels. Furthermore, results from the on-column measurement of single molecules will be discussed in detail. SMD data will be presented as real-time plots of signal as a function of time and in statistical forms including a histogram. Several mathematical treatments will be made on the SMD data including digital filtering and correlation analysis. Descriptions and comparisons of the different presentations of the data will be made to confirm the capability of detection of individual IR 140 molecules separately in each channel. It will then be shown that molecules were efficiently counted sequentially in the two channels.

Preliminary Studies

Background Signal

Prior to engaging in SMD type experiments, it was necessary to assure that the optical alignment of the system was stable over time and that the background signal was at an acceptable level. Stability of the optical alignment includes not only the temporal precision of the focusing and collection optics but also the temporal stability of the laser to maintain its spectral tuning to the absorption transition of the rubidium in the metal vapor filter (MVF). To obtain a unity spatial probing efficiency while maintaining a high laser power density, the laser beam was focused to a spot size of approximately the same diameter as the inside diameter of the capillary (9 μm). Once the laser was focused to match the i.d. of the capillary, the focus lens was backed off slightly so that the capillary was overfilled with laser light ensuring maximum spatial probing efficiency. The probe volume (V_p) was calculated by assuming a cylindrical geometry with the circular part being defined by the inner diameter of the capillary of radius, r_c , and height, h , which was defined by the diameter of the laser beam waist. Using the simple formula of a cylinder, the probe volume was calculated by

$$V_p = 2 \pi (r_c)^2 h \quad (4-1)$$

Given that r_c is 9 μm and h is slightly larger at $\sim 10 \mu\text{m}$, the size of the probe volume was calculated to be 0.636 pL; which is well below the upper limit for SMD of 10 pL as mentioned in chapter one. Because the laser beam will not be a perfect cylinder as it passes through the capillary, the 0.636 pL value is an estimation. To more accurately estimate the

size of the probe volume, the intensity of laser radiation within the capillary will need to be accurately measured or modelled accounting for capillary and laser geometry and refractive index gradients.

Studies were then done to evaluate the magnitude and temporal stability of the amount of background signal. The system was aligned and optimized according to the protocol as explained in chapter 2. Figure 4-1 shows the background signal which was initially obtained upon alignment and optimization at a methanol flow velocity of 1.52 cm/s at a laser power of 50 mW. As can be seen in Figure 4-1, there was a periodic signal burst in both detectors. This fluctuation was thought to be either a result of electronic noise from a source such as an impedance mismatch or fluctuations in the laser power. Both of these factors were ruled out upon further testing. It was then postulated that the periodic nature of the signal could have been due to a vibration in the capillary caused by heating from the laser and/or by flowing air currents in the laboratory. Capillary vibration would cause detector fluctuations resulting from laser scatter; more laser scatter would occur when the laser was focused on the inner wall of capillary would scatter than occurs if the beam was situated in the center of the flowing stream. To validate the heating postulate, the flow rate of the methanol was increased to velocities of 1.87 cm/s (Figure 4-2) and 13.6 cm/s (Figure 4-3). As the flow was increased both the period and size of the signal bursts decreased. Because of this result and the observation that the signal spikes on detector one were always larger than on detector two, capillary vibration was confirmed. The amplitude of vibrations for channel one would be greater than channel two because the probe volume of channel two was situated closer to a point of attachment of the capillary than channel one (see Figure 2-

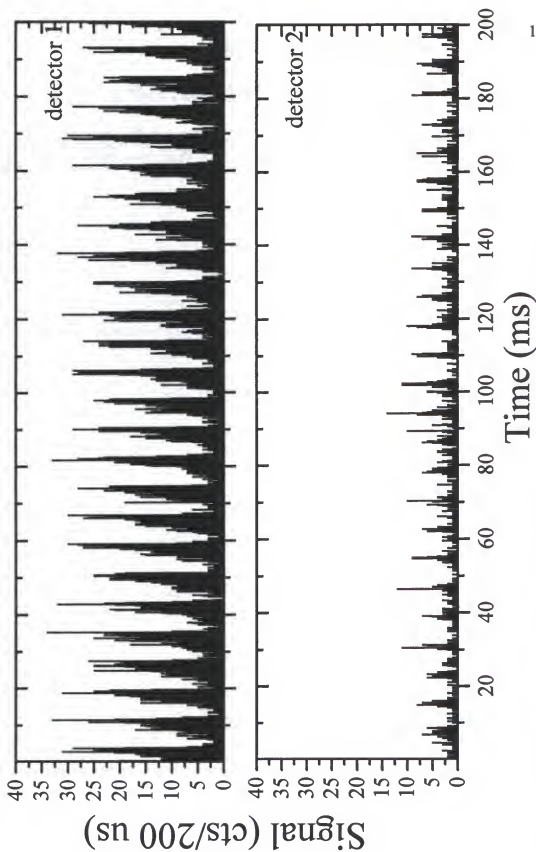


Figure 4-1 Background signal with a methanol flow rate of 1.52 cm/s

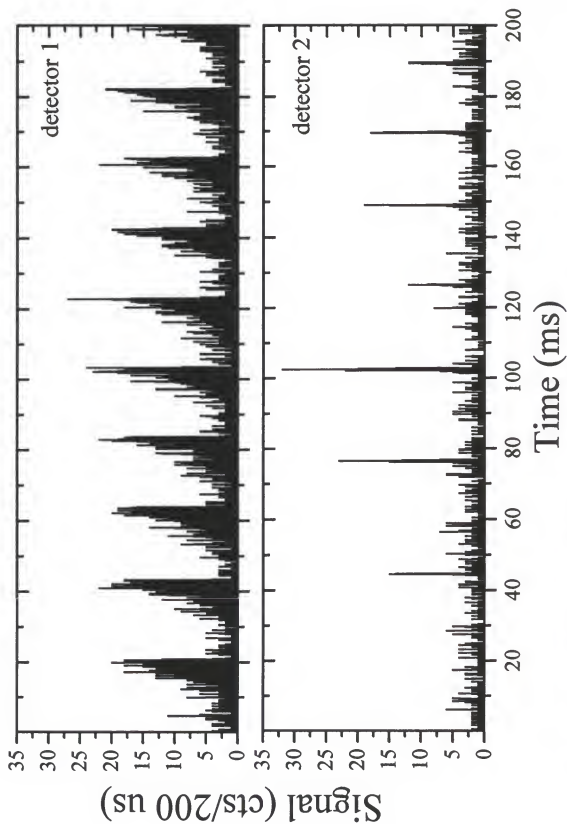


Figure 4-2 Background signal with a methanol flow rate of 1.87 cm/s

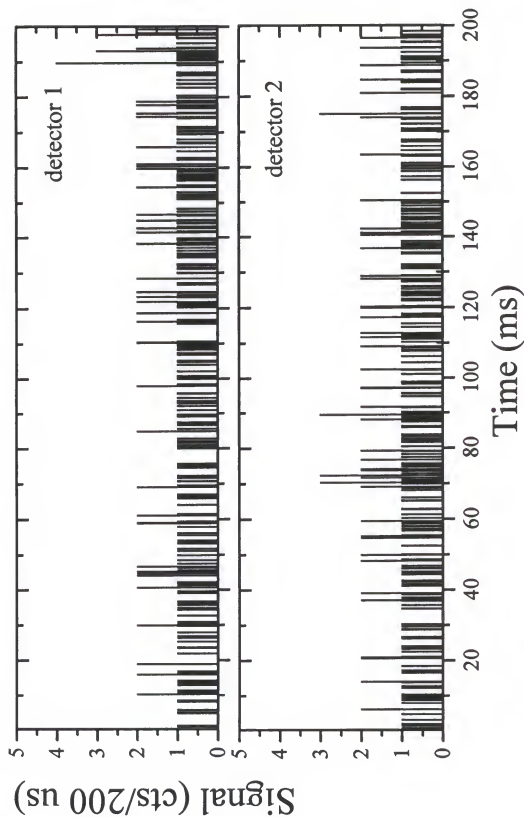


Figure 4-3 Background signal with a methanol flow rate of 13.6 cm/s

5). The temperature increase of a solution of IR 140 in methanol (nM) caused by absorption of laser radiation was calculated by methods used in thermal lens spectroscopy,¹²³

$$\Delta T = \frac{P \alpha}{2 \pi k} \quad (4-2)$$

where ΔT is the temperature difference (K) between the illuminated and nonilluminated sample, P is the laser power (W), α is the absorptivity of absorber (cm^{-1}), k is the thermal conductivity of the solvent ($\text{W K}^{-1} \text{m}^{-1}$). A temperature change of only 2 mK was calculated under the experimental conditions; therefore, the heating of the capillary was due to absorption of laser energy by the capillary fused-silica. The capillary mount was improved by moving the mount fittings closer together so that a shorter distance of capillary was exposed between the fittings (from 8 cm to 3.5 cm) yielding greater capillary tension. This significantly reduced the amount of vibration as can be seen by the background signal at low flow rate (1.2 cm/s) taken after the improvement of the mount (Figure 4-4). The temporal stability of the background was then investigated and is shown in Figure 4-5. Background signal levels were consistent over a nine hour period indicating that the tuning and alignment were stable over that time frame. Hence, the stability was sufficient to allow ultrasensitive fluorescence analysis to take place over an extended period of time.

Linear Flow Velocity

Prior to detecting fluorescence bursts from single molecules, a nominal linear velocity (cm/s) of the bulk solution had to be measured so that fluorescence obtained from

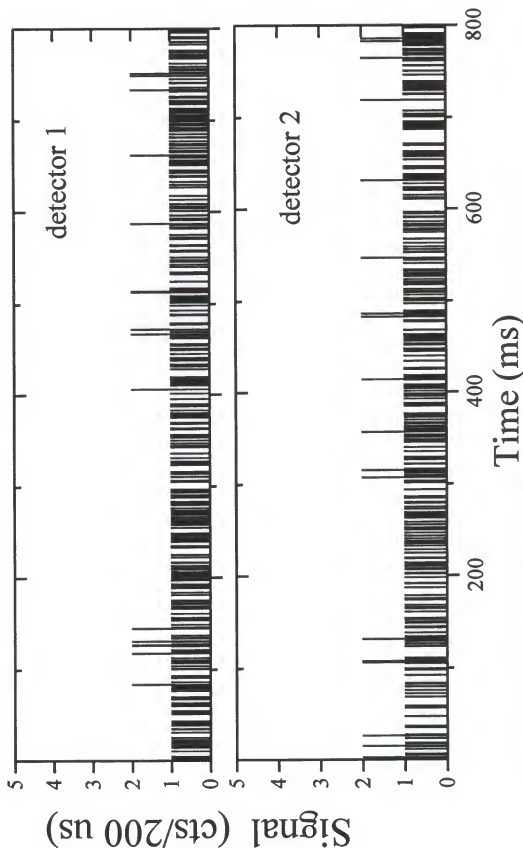


Figure 4-4 Background signal after capillary mount improvements

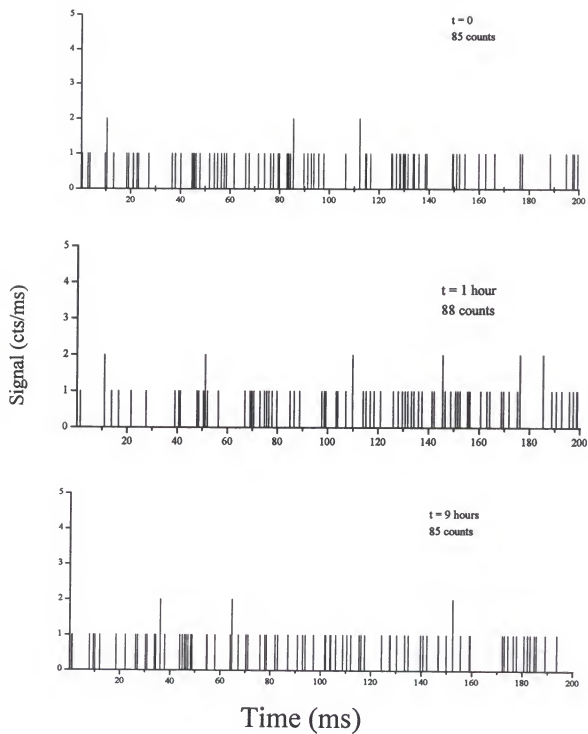


Figure 4-5 Background signal temporal stability

the fluorescent probes could be optimized for high emission with minimal photobleaching. A typical method to make such a flow rate measurement was to perform a flow injection experiment. One type of flow injection measurement would be to inject a plug of sample into the column and measure the time it took to reach the detector knowing the distance of column from the sample injector to the detection volume. Since the SMD system was equipped with sequential on-column detection, another more accurate version of the flow injection method could be performed. Similarly, a sample plug would be injected into the column, but now, instead the distance over which the velocity is timed is between the two detectors. A Gaussian shaped peak would be observed at each detector and the difference between the time of the arrival of the peak centroid at each detector divided by the distance between the detectors would yield the average linear flow velocity ($\langle v \rangle$, cm/s). This method would increase the accuracy of the measured distance and eliminate any imprecision due to temporal injection errors.

A novel method was developed to measure the flow velocity so that an injection valve need not be installed into the SMD apparatus. This method was based on the photobleaching of IR 140 molecules as they passed through the first laser beam. It was noticed that if the first laser beam was blocked that, after a delay, the signal on the second detector would increase. Moreover, it was found that the delay time and the signal level increase were related to the linear velocity of the solution. Hence, it was postulated that if beam-one was blocked rapidly, the velocity of the solution could be calibrated from the delay time and the fluorescence signal increase observed in detector two. This experiment was performed at a bomb pressure of 100 psi and the type of signal obtained is shown in

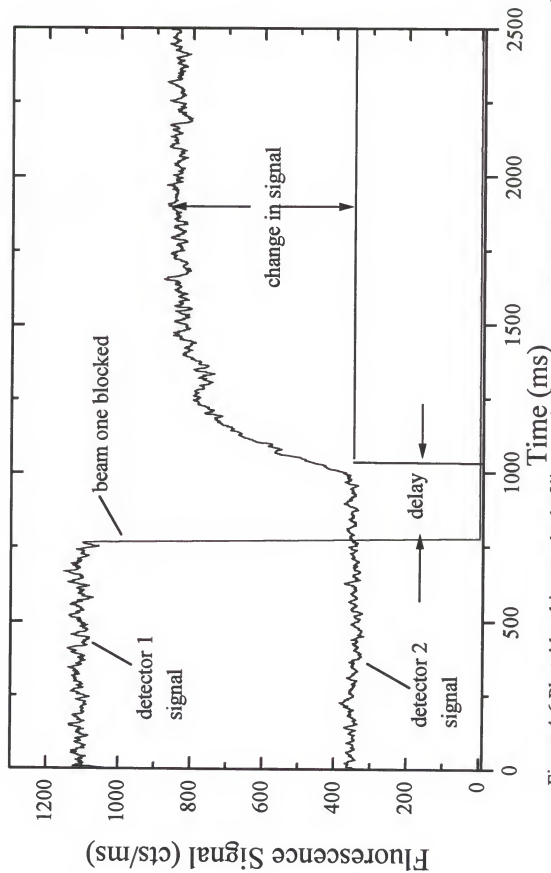


Figure 4-6 Photobleaching method of linear velocity measurement at a bomb pressure of 100 psi

Figure 4-6. The figure shows that after beam 1 is blocked (by rapidly sliding a card in front of the beam), the signal of detector 2 increases and there is a delay time of that increase. The laser powers used to obtain the data the linear velocity by photobleaching were 120 mW for laser one and 60 mW for laser two. Laser one was held at a high laser power to cause considerable photobleaching in the first probe volume and a more dramatic change in signal 2 was observed. Figure 4-7 shows the signals at different pressures (100, 200 and 400 psi respectively). Inspection of the graphs in Figure 4-7 several observations can be made as the flow velocity increased (higher pressure); 1) the overall fluorescence signal in both channels increased, 2) the delay time of the increase in signal in detector 2 decreases and 3) the change in signal of detector 2 decreased. Observations 1 and 3 are indicative of decreasing photobleaching with higher flow rates. The rise profile in detector two was caused by the convolution of the parabolic flow profile of the solution within the capillary, diffusion of the molecules as they exit the first probe volume and the Gaussian-shaped laser intensity. The next step in the study was to find a suitable method of evaluating the photobleaching data to yield a calibrated average flow velocity which could be used as a nominal value for SMD.

The linear velocity was extracted from the photobleaching data either by using the delay time for the channel 2 signal to rise or by using the absolute number of molecules photobleached. Two methods were therefore evaluated to obtain the linear velocity from the delay time (see Figure 4-8). The first method consists of determining the average linear velocity ($\langle v \rangle$) from maximum velocity (v_{\max}) which is given by

$$v_{\max} = \Delta z / \Delta t_{\min} \quad (4-3)$$

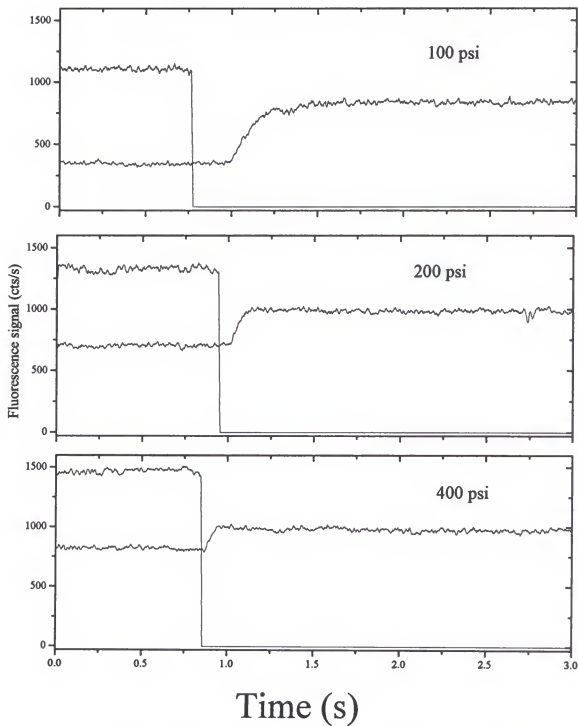


Figure 4-7 Photobleaching signal as a function of bomb pressure.

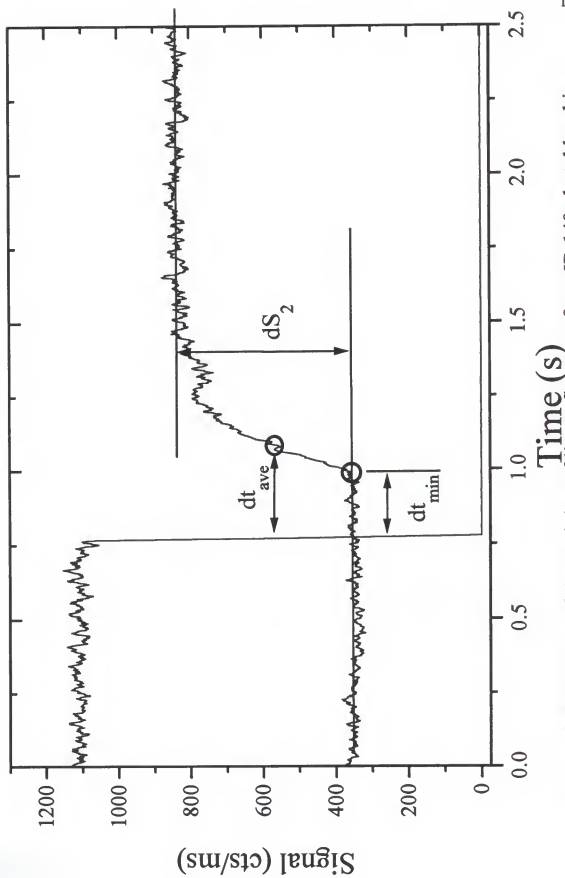


Figure 4-8 Methods of determining of linear flow rate from IR 140 photobleaching.

where Δz is the measured distance between the probe volumes and Δt_{\min} is the change in time from beam 1 being blocked to the time for signal 2 to just begin rising. This point was determined by intersection of the detector 2 average (signal prior to laser one blockage) and a line extrapolated along the signal rise in the same channel. The distance between the probe volumes is accurately measured by translating the collection microscope from the first probe volume up to until the signal from the second probe was detected. Because the probe volumes themselves and the precision of the translation stage (0.001 mm) were small, an accurate inter-probe-volume distance was made ($\Delta z = 1.429 \pm 0.006$ mm). Once v_{\max} was obtained, $\langle v \rangle$ was calculated using the relationship $\langle v \rangle = v_{\max}/2$. The second method resulted in the average linear velocity directly through the relationship

$$\langle v \rangle = \Delta z / \Delta t_{\text{ave}} \quad (4-4)$$

where Δt_{ave} is the time change from the laser blockage to the time when the signal has risen half way up to its maximum value (see Figure 2-8). When the average linear velocities of the two methods are compared they should be in agreement. It was found that the velocity obtained using method 2 was consistently higher than found with method 1. Diffusion and the Gaussian intensity profile of the laser distorts the shape of the rise and therefore affects the measurement of method two to a greater degree. Because of this reason and because method 1 resulted in values closer to the theoretical values, method one would be used to calculate the nominal average linear flow velocity. In Table 4-1 and Figure 4-9 the measured linear flow velocities at various pressure drops across the capillary ($P_{\text{bomb}} - P_{\text{atmosphere}}$) utilizing method 1 are given.

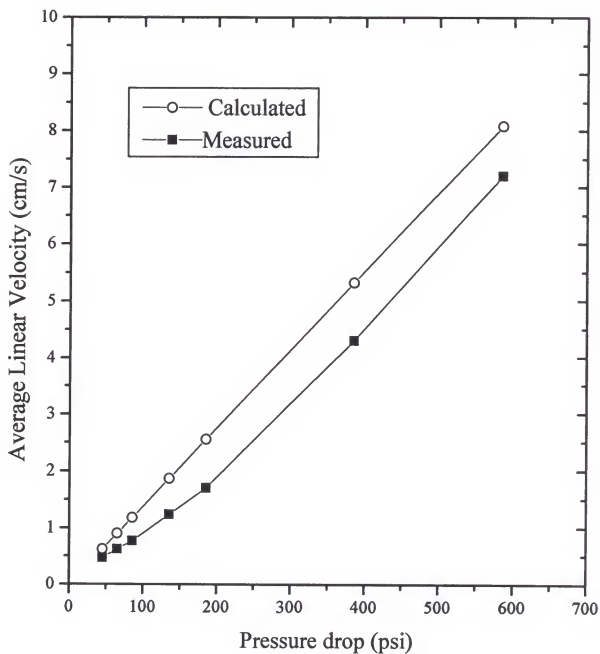


Figure 4-9 Calibration curve of pressure bomb by method 1.

Calculated values were obtained using equation 2-1. Differences between the measured and calculated values could be due to variance in the capillary inner diameter ($9 \pm 1 \mu\text{m}$), miscalibration of pressure regulator, temperature fluctuation, etc.

Table 4-1 Calibration of linear flow velocity by method 1.

Pressure drop (psi)	Linear flow velocity (cm/s)	
	calculated	measured
45.3	0.62	0.47
65.3	0.90	0.62
85.3	1.18	0.77
135.3	1.87	1.24
185.3	2.55	1.70
385.3	5.32	4.30
585.3	8.08	7.20

As mentioned previously, the average linear velocity could also be measured by the degree of photobleaching of the molecules as they pass through the laser beam. Mathies *et al*¹⁸ and Larson *et al*²⁴ have developed the mathematics to describe the degree of photobleaching of a molecule as it flowing by a laser beam. The equations were developed to quantify the photodestruction quantum yield (Q_d) from the measured fluorescence intensity ($S(F)$) as a function of linear flow velocity. One of the main parameters of the model was the photoalteration constant (F) and is given by

$$F = \frac{3.8 \times 10^{-21} \epsilon P Q_d}{\sqrt{\pi} \omega v} \quad (4-5)$$

where ϵ is the molar absorptivity of the fluorophore ($\text{cm}^{-1} \text{M}^{-1}$), P is the laser power (photons

s^{-1}), Q_d is the photodestruction quantum yield, ω is the focused laser beam radius (cm) and v is the linear flow velocity (cm/s). The normalized fluorescence intensity (S') is given by

$$S' = \frac{1}{F} \sqrt{\frac{2}{\pi}} \times \int_0^1 \frac{1 - \exp(-\sqrt{2} F u)}{2 u \sqrt{-\log u}} du \quad (4-6)$$

where u is an integration variable and S' is the normalized fluorescence intensity given by

$$S' = S(F) / S(0) \quad (4-7)$$

where $S(F)$ is the fluorescence intensity measured at a given F and $S(0)$ is the intensity that would be observed if the dye was not photolabile. Since the photodestruction yield for IR 140 has been measured (2.6×10^{-6})⁶⁷ and the fluorescence intensity can be measured, the flow rate can be calculated by equation 4-6. Figure 4-10 shows the calculated normalized fluorescence intensity as a function of flow velocity and measured values obtained in this study. Measured points on Figure 4-10 were obtained from the change in fluorescence intensity data of channel 2 from the previous method of velocity calibration. In this case, the measured relative fluorescence intensity change in detector 2 was measured and then related to the calculated photodestruction curve shown in Figure 4-10 to obtain the flow rate. As can be seen, the measured values match fairly well to the calculated curve. These velocity measurement methods illustrate the wealth of information which can be gained in the on-column sequential dual channel LIF system.

As elucidated by Lee,⁶⁷ the optimum transit time of a molecule through a 1 pL probe volume for SMD of IR 140 with this system was ~ 1 ms. Since the radius of the capillary and laser focus used in this work were $1 \mu\text{m}$ smaller than used previously, the optimum

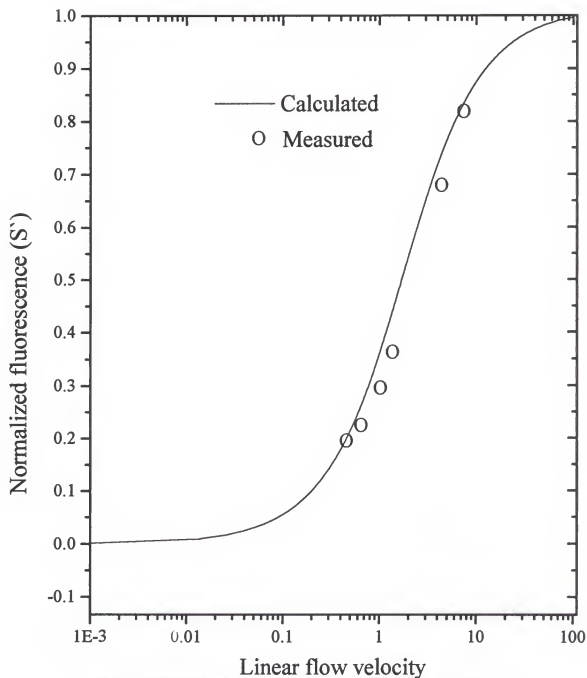


Figure 4-10 Photodestruction curve for IR 140 with fitted values using method 1

linear flow velocity needed to be recalculated. The transit time (τ_p , s) estimated by

$$\tau_p = (\pi \omega) / (4 \langle v \rangle) \quad (4-8)$$

where ω is the width of the laser beam (cm) and $\langle v \rangle$ is average linear velocity (cm/s). At a pressure of 150 psi, the linear velocity is 1.2 cm/s (see Table 4-1) and at a 9 μ m laser width, the transit time was calculated to be 0.58 ms. This flow rate was used throughout the remainder of the experiments described in this research.

Fluorescence Signal Saturation

To maximize the observed fluorescence signal while minimizing the degree of photobleaching, a study was undertaken to simultaneously measure the fluorescence and photobleaching under varying laser power. This was done at the constant average linear flow velocity chosen for the SMD experiments (1.2 cm/s). Figure 4-11 shows the observed fluorescence signal obtained at both detectors as a function of the laser power of beam 1. The laser power of channel 2 was held at 60 mW so that information about the photobleaching could be obtained along with fluorescence saturation. The deviation from linearity in the signal of detector 1 is a convolution of the saturation of the optical transition and photobleaching effects. Linearity of detector one begins to deviate at ~ 20 mW and significantly above 50 mW. The decreasing signal in detector 2 is a result of increasing photobleaching at higher laser powers. As can be seen in Figure 4-11, photodestruction levels off at a laser power of ~ 110 mW. In order to maximize the fluorescence signal to photobleaching ratio, a laser power of 20 mW (power density = 19.6 kW cm²) was chosen for the SMD experiments. It is of paramount importance to the sequential detection of

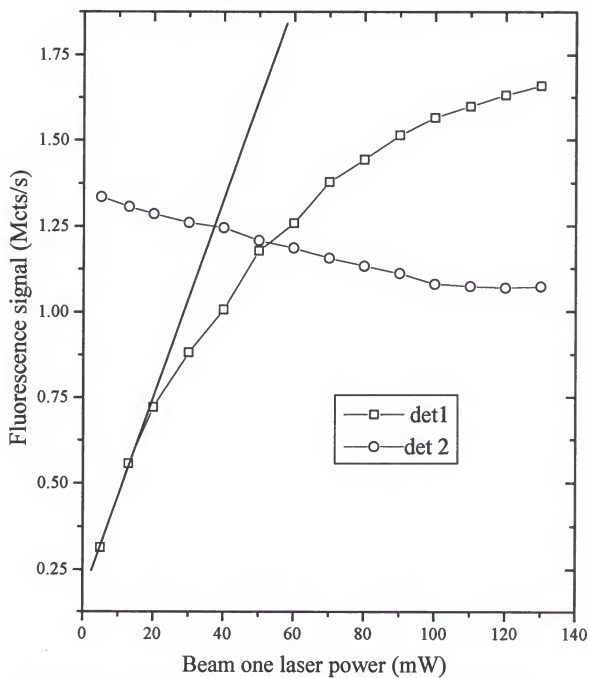


Figure 4-11 Saturation of fluorescence signal while monitoring photobleaching.

single molecules that photobleaching not be complete as they pass through the first laser beam. Otherwise, molecules observed in the first channel would not be observed in the second.

Calibration Curve

To demonstrate the sensitivity and linear dynamic range of both channels, calibration curves of fluorescence versus concentration of IR 140 in methanol were constructed. These curves were obtained utilizing an average linear flow velocity of 1.2 cm/s ($\tau_p = 0.74$ ms) and an equal laser power at each channel of 70 mW. Solutions were made through serial dilutions of a 10 μ M stock solution on the day of the experiment. To help alleviate photobleaching of the solutions prior to analysis, they were placed in a dark box until they were analyzed. Figure 4-12 is a calibration curve with the signals from each channel obtained independently, i.e., laser beam one was blocked for the detector two measurements. The curves both show a linear dynamic range from 0.1 nM to 10 pM and show good correlation between channels in terms of sensitivity and absolute signal. Detector one shows a slightly higher sensitivity at low concentrations. This was most likely because the fluorescence collection interference filter on channel one has a ~ 5 % higher transmission at its bandpass maximum than the filter on channel two. Below 10 pM, the sensitivity of the calibration curve decreases dramatically for both channels. Below a concentration of 2.9 pM, less than one molecule resides in the probe volume for a given transit time. Therefore, the signal levels off due to the lack of molecules in the probe volume as dictated by sampling statistics and the limitation of the blank signal. Figure 4-13 is a calibration curve obtained

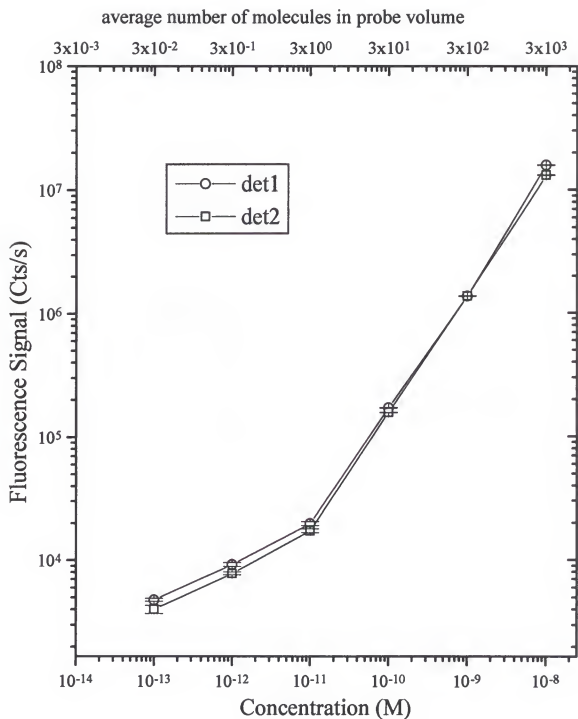


Figure 4-12 IR 140 calibration curve with channels measured independently.

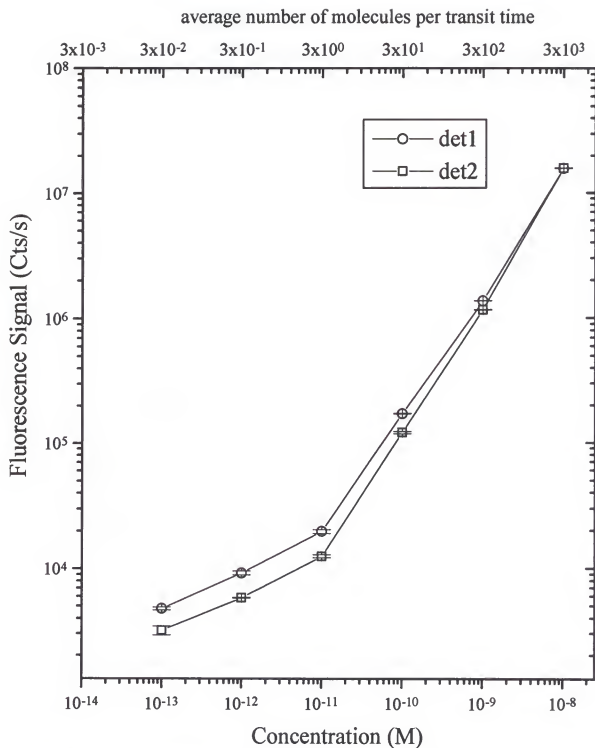


Figure 4-13 IR 140 calibration curve obtained simultaneously in both channels

with both channels operating simultaneously. Photobleaching of the molecules as they pass through beam one is observed through the slight decrease in the fluorescence signal in detector 2. The linear dynamic range of this system may be extended above 0.01 μM through the use of neutral density filters.

Single Molecule Measurement

With the knowledge gained from the previous studies, namely, the characterization of the background, linear flow velocity, and optimization of laser power, experiments involving the measurement of single molecules were performed. Table 4-2 summarizes the experimental parameters used for single molecule measurement (SMM) studies described in this chapter. Utilizing equation 1-9, the Poisson probability of n molecules occupying the probe volume in a given transit time were calculated for an IR 140 concentration of 0.1 μM and a 0.64 pL probe volume (see Table 4-3). As can be noticed, most of the time, there are no molecules in the probe volume with rapidly decreasing probability of 1, 2, and 3 molecules. On only very rare occasions, more than one molecule will be present in the probe volume. Thus, the signals obtained at 0.1 μM were considered to be from single molecules. Initially, SMM was performed on each channel independently to assure that both of them were capable of single molecule sensitivity. In other words, data collected for channel 2 were carried out with laser beam one blocked. Figures 4-14 and 4-15 show the collected data for the darkcount, blank and 0.1 μM IR 140 for channels 1 and 2 respectively. The the dark counts in the detector were negligible in each case.

Table 4-2 Experimental parameters for SMM studies.

dye	IR 140 @ 0.1 pM
solvent	methanol
capillary	9 μm o.d. and 150 μm i.d.
laser power	beam 1 = beam 2 = 20 mW
probe volume	0.64 pL
calculated transit time	0.58 ms
linear flow velocity	1.21 cm/s
MVF temperature	149 $^{\circ}\text{C}$

Table 4-3 Occupation probability for different numbers of molecules in the probe volume at any given time ([IR 140] = 0.1 pM, probe volume = 0.64 pL).

# of molecules in probe volume (n)	Occupation Probability
0	0.962
1	0.037
2	0.0007
3	9×10^{-6}

Furthermore, the signal counts in each channel for the IR 140 solution were clearly greater than that obtained for the blank. As will be shown, spikes in the IR 140 data stream were due to single molecules passing through the focused laser beam. As mentioned in Chapter 1, there are three criteria to confirm the detection of single molecules 1) higher signal counts per integration time for the fluorophore than the blank in the histograms of the data, 2) a nonrandom correlation of the autocorrelation function for the fluorophore corresponding to the transit time of the molecule through the probe volume and 3) direct observation of fluorescence bursts from individual molecules. Each criterion to confirm

Channel 1

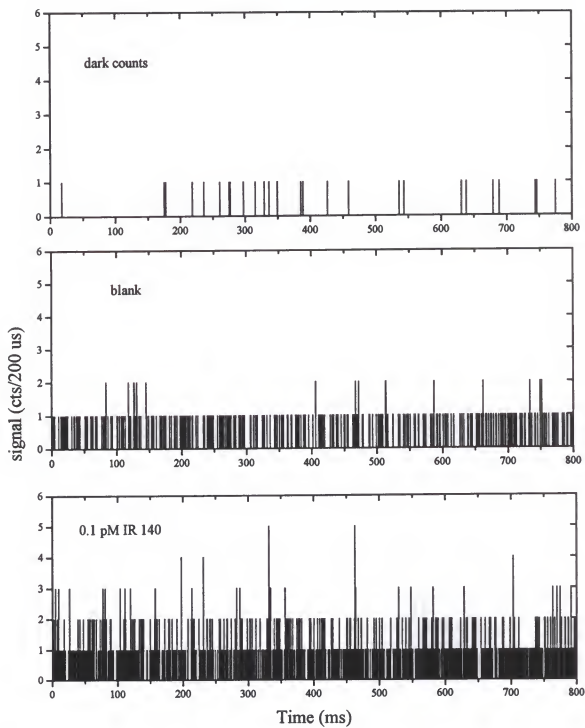


Figure 4-14 Channel one signal from dark counts, blank and 0.1 pM IR 140

Channel 2

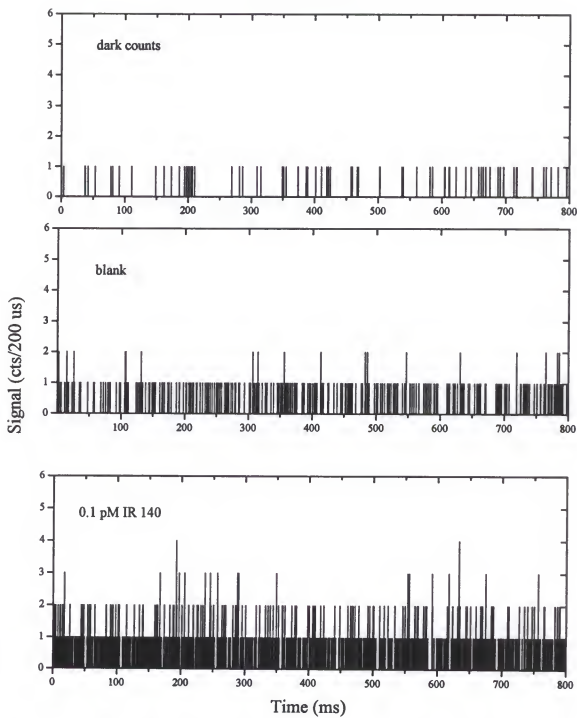


Figure 4-15 Channel two signals for dark counts, blank and 0.1 pM IR 140.

SMD was used to evaluate the data in order to show the detection of single molecules independently in each channel. The first criterion was met and can be seen in the histograms of the blank and IR 140 signals shown in Figure 4-16. Of the total 4000 integration bins, over 3000 of them had zero counts for the blank and the other 1000 were split between 1 and 2 counts per bin. Conversely, for the IR 140 solutions, a greater frequency of 1 and 2 counts were obtained and counts of 3, 4, and 5 were detected as well. This evaluation provides indirect proof that single molecules were detected in each channel.

The second method of confirming the observation of single molecules was performed through the use of the autocorrelation function, $G(\tau)$ (see equation 1-10 in Chapter 1). Autocorrelation analysis was performed utilizing a data reduction software package called DaDISP 4.0 SE running on a P-100 MHz PC. Figure 4-17 gives the autocorrelation plots for the raw unprocessed IR 140 and blank data (from Figures 4-14 and 4-15) for both channels. Nonrandom correlations were found in the IR 140 data and none were noticed in the blank data. Peaks at a delay time of zero, as seen in the IR 140 autocorrelations, are indicative of nonrandom events. Nonrandom correlations in the IR 140 $G(\tau)$ were due to correlated photon bursts given off as the molecule traversed the laser beam. The width of the correlated peak in the IR 140 autocorrelation revealed the average transit time of the molecule passing through the probe volume. No peak in the blank autocorrelation showed that only the random part of the correlation was present. Average transit times were interpolated from the IR 140 autocorrelation peaks Figure 4-17 for both channels and were found to be the same at a value for each at 0.58 ms. This compared rather well to the transit time of 0.58 ms which was estimated in the previous section using the measured average

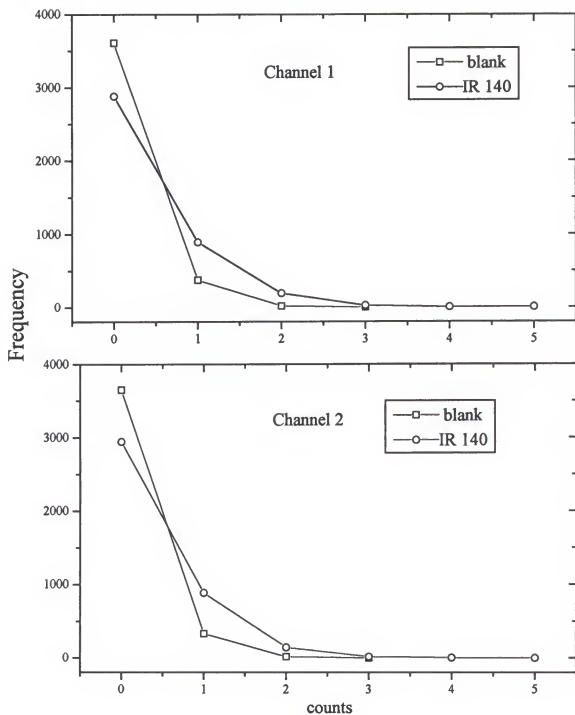


Figure 4-16 Histograms of the raw data for the blank and IR 140 in both channels.

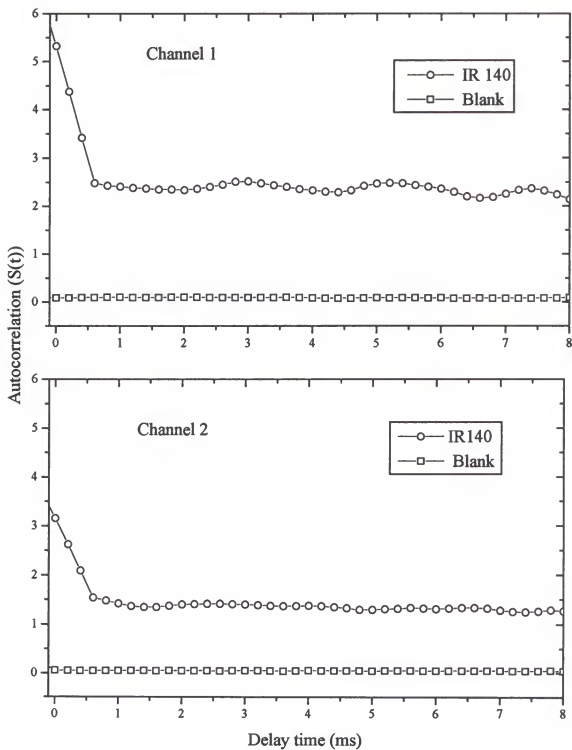


Figure 4-17 Autocorrelation plots for IR 140 and blank data in both channels.

linear flow velocity. As was noticed in the calibration studies, a higher sensitivity of channel one over channel two was observed in the autocorrelation analysis as indicated by the larger nonrandom correlation peak calculated for channel one (see Figure 4-17). Despite the information gained from the histograms and autocorrelation analysis, direct proof of fluorescence bursts due to individual fluorophores remains to be clearly seen.

Fluorescence photon bursts emanating from single molecules are difficult to visualize in the raw data obtained with the modest signal-to-noise ratios observed and because of the way in which the data is binned (see Figures 4-14 and 4-15). To enhance the visibility of photon bursts, the data was passed through a mathematical summing filter which selectively enhanced correlated photon events over random noise. As mentioned in Chapter 1, there are two types of filters used throughout SMD literature to enhance photon bursts; the sliding sum filter (SSF, eqn. 1-13) and a weighted quadratic summing filter (WQS, eqn. 1-12). These filters sum the average number of integration bins per molecular transit time to augment the height of the photon burst. SSF and WQS filtering was implemented on the obtained data for the blank and 0.1 IR 140 solutions in both channels (see Figures 4-18, 4-19, 4-20 and 4-21). By running the filters over the raw data, the photon bursts are greatly enhanced over the random background and become clearly visible. As stated in Chapter one, the weighting factor in the filter was chosen to best describe the distribution of the photon burst. The weighting factor used for both filters was $w(t) = 1$, because it was found in a statistical study that the sensitivity of the filter was best with this factor despite the actual shape of the photon burst (see the Appendix). The number of integration bins per transit time, $k = 3$, used in the filters, was calculated by dividing the measured transit time (0.58 ms)

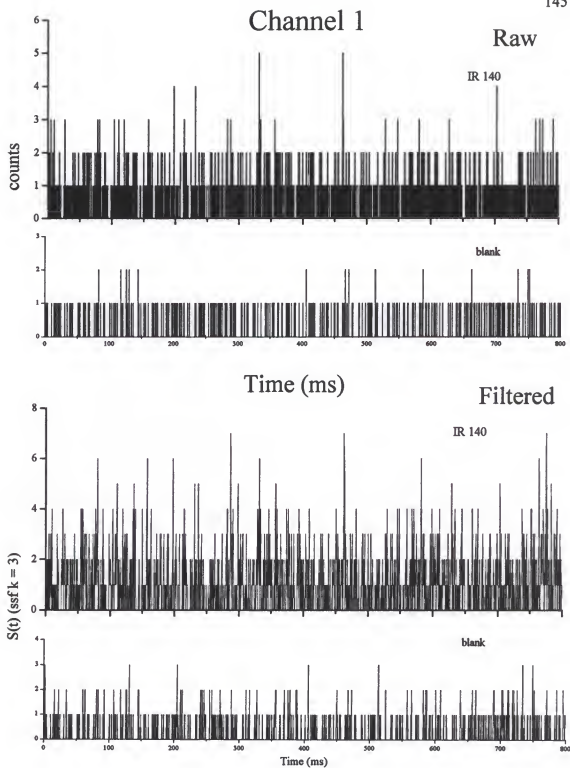


Figure 4-18 Comparison of raw and SSF data for channel 1.

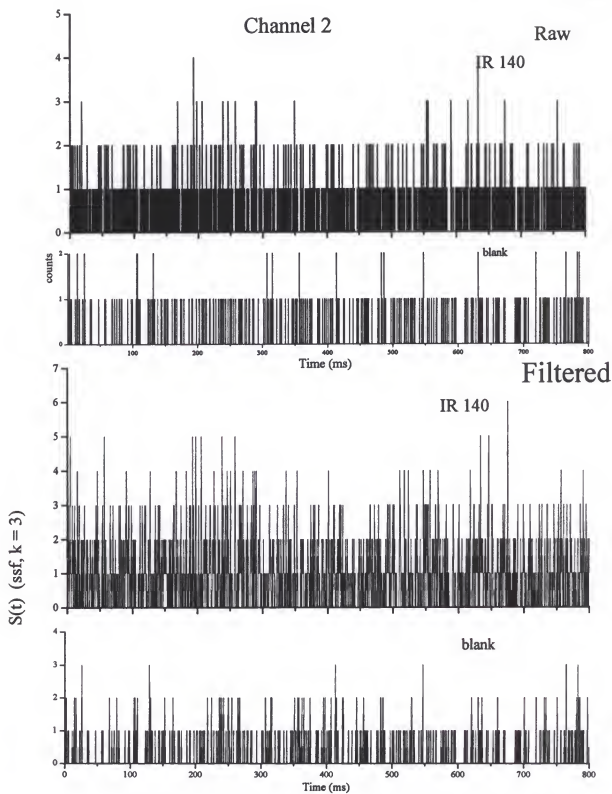


Figure 4-19 Comparison of raw and SSF data for channel 2.

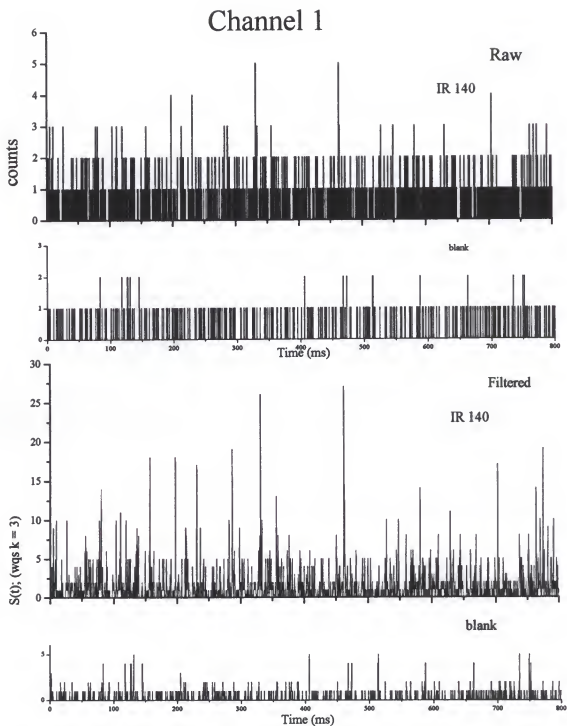


Figure 4-20 Comparison of raw and WQS data for channel 1.

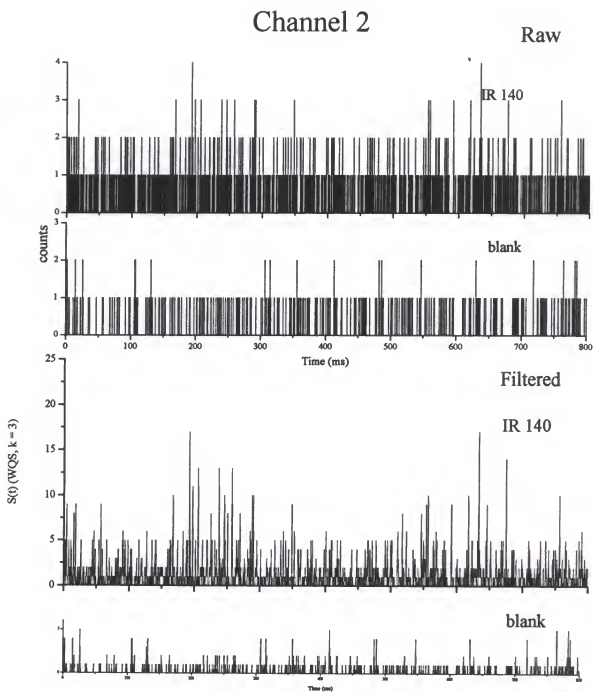


Figure 4-21 Comparison of raw and WQS data for channel 2.

by the width of the integration bin (200 μ s). By comparison, the WQS filter enhanced the photon burst to a larger degree than the SSF (comparing Figures 4-18 and 4-20). The variations in peak height are attributed to the convolution of spatial variations in laser intensity and the random emission of photons from the molecules and the blank.

The average number of expected events from a single molecule as it passes through the laser beam may be calculated. These events are the number of time integrations with counts from IR 140 above the discriminator level. The number of events (N_e) for a given measurement time (T) is given by

$$N_e = \langle N_p \rangle T k / \tau_p \quad (4-8)$$

where $\langle N_p \rangle$ is the average number of molecules in the probe volume (0.039, from eqn. 1-8), k is the number of integration bins per transit time ($k = 3$) and τ_p is the transit time (0.58 ms). For this experiment, the expected number of events over the 800 ms measurement time was calculated to be 165. By dividing the expected number of events by the number of bins per transit time (k), the approximate number of molecules (n) detected during the measurement time is obtained. For this experiment, with a measurement time of 800 ms, approximately 55 molecules would pass through the probe volume. The detection efficiency (ϵ_d) is defined as the ratio of the number of molecules detected (n_d) to the expected number of molecules passing through the probe volume (n). This is given by

$$\epsilon_d = n_d / n \quad (4-9)$$

To differentiate between background and photon bursts from single molecules, a discrimination level is set. To minimize the probability of false positives, the discriminator value is set to the maximum peak size in the histogram of the background. All events above

the discriminator are then recorded as being from individual molecules. A discriminator level for the SSF data was found to be 3 in both channels and for the WQS data, 5 in both channels. Upon further inspection of SSF and WQS histograms, the number of observed events for channel one was 128 (SSF), 155 (WQS) and for channel two 122 (SSF), 153 (WQS). The number of detected molecules by SSF was 43 and 40 for channels one and two. For the WQS filter, channel one detected 52 molecules and channel two 51 molecules. Hence, the detection efficiencies for channel one were 0.78 (SSF) and 0.95 (WQS). Channel two detection efficiencies were 0.73 (SSF) and 0.93 (WQS). Increased detection efficiency by filtering with the quadratic summing filter indicates that it should be used to analyze single molecule data. Errors in dilution, the size of the probe volume and the linear velocity could have caused the detection efficiency to be less than unity.

The overall measurement efficiency for each channel was calculated using equation 1-10 ($\epsilon_m = \epsilon_T \epsilon_d \epsilon_p$). The transfer efficiency of transporting the sample to the probe regions was assumed to be unity (adsorption of the molecules to the capillary wall was assumed to be negligible). Using CW excitation and overfilling the capillary with laser light, a laser probing efficiency of unity was obtained. Given the detection efficiencies for channel one, 0.95 and channel two, 0.93, the overall measurement efficiency for each channel was therefore 0.95 and 0.93, respectively. Because of such a high measurement efficiency, it can be stated that molecules are being efficiently *measured*. Other SMD methods have higher signal-to-noise ratios, however, none can claim measurement efficiencies near unity as does the technique given in this research. The results from these SMD experiments is summarized in table 4-4.

Table 4-4 Results from Independent SMM experiments

SSF discriminator (channels 1 and 2)	3
WQS discriminator (channels 1 and 2)	5
expected number of events	165
<u>measured number of events channel 1</u>	
SSF data	128
WQS	155
<u>measured number of events channel 2</u>	
SSF data	122
WQS data	153
<u>detection efficiency</u>	
channel 1	0.95
channel 2	0.93
laser probing efficiency	~1
sample transport efficiency	~1
<u>overall measurement efficiency</u>	
channel 1	0.95
channel 2	0.93
<u>ave photoelectrons per molecule*</u>	
channel 1	12
channel 2	9

* The average number of photoelectrons per molecule was calculated with $(\Sigma C)/n$, where n is the number of molecules measured in the measurement time above the WQS discriminator and C is the number of photon counts from an individual molecule using the raw data.

Sequential Single Molecule Measurement

The next step in the research was to measure photon bursts from individual molecules sequentially as they pass through two detection channels. It has been shown in this chapter that efficient single molecule measurement is possible in each channel. Here, counting in

both channels occurs simultaneously so that a molecule detected in channel will be interrogated again upstream in the second channel and detected. Because the detection volumes were so close together (1.429 mm) there were concerns about crosstalk between the two channels. In other words, the detection of light in channel one would originate from the second probe volume and vice-versa. To test for this problem, an experiment was devised in which channel one was monitored under two different conditions. In one condition, beam one was blocked while beam 2 was engaged. The other condition involved the blockage of both laser beams. In this manner, the amount of crosstalk was measured by taking the difference between the signal obtained in channel one with and without beam two being engaged. Figure 4-22 shows the results of this experiment. As seen in that figure, there is a significant decrease of signal in channel 1 when laser two was blocked (>100 cts). Although this value is small compared to the signal from the blank, for the sequential SMM experiments, the inter-probe-volume distance was increased to 2.78 mm to minimize crosstalk. At that distance, the crosstalk decreased dramatically and it found to be negligible for sequential SMM. At an average linear flow velocity of 1.2 cm/s and an inter-probe-volume distance of 2.78 mm, the average time for a molecule to travel between the probe volumes is 232 ms.

With the exception of the increased inter-probe-volume distance, all of the conditions for the sequential SMM studies were the same as used previously in independent single molecule measurements (see Table 4-2). Typical, unprocessed data streams obtained simultaneously for IR 140 and the blank are shown in Figure 4-23. Indeed, both channels had a larger IR 140 signal than the blank indicating the detection of single molecules.

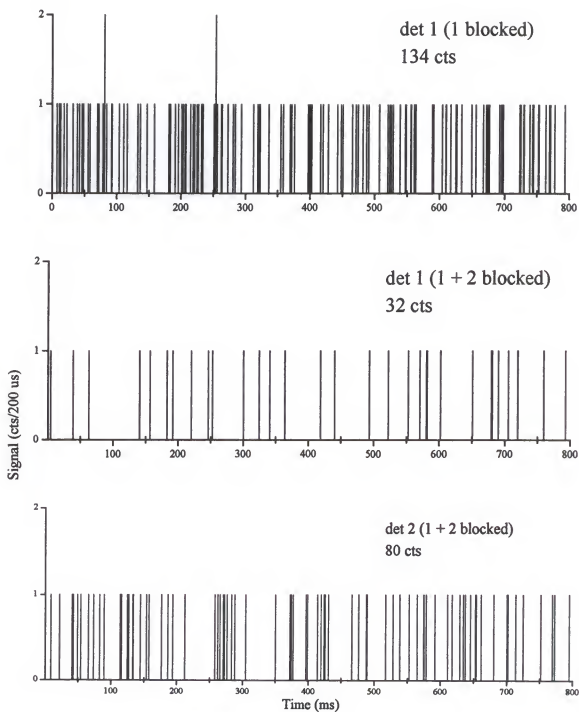


Figure 4-22 Crosstalk between detectors one and two.

IR 140

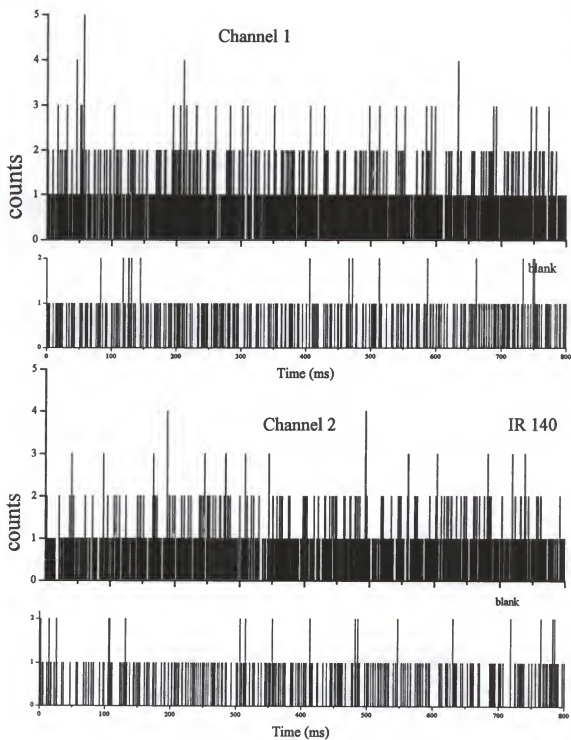


Figure 2-23 Raw data for simultaneous detection in two channels

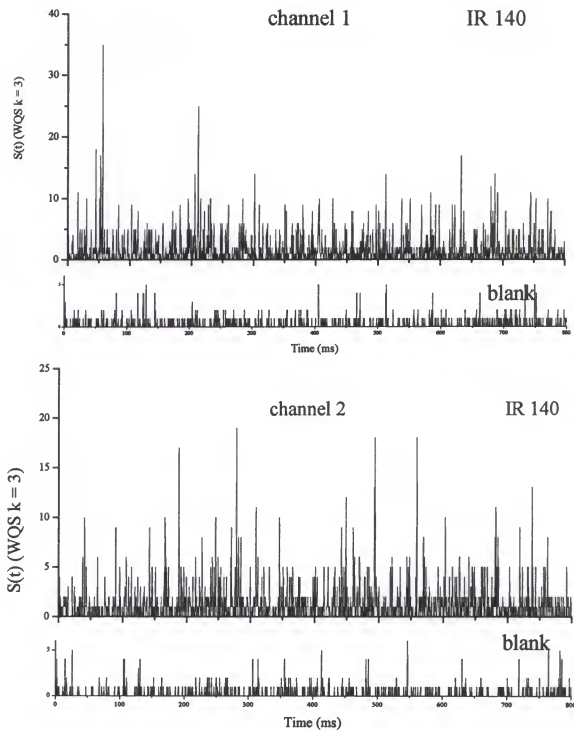


Figure 4-24 WQS data for simultaneous detection in 2 channels.

The observation of sequential detection here is precluded by the lack of visibility of the individual photon bursts. As performed previously, the data streams were run through the WQS summing filter to enhance the visibility of the bursts and increase the detection efficiency. The WQS filter was used exclusively because it gave the best detection efficiencies.

Figure 4-24 shows the data presented in Figure 4-23 after having been processed through the WQS filter. The expected average number of events for each channel was 165, equivalent to ~ 55 molecules over the 800 ms measurement time. Channel one recorded 174 events (58 molecules) and channel two detected 125 events (42 molecules) above the WQS discriminator of 5. Since the expected number of events is an average value and not an absolute value, the higher number of detected events in channel one was unexpected for SMM analysis. What was important was the fairly large decrease (28 %, $(58-42)/58 \times 100\%$) in the number of molecules counted in channel 2 as compared to channel 1. Although channel two was found to have a slightly lower detection efficiency, the main contribution to the decrease was photobleaching. By interpolating the normalized fluorescence intensity at the flow rate used for sequential SMM (1.2 cm/s) in Figure 4-10, the theoretical percentage of photobleaching was 40 %. The calculated photobleaching value was obtained assuming ensembles of molecules existed in the probe volume and not only a single molecule. Therefore, the extent of photobleaching in this experiment was actually less than predicted by theory. To decrease the amount of photobleaching, either a lower laser power for beam one should be used or the flow rate should be increased. With the current apparatus, significant changes in either one would not be trivial to perform. Unfortunately,

by significantly decreasing beam one laser power and/or increasing the flow rate, the signal-to-noise ratio would also be decreased.

WQS data streams from Figure 4-24 were expanded so that visual confirmation of sequential detection of individual fluorophores could be made (see Figure 4-25). Because it was expected that it would take 232 ms for a molecule to pass between the detection volumes, the data stream for the second channel was delayed by that amount of time. A distinct similarity in *position* between the peaks in channel one and two was observed. Recall that peaks heights will fluctuate inherently because of the random emission of photons and depending upon the amount of laser intensity they receive. Corresponding peaks in each channel are numbered to show the correlation between the channels. Peak numbers on channel two with arrows below indicate peaks lost due most likely to photobleaching. However, absent peaks could also represent a false negative signal or a molecule "darkened" in a long lived triplet state. Over the 260 ms time frame, detector one counted 19 molecules above the discriminator while detector two counted 11 molecules (42 % photobleaching). Peak assignments were based on visual observation first and confirmed by the time difference observed for each peak in the two channels. Of the 11 molecules counted in both channels, the measured average time to travel the distance between the probe volumes was 229.5 ± 5.2 ms in excellent agreement with the calculated value of 232 ms. The variance in the measured value could be due to diffusion of the molecule and the parabolic flow profile within the capillary. The average distance traveled by an individual molecule due to diffusion (σ_d) can be estimated using the relationship

$$\sigma_d = (2Dt)^{1/2} \quad (4-10)$$

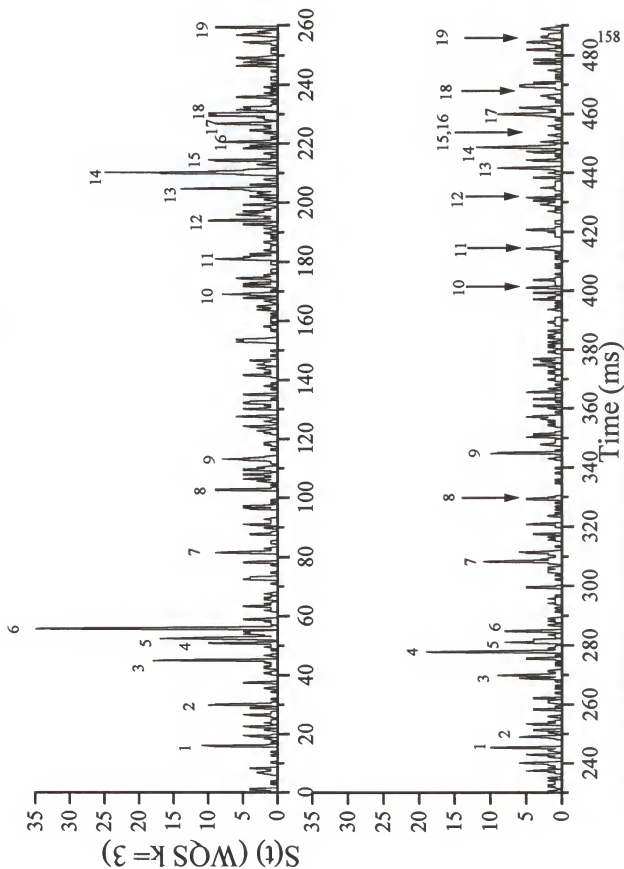


Figure 4-25 Sequential single molecule measurement. Numbers with arrow underneath indicate a photobleached molecule.

where D is the apparent diffusion coefficient ($5.13 \times 10^{-6} \text{ cm}^2/\text{s}$ for IR 140 in methanol) and t is the time over which the diffusion occurs (230 ms in our case). A spatial standard deviation of $\pm 2.19 \text{ } \mu\text{m}$ was obtained yielding a time deviation in each peak of $\pm 0.18 \text{ ms}$ (given the 1.2 cm/s linear velocity). Hence, diffusion was not the major cause of random in molecular travel between probe volumes. Primarily, this effect was due to the change in linear velocity of the molecule caused by the parabolic flow behavior within the capillary.

The observations made in these experiments, confirmed that individual molecules could be counted sequentially in 2 channels with the experimental apparatus described in this dissertation. Counting molecules sequentially in two channels is, arguably, the highest form of confirmation that individual molecules are being detected. The results from the sequential SMM experiments are listed in Table 4-5.

Table 4-5 Results from sequential SMM studies.

expected number of events	165 (55 molecules)
<u>measured number of events</u>	
channel 1	174 (58 molecules)
channel 2	125 (42 molecules)
average percentage of photobleaching*	28.0 %
<u>travel time between channels</u>	
calculated	232 ms
observed	$229.5 \pm 5.2 \text{ ms}$

* The average percent of photobleaching was calculated from the % relative difference between the number of molecules detected in channel 1 and channel 2.

CHAPTER FIVE

CONCLUSIONS AND FUTURE WORK

Conclusions

In summary, the work in this dissertation has characterized in detail a rubidium metal vapor filter for its use in single molecule detection and has shown the sequential on-column detection of single IR 140 molecules with high efficiency. Experimental and theoretical evaluations of the rubidium metal vapor filter (MVF) elucidated several interesting results. It was shown that the laser scatter from the capillary, attenuated by the metal vapor filter, was limited by a broadband emission originating from the titanium:sapphire laser. Transmission spectra of MVF revealed other sources of background radiation; e.g. collisionally populated rubidium fluorescence at 795.76 nm and Raman scatter from the methanol solvent at 1055 cm^{-1} . The capability of the system to measure Raman scatter from a 1.05 pL volume, demonstrated the high sensitivity of the Ti:sapphire, MVF and single photon avalanche photodiode combination. Transmission spectra of the MVF were obtained experimentally under different conditions of temperature, fill-gas pressure and laser power. It was found that the MVF operated most efficiently under conditions of high temperature, high pressure and low laser power.

The 2-channel SMD apparatus was characterized with each channel acting independently first and then with both channels detecting simultaneously. Sensitivity in each channel was illustrated with fluorescence calibration curves for IR 140 in methanol.

Each channel exhibited 3 decades of linearity (10^{-8} M - 10^{-11} M) and appreciable signal with less than one molecule in the probe volume per transit time. Calibration curves obtained in both channels simultaneously resulted in a decreased sensitivity in channel two due to significant photobleaching which occurred in channel one. Raw single molecule detection data was processed using sliding sum filtering and analyzed using statistical and autocorrelation analysis. The molecular transit time through the probe volume was calculated (0.58 ms) and obtained from the autocorrelation data for each channel. Autocorrelation analysis yielded a transit time of 0.58 ms for both channels confirming that the correlated events detected were indeed due to single molecules. Photon bursts were enhanced by two different sliding summing filters; weighted quadratic summing (WQS) and linear sliding summing (SSF) filters. It was found that the WQS filter visually enhanced the correlated photon bursts to a larger extent, but more importantly, had a higher detection efficiency than the SSF (0.95 vs 0.78 for channel 1 and 0.93 vs 0.73 for channel 2). Because the detection, laser probing and sample transport efficiencies were all near unity, it can be stated that the single molecules were *measured*. No other SMD technique can make that claim, even though signal-to-noise ratios of other techniques is often higher.

On-column sequential measurement of a single molecule was successfully achieved. Confirmation of sequential detection was performed visually and by matching the time difference for the molecule to traverse the inter-probe-volume distance. The calculated average time of 232 ms matched the average measured time of 229 ± 5 ms for the molecules to traverse the inter-probe volume distance. This confirmed the sequential detection of the individual fluorophores. It was shown that the variations of flow due to the parabolic flow

profile within the capillary caused the deviation of the measured value of inter-channel traversing time from the calculated value. The highest validation of the detection of single molecules was accomplished with the on-column sequential SMM technique presented in this dissertation.

Future Work

Work to be performed in the future on this project should include improving the instrument and applying the technique to an analytical problem. Improvements to the system should be done in order to increase the number of photoelectrons obtained from individual molecules. One way this could be achieved is by using a microscope objective of higher numerical aperture ($NA > 0.65$) to collect a greater solid angle of the emitted fluorescence. Furthermore, the SPAPD's used in this research have dead times on the order of 200 ns which significantly reduced the photon detection efficiency (number of photons emitted from molecule/number of photoelectrons counted). Detectors with dead times of 50 ns are now available which would greatly enhance the photon detection efficiency. A computer program based on a Monte Carlo simulation was used to show that the number of photoelectrons obtained per molecule with a 50 ns dead time detector could be as many as 80 (compared to the 9-12 photoelectrons obtained with the current detectors).

A very interesting application of the sequential on-column single molecule measurement system would be to perform a technique which we have coined single molecule electrophoretic-migration measurement (SMEM). In this technique, the molecules will flow through the capillary under the influence of electroosmotic flow. Because our system has the ability to efficiently measure single molecules sequentially on-column, the inherent

electrophoretic mobility of the fluorophore could be measured. This would be done by relating the electrophoretic velocity, obtained by timing the molecule across the known inter-probe-volume distance, to the inherent electrophoretic mobility of the molecule. In this manner, single molecules could be identified based on their electrophoretic velocity. Because such small capillaries are used on our SMM system, high electric fields could be used (>10 kV/cm); therefore enabling rapid solution determinations. This technique could prove useful where the rapid analysis of dilute solutions ($< \text{pM}$) was desired.

APPENDIX

STATISTICS OF SINGLE MOLECULE DETECTION

As the number of detected molecules is decreased to individual level, the processes which are detected in those molecules lose their "bulk" character and become more random in nature. In other words, instead of observing ensembles of molecules averaged out in large distributions, detection events are monitored which are random in nature. For this reason, many concepts typically used in analytical chemistry are no longer useful in the realm of single molecule detection. For example, the fluorescence burst profile obtained from a single molecule as it passes through a focused laser should reflect the spatial intensity of the laser. However, because only a few of the photons emitted from the molecule are collected and detected, the photon emission follows a Poisson distribution (which describes random events). Thus, the fluorescence burst profile of the molecule as it passes through the laser beam does not mirror the spatial intensity of the laser because it is severely distorted by the Poisson distribution of photons seen by the detector. Working with Chi-Hse Teng and Professor Mark K.C. Yang at the University of Florida Department of Statistics some of the statistical problems associated with single molecule detection were addressed. A brief description of the work performed will be discussed in this Appendix.

Occupancy of a Single Molecule

To reliably detect a single molecule, the probability of more than one molecule

occupying the probe volume must be minimized. In very dilute solutions, the arrival of the molecule to the probe volume is random and follows a Poisson probability distribution. Assuming the arrival *rate* is constant, the probability that n molecules will occupy the probe volume at one time can be given by

$$P(N_{t,k} - N_t = n) = \frac{(k \lambda_p)^n e^{-k \lambda_p}}{n!} \quad (A-1)$$

where N_t is the number of molecules arrived at time t , k is the number of time segments (integration bins) per transit time and λ_p is the average number of molecule in the probe volume per time segment. This equation holds true assuming that events occur independently, in other words, the occurrence of an event in one period does not change the probability of an event occurring at a later time period. This equation has been very useful for accurately planning solution concentrations for SMM experiments.

Photon Detection Model

A model was devised to describe the detection of photons from molecules in a flowing stream as they passed through laser beam. Again, this assumes that the appearance of a molecule in the probe volume follows a random process. Furthermore, the distribution of photons detected during the transit time will follow a Poisson distribution because of the random nature of the distribution of the number of molecules in the probe volume (N_p). The observed number of detected counts $X(t)$ in time, t , is given by

$$X(t) = Z(t) + B(t) \quad (A-2)$$

(if there is a least one molecule in one of the measured time segments)

or

$$X(t) = B(t) \quad (A-3)$$

(if there are no molecules in any time segment)

where $Z(t)$ is the number of signal counts from the molecule and $B(t)$ is the number of signal counts due to the blank. It is assumed that the counts from analyte and the blank occur independently and follow Poisson distributions. Therefore, the probability to detect n signal counts, $P(X_t = n)$ is given by

$$P(X_t = n) = \Gamma P(B_t = n) + (1 - \Gamma) P(Z_t + B_t = n) \quad (A-4)$$

where $P(X_t = n)$ is defined as the probability to detect n signal counts from the analyte data in time t , $P(B_t = n)$ is defined as the probability to detect n signal counts from the data in time t , $P(Z_t + B_t = n)$ is the probability to detect n signal counts from both the analyte and the blank in time t and Γ is a proportionality constant to be evaluated. Assuming Poisson distributions for all processes, equation A-4 can be rewritten as

$$\frac{\lambda_x^n e^{-\lambda_x}}{n!} = \Gamma \frac{\lambda_B^n e^{-\lambda_B}}{n!} + (1 - \Gamma) \frac{(\lambda_x + \lambda_B)^n e^{-(\lambda_x + \lambda_B)}}{n!} \quad (A-5)$$

where λ_x , λ_B , and λ_z are the average numbers of signal counts per time segment for the total signal (analyte plus blank), the blank and analyte (to be evaluated), respectively. Since λ_x and λ_B can be obtained from the raw data, λ_z and Γ are estimated by solving a nonlinear equation for $n = 0$ and $n = 1$. From SMM data for IR 140 obtained in this dissertation at a laser power of 20 mW the values of λ_x and λ_B were 0.482 and 0.101 respectively. Equation

A-5 was evaluated to obtain Γ as well as the values of signal counts due to methanol and IR 140. The frequency of counts for a given n and the probability distribution for methanol and IR 140 were calculated using the obtained parameters λ_z and Γ (see Table A-1)

Table A-1 Observed and fitted probability distributions for IR 140 and methanol.

	methanol		IR 140	
	observed	fitted	observed	fitted
$n = 0$	3616 (0.904)*	3616 (0.904)	2956 (0.739)	2960 (0.740)
$n = 1$	364 (0.091)	364 (0.091)	812 (0.203)	800 (0.200)
$n = 2$	20 (0.005)	20 (0.005)	208 (0.052)	188 (0.147)
$n = 3$	0 (0.00)	0 (0.00)	20 (0.005)	36 (0.009)
$n = 4$	-	-	4 (0.001)	4 (0.001)
$n = 5$	-	-	0 (0.000)	4 (0.001)

*The number in parenthesis is the probability.

As can be seen in Table A-1, the fitted values of signal count compare very well the observed values. Furthermore, a larger number of high signal counts ($n > 3$) are obtained in the IR 140 data as compared to the methanol data. The goodness of the fit to observed values validated the assumption that the noise in the detection process was limited by the photon statistics described by a Poisson distribution.

Simulation of Data

A computer simulation was performed to examine the sensitivity enhancement gained using different sliding sum filters used process raw single molecule detection data. To do this, random solution data was generated using the parameters estimated in the previous section (λ_z and Γ). The generated data was analyzed using different summing

filters and the results were compared to the simplest case linear nonweighted summing filter (SSF from Chapter 4) for change in sensitivity. Detection sensitivities were all compared at given false detection rates (false positives and false negatives) of 0.1%.

The simple linear nonweighted summing filter (SSF) is given by

$$S_t = \sum X_t + X_{t+1} + X_{t+2} + X_{t+k} \quad (\text{A-6})$$

where S_t is the value of the summing filter at time t , X_t is the data point at time t and k is the number of time segments per molecular transit time. Other filters which were compared to the SSF included

1) Triangularly weighted sum

$$S_t = \sum 1X_t + 2X_{t+1} + 3X_{t+2} + 4X_{t+k} \quad (\text{A-7})$$

2) Symmetrically weighted sum

$$S_t = \sum 2X_t + 5X_{t+1} + 5X_{t+2} + 2X_{t+k} \quad (\text{A-8})$$

3) Triangularly weighted quadratic sum

$$S_t = \sum 1(X_t)^2 + 2(X_{t+1})^2 + 3(X_{t+2})^2 + 4(X_{t+k})^2 \quad (\text{A-9})$$

4) Symmetrically weighted quadratic sum

$$S_t = \sum 2(X_t)^2 + 5(X_{t+1})^2 + 5(X_{t+2})^2 + 2(X_{t+k})^2 \quad (\text{A-10})$$

The weighting in the filter is designed to emulate the shape of the photon burst from the molecule as it passes through the laser beam. Thus, the shape of the photon bursts in the simulated data (called true intensities) were varied to investigate how the weighting factors affected the results. Since this shape was not easy to quantify at the signal-to-noise ratios

obtained in this work, many types were investigated. It was found in this simulation that a linear weighting factor gave the best results regardless of the true intensity profile of the photon bursts. Furthermore, it was found that the linear summing filter (SSF) gave better sensitivity than the quadratic summing filter (WQS). This finding is contrary to what was found in the analysis of the data presented in this research (see Chap 4). It was found in this research that the WQS filter gave a significantly higher sensitivity as compared to the SSF. For example, channel one had a detection efficiency of 0.78 with SSF analysis and 0.95 with WQS analysis. The discrepancy in these findings will need to be investigated to elucidate the cause.

References

1. W.E. Moerner and L. Kador *Anal. Chem.* **1989**, *61*, 1217A-1223A
2. W.E. Moerner, *Science*, **1994**, *265*, 46-53
3. M. Orrit and J. Benard, *Phys.Rev. Lett.* **1990**, *65*, 2716-2719
4. Th. Basche, W.E Moerner, M. Orrit and H. Talon, *Phys. Rev. Lett.* **1992**, *69*, 1516-1519
5. R. Kettner, J. Tittel, Th. Basche, and C. Brauchle, *J. Phys. Chem.* **1994**, *98*, 6671-6674
6. F. Guttler, T. Irngartinger, T. Plakhotnik, A. Renn and U.P. Wild, *Chem. Phys. Lett.* **1994**, *217*, 393-397
7. T. Plakhotnik, D. Walser, M. Pirotta, A. Renn and U. P. Wild, *Science*, **1996**, *271*, 1703-1705
8. J. Wrachtrup, C. von Borczyskowski, J. Bernard, M. Orrit, and R. Brown, *Nature*, **1993** *363*, 244-245
9. J. Kohler, A.C. Brouwer, E. J. J. Groenen and J. Schmidt, *Science*, **1995**, *268*, 1457-1460
10. M. M. Collinson and R. M. Wightman, *Science*, **1995**, *268*, 1883-1885
11. F. F. Fan and A. J. Bard, *Science*, **1995**, *267*, 871-874
12. T. Hirschfeld, *Appl. Opt.* **1976**, *15*, 2965-2966
13. T. Hirschfeld, *Appl. Opt.* **1976**, *15*, 3135-3139
14. D.C. Nguyen, R. A. Keller, J. H. Jett and J. C. Martin, *Anal. Chem.* **1987**, *59*, 2158-2161
15. Q. Xue and E. S. Yeung, *Nature*, **1995**, *373*, 681-83
16. D. Craig, E. A. Arriaga, P. Banks, Y. Zhang, A. Renborg, M. M. Palcic and N. J. Dovichi, *Anal. Biochem.* **1995**, *226*, 147-153

17. K. Peck, L. Stryer, A. N. Glazer and R. A. Mathies, *Proc. Natl. Acad. Sci.* **1989**, *86*, 4087-4091
18. R. A. Mathies, K. Peck and L. Stryer, *Anal. Chem.* **1990**, *62*, 1786-1791
19. S. A. Soper, L. M. Davis, F. R. Fairfield, M. L. Hammond, C. A. Harger, J. H. Jett, R. A. Keller, B. L. Marrone, J. C. Martin, H. L. Nutter, E. B. Shera and D. J. Simpson, *Proc. Int. Soc. Opt. Eng.* **1991**, *1435*, 168-178
20. S. A. Soper, Q. L. Mattingly and P. Vegnuta, *Anal. Chem.* **1993**, *65*, 740-747
21. Y.H. Lee, R. G. Maus, B. W. Smith and J. D. Winefordner, *Anal. Chem.* **1994**, *66*, 4142-4149
22. M. Ishikawa, K. Hirano, T. Hayakawa, S. Hosoi and S. Brenner, *Jpn. J. Appl. Phys.* **1994**, *33*, 1571-1576
23. L. Q. Li and L. M. Davis, *Appl. Opt.* **1995**, *34*, 3208-3217
24. S. A. Soper, L. M. Davis and E. B. Shera, *J. Opt. Soc. Am. B*, **1992**, *9*, 1761-1769
25. P. M. Goodwin, C. W. Wilkerson, W. P. Ambrose, and R. A. Keller, *SPIE Proc SPIE*, **1993**, *79*, 1895-1898
26. R. C. Dunn, E. V. Allen, S. A. Joyce, G. A. Anderson and X. S. Xie, *Ultramicroscopy*, **1995**, *57*, 113-117
27. A. Castro, F. R. Fairfield and E. B. Shera, *Anal. Chem.* **1993**, *65*, 849-852
28. J. K. Trautman, J. J. Macklin, L. E. Brus and E. Betzig, *Nature*, **1994**, *369*, 40-42
29. J. J. Macklin, J. K. Trautman, T. D. Harris and L. E. Brus, *Science*, **1996**, *272*, 255-258
30. N. J. Dovichi, J. C. Martin, J. H. Jett, M. Trkula and R. A. Keller, *Anal. Chem.* **1984**, *56*, 348-354
31. E. B. Shera, N. K. Seitzinger, L. M. Davis, R. A. Keller and S. A. Soper, *Chem. Phys. Lett.* **1990**, *174*, 553-557
32. M. D. Barnes, W. B. Whitten and J. M. Ramsey, *Anal. Chem.* **1995**, *67*, 418A-423A
33. S. A. Soper, E. B. Shera, J. C. Martin, J. H. Jett, J. H. Hahn, H. L. Nutter and R. A. Keller, *Anal. Chem.* **1991**, *63*, 432-437
34. R. Rigler, J. Widengren and U. Mets in *Fluorescence Spectroscopy*, O. S. Wolfbeis, Ed. (Springer-Verlag, Berlin, 1993) Chap. 2

35. H. Kaiser, *Two Papers on the Limit of Detection of a Complete Analytical Procedure*, Jafner Publishing, New York, 1969
36. J. D. Winefordner, G.A. Petrucci, C.L. Stevenson and B.W. Smith, *J. Anal. At. Spectrom.* **1994**, *9*, 131-139
37. J. D. Winefordner and C.L. Stevenson, *Spectrochim. Acta.* **1993**, *44B*, 757-764
38. C. Th. Alkemade, *Appl. Spectrosc.* **1981**, *35*, 1-9
39. C. Th. Alkemade in *Analytical Applications of Lasers*, ed. E. H. Pipmeier, Wiley-Interscience, New York, **1986**, ch 4
40. C. L. Stevenson and J. D. Winefordner, *Appl. Spectrosc.*, **1991**, *44*, 1217-1224
41. C. L. Stevenson and J. D. Winefordner, *Appl. Spectrosc.* **1992**, *45*, 407-419
42. C. L. Stevenson and J. D. Winefordner, *Appl. Spectrosc.* **1992**, *45*, 715-724
43. B. B. Haab and R. A. Mathies, *Anal. Chem.* **1995**, *67* 3253-3260
44. J. H. Hahn, S. A. Soper, H. L. Nutter, J. C. Martin, J. H. Jett and R. A. Keller, *Appl. Spectrosc.*, **1991**, *45*, 743-746
45. D. C. Nguyen, R. A. Keller, J. H. Jett and J. C. Martin, *Anal. Chem.* **1987**, *59*, 2158-2161
46. D. C. Nguyen, R. A. Keller and M. Trkula, *J. Opt. Soc. Am. B*, **1987**, *4*, 138-143
47. J. H. Jett, R. A. Keller, J. C. Martin, D. C. Nguyen and G. C. Saunders, in *Flow Cytometry and Sorting*, **1990**, Wiley-Liss Inc. New York, 381-396
48. C. W. Wilkerson, P. M. Goodwin, W. P. Ambrose, J. C. Martin and R. A. Keller, *Appl. Phys. Lett.* **1993**, *62*, 2030-2032
49. J. Tellinghuisen, P.M. Goodwin, W. P. Ambrose, J. C. Martin and R. A. Keller, *Anal. Chem.* **1994**, *66*, 64-72
50. R. L. Affleck, W. P. Ambrose, J. N. Demas, P. M. Goodwin, J. A. Schecker, M. Wu and R. A. Keller, *Anal. Chem.* **1996**, *68*, 2270-2276
51. S.A. Soper, Q. L. Mattingly and P. Vegnuta, *Anal. Chem.* **1993**, *65*, 740-747
52. S. A. Soper, B. L. Lengendre and J. Huang, *Chem. Phys. Lett.* **1995**, *237*, 339-345
53. L.Q. Li and L. M. Davis, *Rev. Sci. Instrumen.* **1993**, *64*, 1524-1529

54. L. Q. Li and L. M. Davis, *Appl. Opt.* **1995**, *34*, 3208-3217
55. R. A. Keller, W. P. Ambrose, P. M. Goodwin, J. H. Jett, J. C. Martin and M. Wu, *Appl. Spectrosc.* **1995**, *50*, 12A-32A
56. D. Y. Chen, K. Adelhelm, X. L. Cheng and N. J. Dovichi, *Analyst*, **1994**, *119*, 349-354
57. S. A. Soper and Q. L. Mattingly, *J. Am. Chem. Soc.* **1994**, *116*, 3744-3752
58. G. Patonay and M. D. Antoine, *Anal. Chem.* **1991**, *63*, 321A-327A
59. L. Strekowski, M. Lipowska and G. Patonay, *J. Org. Chem.* **1992**, *57*, 4578-4580
60. L. Strekowski, M. Lipowska and G. Patonay, *Synth. Comm.* **1992**, *22*, 2593-2598
61. D. B. Shealy, R., Lohrmann, J. R. Ruth, N. Narayanan, S. L. Sutter, G. A. Casay, L. Evans and G. Patonay, *Appl. Spectrosc.* **1995**, *49*, 1815-1820
62. T. Fuchigami, T. Imasaka and M. Shiga, *Anal. Chim. Acta.* **1993**, *282*, 209-213
63. K. Sauda, T. Imasaka and N. Ishibashi, *Anal. Chim. Acta.* **1986**, *187*, 353-356
64. R. J. Williams, N. Narayanan, G. A. Casay, M. Lipowska, L. Strekowski, G. Patonay, J. M. Peralta and V. C. W. Tsang, *Anal. Chem.* **1994**, *66*, 3102-3107
65. L. R. Middendorf, J. C. Bruce, R. C. Bruce, R. D. Eckles, D. L. Grone, S. C. Roemer, G. D. Sloniker, D.L. Steffans, S. L. Sutter, J. A. Brumbaugh and G. Patonay, *Electrophoresis*, **1992**, *13*, 487-494
66. D. B. Shealy, M. Lipowska, J. Lipowski, N. Narayanan, S. Sutter, L. Strekowski and G. Patonay. *Anal. Chem.* **1995**, *67*, 247-251
67. Y.H. Lee, Ph.D. Dissertation, University of Florida, **1995**
68. W. B. Whitten, J. M. Ramsey, S. Arnold and B. V. Bronk, *Anal. Chem.* **1991**, *63*, 1027-1031
69. K. C. Ng, W. B. Whitten, S. Arnold and J. M. Ramsey, *Anal. Chem.* **1992**, *64*, 2914-2919
70. W.B. Whitten, J. M. Ramsey, *Appl. Spectrosc.* **1992**, *46*, 1487-1589
71. M. D. Barnes, K. C. Ng, W. B. Whitten and J. M. Ramsey, *Anal. Chem.* **1993**, *65*, 2360-2365
72. M. D. Barnes, W. B. Whitten, S. Arnold and J. M. Ramsey, *J. Chem. Phys.* **1992**, *97*, 7842-7845

73. M. D. Barnes, W. B. Whitten and J. M. Ramsey, *Chem. Phys. Lett.* **1994**, *227*, 628-632
74. K. Morikawa and M. Yanagida, *J. Biochem.* **1981**, *89*, 696-696
75. S. B. Smith, P. K. Aldridge and J. B. Callis, *Science*, **1989**, *243*, 203-206
76. N. J. Rampino and A. Chrambach, *Anal. Biochem.* **1991**, *194*, 278-283
77. T. T. Perkins, D.E. Smith and S. Chu, *Science*, **1994**, *264*, 819-822
78. T. T. Perkins, S. R. Quake, D. E. Smith and S. Chu, *Science*, **1994**, *264*, 822-826
79. X. Meng, K. Benson, K. Chada, E. J. Huff and D. C. Schwartz, *Nature Genetics*, **1995**, *9*, 432-438
80. H. Kabata, O. Kurosawa, I. Arai, M. Washizu, S. A. Margaron, R. E. Glass and N. Shimamoto, *Science*, **1993**, *262*, 1561-1562
81. R. Rigler and U. Mets, *SPIE Proc.-Soc. Int. Opt. Eng.* **1992**, *1921*, 239-248.
82. R. Rigler and U. Mets, *Eur. Biophys. J.* **1993**, *22*, 169-175
83. E. Eigen and R. Rigler, *Proc. Natl. Acad. Sci. USA*, **1994**, *91*, 5740-5747
84. U. Mets, R. Rigler, *J. Fluoresc.* **1994**, *4*, 259-264
85. J. Windengrin, R. Rigler and U. Mets, *J. Fluoresc.* **1994**, *4*, 255-258
86. M. Kinjo and R. Rigler, *Nucl. Acids. Res.*, **1995**, *23* 1795-1799
87. R. Rigler, *J. Biotech.* **1995**, *41*, 177-186
88. S. Nie, D. T. Chiu and Richard Zare, *Science*, **1994**, *266*, 1018-1021
89. S. Nie, D.T. Chiu and R. N. Zare, *Anal. Chem.* **1995**, *67*, 2849-2857
90. Th. Schmidt, G. J. Schultz, W. Baumgartner, H. J. Gruber and H. Schindler, *Proc. Natl. Acad. Sci.* **1996**, *93*, 2926-2929.
91. R. Kopelman and W. Tan, *Science*, **1993**, *262*, 1382-1384
92. K Betzig and R. J. Chechester, *Science*, **1993**, *262*, 1422-1425
93. W. P. Ambrose, P. M. Goodwin, J. C. Martin and R. A. Keller, *Phys. Rev. Lett.* **1994**, *72*, 160-163
94. X. S. Xie and R. C. Dunn, *Science*, **1994**, *265*, 361-364


95. W. P. Ambrose, P. M. Goodwin, J. C. Martin and R. A. Keller, *Science*, **1994**, *265*, 364-367
96. G. Tarrach, M. A. Bopp, D. Zeisal and A. J. Meixner, *Rev. Sci. Instrumen.* **1995**, *66*, 3569-3575
97. J. H. Jett, R. A. Keller, J. C. Martin, B. L. Marrone, R. K. Moyzis, R. L. Ratcliff, N. K. Seitzinger, E. B. Shera and C. C. Stewart, *J. Biomol. Struc. Dyn.* **1989**, *7*, 301-309
98. S. A. Soper, L. M. Davis, F. R. Fairfield, M. L. Hammond, C. A. Harger, J. H. Jett, R. A. Keller, B. L. Marrone, J. C. Martin, H. L. Nutter, E.B. Shera and D. J. Simpson, *Proc. Int. Opt. Eng.* **1991**, *1435*, 168-178
99. W. P. Ambrose, P. M. Goodwin, J. H. Jett, M. E. Johnson, J. C. Martin, B. L. Marrone, J. A. Schecker, C. W. Wilkerson, R. A. Keller, A. Haces, P. J. Shih, and J. D. Harding, *Ber. Bunsenges. Phys. Chem.* **1993**, *97*, 1535-1542
100. A. Castro and E. B. Shera, *Appl. Opt.* **1995**, *34*, 3218-3222
101. A. Castro and E. B. Shera, *Anal. Chem.* **1995**, *67*, 3181-3186
102. T. Funatsu, Y. Harada, M. Tokunaga, K. Saito, and T. Yanagida, *Nature*, **1995**, *374*, 555-559
103. CRC Handbook of Chemistry and Physics, 71st Edition, Boca Raton, 8-44
104. A. Gallager and E. L. Lewis, *J. Opt. Soc. Am.* **1973**, 864-869
105. D. S. Birch, G. Hungerford, B. Nidolshi, R. E. Imhof and A. D. Dutch, *J. Phys. E.: Sci. Instrumen.* **1988**, *21*, 857-860
106. R. Indralingam, J. B. Simeonsson, G. A. Petrucci, B. W. Smith and J. D. Winefordner, *Anal. Chem.* **1992**, *64*, 964
107. L. A. Woodard, in Raman Spectroscopy: Theory and Practice; vol. 2, H. A. Szymanski, ed; Plenum Press: New York, **1970**
108. D. A. Long, Raman Spectroscopy; Mc Graw Hill Inc: New York, **1970**
109. G. J. Puppels, A. Huzinga, H. W. Krabbe, H. A. de Boer, G. Gijsbers and F. F. M. de Mul, *Rev. Sci. Instrumen.* **1990**, *61*, 3709
110. F. Rasetti, *Nuovo Cimento*, **1930**, *46*, 395
111. M. J. Pelletier, *Appl. Spectrosc.* **1992**, *46*, 395

- 112. M. J. Pelletier, *Appl. Spectrosc.* **1993**, *47*, 69
- 113. P. J. Horosyski and M. L. Thewalt, *Appl. Spectrosc.* **1994**, *48*, 843
- 114. J. Sabbaghzadeh and M. Fink, *J. Raman. Spectrosc.* in press
- 115. T. D. Raymond and A. V. Smith, *Opt. Lett.* **1991**, *16*, 33
- 116. C. Th. Alkemade, Tj. Hollander, W. Snelleman, and P. J. Th. Zeegers, Metal Vapors in Flames, Pergamon Press, Elmsford, New York, **1982**
- 117. J. Puerta and P. Martin, *Appl. Opt.* **1981**, *20*, 259
- 118. R. A. Mathies and K. Peck, *Anal. Chem.* **1990**, *62*, 1786
- 119. N. Omenetto, J. D. Winefordner and C. Alkemade, *Spectrochim. Acta*, **1975**, *30B*, 335
- 120. A. Gallager and E. L. Lewis, *J. Opt. Soc. Am.* **1973**, *63*, 864
- 121. J. R. Beacham and K. L. Andrew, *J. Opt. Soc. Am.* **1971**, *61*, 231
- 122. H. P. Hooymayers, *Spectrochim. Acta.* **1968**, *23B*, 567
- 123. G. Cai, H. Zong, Q. Yu and R. Lin, *J. Chem. Eng. Data*, 332-335
- 124. A. P. Larson, H. Ahlberg and S. Folestad, *Appl. Opt.* **1993**, *32*, 794-798


BIOGRAPHICAL SKETCH

Robert D. Guenard was born on March 24, 1965, in Laconia, NH, and was raised on Cape Cod in Hyannis, Massachusetts. After graduating from Barnstable High School, in Hyannis, he worked as a bicycle mechanic and a machinist for four years. In 1988, he went back to school and attended Cape Cod Community College where he graduated with an Associate's degree. He then attended University of Massachusetts at Lowell where he majored in chemistry and gained a Bachelor of Science degree in 1992. He entered the University of Florida in the fall of 1992 and joined Professor Jim Winefordner's research group to work on his doctoral degree in analytical chemistry.

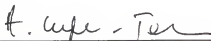
I certify that I have read this study and that in my opinion it conforms to acceptable standards of scholarly presentation and is fully adequate, in scope and quality, as a dissertation for the degree of Doctor of Philosophy.


James D. Winefordner, Chairman
Graduate Research Professor of Chemistry

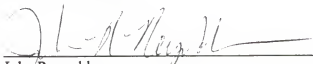
I certify that I have read this study and that in my opinion it conforms to acceptable standards of scholarly presentation and is fully adequate, in scope and quality, as a dissertation for the degree of Doctor of Philosophy.


Robert T. Kennedy
Associate Professor of Chemistry

I certify that I have read this study and that in my opinion it conforms to acceptable standards of scholarly presentation and is fully adequate, in scope and quality, as a dissertation for the degree of Doctor of Philosophy.


Anna Brajter-Toth
Associate Professor of Chemistry

I certify that I have read this study and that in my opinion it conforms to acceptable standards of scholarly presentation and is fully adequate, in scope and quality, as a dissertation for the degree of Doctor of Philosophy.


John Reynolds
Professor of Chemistry

I certify that I have read this study and that in my opinion it conforms to acceptable standards of scholarly presentation and is fully adequate, in scope and quality, as a dissertation for the degree of Doctor of Philosophy.


Joseph J. Delfino
Professor of Environmental Engineering Sciences

This dissertation was submitted to the Graduate Faculty of the Department of Chemistry in the College of Liberal Arts and Sciences and to the Graduate School and was accepted as partial fulfillment of the requirements for the degree of Doctor of Philosophy.

December, 1996

Dean, Graduate School